

Aus dem Bereich Klinische Medizin
der Medizinischen Fakultät
der Universität des Saarlandes, Homburg/Saar

Quantification of periaortic fat tissue in contrast-enhanced computed tomography

Dissertation zur Erlangung des Grades eines Doktors der Medizin

der Medizinischen Fakultät

der UNIVERSITÄT DES SAARLANDES

2022

vorgelegt von: Apostolos Theodosiou Mamopoulos
geb. am: 10.05.1979 in Thessaloniki

Dekan: Univ.- Prof. Dr. med. M. D. Menger
1. Berichterstatter: Prof. Dr. med. M. Katoh
2. Berichterstatter: Prof. Dr. med. W. Reith
Tag der mündlichen Prüfung: 13. Oktober 2022

TABLE OF CONTENTS

TABLE OF CONTENTS.....	II
LIST OF ABBREVIATIONS.....	III
1. SUMMARY.....	1
2. INTRODUCTION.....	3
2.1 Background of the present study.....	3
2.2 Pathophysiology of perivascular fat tissue.....	3
2.3 Clinical significance and histological characteristics of periaortic fat tissue.....	5
2.4 Periaortic fat tissue and aortic aneurysm formation.....	7
2.5 Periaortic fat tissue measurement using computer tomography.....	8
2.6 Correlation of periaortic fat tissue and aortic diameter on computer tomography.....	11
2.7 Objective of current study.....	11
3. MATERIALS AND METHODS.....	13
3.1 Existing PaFT quantification CT-protocols and their limitations.....	13
3.2 Methodological considerations for the present study.....	16
3.2.1 Impact of patient and CT-scanner variability on tissue attenuation values...	16
3.2.2 Impact of CT-tube voltage on tissue attenuation values.....	16
3.2.3 Impact of CT-tube current on tissue attenuation values.....	17
3.2.4 Impact of slice thickness and increment on volume reconstructions.....	17
3.3 Applied method.....	18
3.3.1 General considerations.....	18
3.2.2 Method for periaortic fat tissue quantification.....	21
3.3. Statistical Analysis.....	29
3.3.1 Normality of distribution.....	29
3.3.2 Periaortic fat tissue quantification.....	29
4. RESULTS.....	31
4.1 Normality of distribution.....	31
4.2 Derivation study.....	33
4.2.1 Correlation of periaortic fat tissue between arterial and native scans.....	35
4.2.1.1 Periaortic fat tissue Volume.....	35
4.2.1.2 Periaortic fat tissue Mean HU.....	37
4.2.2 Linear regression of periaortic fat tissue in arterial and native scans.....	39
4.2.2.1 Periaortic fat tissue Volume.....	39
4.2.2.2 Periaortic fat tissue Mean HU.....	41
4.3 Validation study.....	43
4.3.1 Periaortic fat tissue Volume.....	45
4.3.2 Periaortic fat tissue Mean HU.....	46
4.4 Secondary study.....	48
4.5 Reproducibility Study.....	49
5. DISCUSSION.....	53
5.1 Study background.....	53
5.2 Study results.....	55
5.2.1 Study results-PaFT Volume.....	55
5.2.2 Study results-PaFT Mean HU value.....	57
5.2.3 Study results-Secondary study.....	59
5.2.4 Study results-Reproducibility study.....	60
5.2.5 Study results-Sample size.....	60
5.2.6 Study results-Potential confounding factors.....	60
5.2.7 Study results-Study limitations.....	62
5.3 Methodological considerations.....	63
5.4 Conclusion – Future prospectives.....	68
6. REFERENCE LIST.....	70
7. PUBLICATIONS /ACKNOWLEDGEMENTS.....	76
8. CURRICULUM VITAE.....	77

LIST OF ABBREVIATIONS

AAA	Abdominal Aortic Aneurysm
ABI	Ankle-brachial index
BMI	Body Mass Index
CAD/CVD	Coronary Artery Disease/ Cardiovascular Disease
CE	Conformitè Européenne (EU)
CF	Conversion Factor
CM	Contrast Medium
CRP	C-Reactive Protein
CTA	Computer tomographic angiography
DICOM	Digital Imaging and Communications in Medicine (standard format)
EVAR	Endovascular Aortic Reconstruction
FAI	Fat Attenuation Index
FDA	Federal Drug Administration (USA)
GFR	Glomerular Filtration Rate
HU	Hounsfield Unit
ICC	Intraclass Correlation Coefficient
kV/kVp	kilovolt/kilovolt peak
MDCT	Multi-Detector Computer Tomography
mAs	milliamperesecond
MCP	Monocyte Chemoattractant Protein
MFT	Mesenteric Fat Tissue
MMP	Matrix Metaloproteinases
MR	Magnetic Resonance
PaFT	Periaortic Fat Tissue
PET-CT	Positron Emission Tomography – Computer Tomography
ROI	Region of Interest
SD	Standard Deviation
SFT	Subcutaneous fat tissue
TAA	Thoracic Aortic Aneurysm
TNF	Tumor Necrosis Factor
VAT	Visceral Adipose Tissue
VSMC	Vascular Smooth Muscular Cell

1. SUMMARY

Objective. Periaortic fat tissue (PaFT) has been implicated in the progression of abdominal aortic aneurysms (AAAs). Therefore, its quantification as a prognostic marker for aneurysm expansion has attracted clinical interest. Most existing research on PaFT, however, is based on unenhanced aortic CT-scans, whereas the CT diagnosis of aortic aneurysms is usually performed with enhanced CT angiographies. The objective of this study is to examine the feasibility of measuring abdominal periaortic fat tissue in enhanced aortic CT-scans using a new method based on the OsirixMD post-processing software and evaluate any methodological issues/considerations arising from it, in order to reliably quantify periaortic fat tissue from enhanced and unenhanced CT-scans.

Methods. In a derivation cohort (n= 101), PaFT Volume and PaFT mean HU value were measured within a 5 mm-wide periaortic ring in arterial phases and compared to the same values from native scans. Fat tissue was defined within the range of -45 to -195 Hounsfield Units (HU). After testing their correlation, fat tissue values from both CT phases underwent linear regression through the origin to define a correction factor (slope of the line of best fit), allowing the conversion of arterial back to native scores. This conversion factor was then applied to fat tissue values in a different validation cohort (n=47) and the agreement of the corrected fat tissue values and values in the native scans was examined using Bland-Altman plots and Passing-Bablok regression. In a secondary study the pooled data sets from both studies (n=148) were stratified in an AAA and non-AAA group and the average fat tissue values for both groups (with PaFT volumes adjusted for aortic size) were calculated using both native and corrected arterial values.

Results. In the derivation cohort, periaortic fat tissue Volume and mean HU value showed very high correlations between arterial and native scans ($r > .99$ and $r = .95$ respectively, $p < .0001$ both). Linear regression defined a conversion factor of 1.1057 for arterial periaortic fat tissue Volume and 1.0011 for arterial periaortic fat tissue mean HU. Potential confounding factors (mean intraluminal contrast density, aortic wall calcification, longitudinal contrast dispersion, aortic diameter, CT-tube voltage, slice thickness, image noise) showed no significant impact in multivariate regression. Application of the conversion factors in arterial scans of the validation study resulted in corrected arterial fat tissue values that showed very good agreement with PaFT values in native scans. Bland Altman analysis showed the following mean differences [95% confidence interval]: 0.36 [-0.01 to 0.73] for periaortic fat tissue Volume and 0.83 [-1.08 to 0.1] for periaortic fat tissue mean HU. Passing-Bablok regression confirmed minimal/no residual bias. Median periaortic fat tissue size-adjusted PaFT Volumes and Mean HU values from the Mann-Whitney test showed no significant difference between the AAA and non-AAA groups.

Conclusion. Periaortic fat tissue Volume and mean HU values demonstrate only minimal variation between arterial and native scans and can be measured in enhanced aortic CT scans with very high reliability. Periaortic fat tissue Mean HU value, unlike Volume, is independent from the presence of paraaortic organs. Certain issues, like non-circular aortic discs, histological boundaries of periaortic fat tissue and dependence from Body Mass Index and other fat tissue depots need to be explored further.

1. ZUSAMMENFASSUNG

Ziel. Das periaortale Fettgewebe spielt bei der Progression von Aortenaneurysmen eine Rolle, so dass seine Quantifizierung als prognostischer Marker für die Aneurysmaprogression von besonderem klinischem Interesse ist. Die aktuelle Forschung ist basiert jedoch fast ausschließlich auf nativen CTs, während Aortenaneurysmen üblicherweise nur mittels kontrastmittelverstärkten CT angiographien dargestellt werden. Das Ziel dieser Studie ist die methodische Überprüfung der Bestimmung vom abdominalen periaortalen Fettgewebe in kontrastmittelverstärkten CTs mit der frei verfügbaren OsirixMD Softwareanwendung und die Evaluation von potenziellen Faktoren, die eine zuverlässige periaortale Fettgewebsquantifikation in nativen und kontrastverstärkten CTs ermöglichen.

Methodik. In einer Derivationsgruppe (n=101), wurde das Fettgewebsvolumen und die HU Mittelwerte innerhalb von einem 5 mm breiten periaortalen Ring in arteriellen CTs bestimmt und die Werte wurden mit entsprechenden Werten aus nativen CTs verglichen. Das Fettgewebe wurde als HU Werte -45 bis -195 HU definiert. Die Fettgewebswerte von beiden CT-Phasen wurden auf Korrelation überprüft und anschließend einer linearen Regressionsanalyse unterzogen, wobei ein Konversionsfaktor bestimmt wurde, um arterielle in nativen Fettgewebswerten zu konvertieren. Der Konversionsfaktor wurde danach in einer zweiten Validierungsgruppe (n=47) angewendet. Sodann wurde die Übereinstimmung von korrigierten arteriellen und nativen Fettgewebswerten mittels Bland-Altman Plots und Passing-Bablok Regressionsanalyse überprüft. In einer Sekundärstudie, wurden die gepoolten Datasets beider Studien (n=148) in einer Bauchaortenaneurysma- und einer Nichtbauchaortenaneurysmagruppe stratifiziert, um die Mittelwerte von Fettgewebsvolumen (adjustiert für Aortengröße) und HU Mittelwert in beiden Gruppen zu bestimmen.

Ergebnisse. In der Derivationsgruppe, zeigte das Fettgewebsvolumen und der HU Mittelwert eine sehr hohe Korrelation zwischen kontrastverstärkten und nativen CTs ($r > 0,99$ und $r = 0,95$ entsprechend, $p < 0,0001$ für beide). Die lineare Regressionsanalyse ergab einen Konversionsfaktor von 1,1057 für das Fettgewebsvolumen und 1,0011 für den Fettgewebs-HU Mittelwert. Potenzielle Störfaktoren (intraluminal Kontrastmitteldichte, Aortenwandkalzifikation, longitudinale Kontrastmittelverteilung, Aortendiameter, CT-Röhrenspannung, Slicestärke, Größe der intraluminalen Kontrast-ROI, Bildrauschen) zeigten keinen signifikanten Einfluss in der multiplen Regressionsanalyse. In der Validierungsgruppe, zeigten die mittels Konversionsfaktor korrigierten Fettgewebswerte der arteriellen Phase eine sehr hohe Übereinstimmung mit den Fettgewebswerten der nativen CT-Phase. Die Bland-Altman Analyse ergab folgende mittlere Differenzen [95% Konfidenzintervall]: 0,36 [-0,01 bis 0,73] fürs Volumen und 0,83 [-1,08 bis 0,1] für den HU Mittelwert. Die Passing-Bablok Regressionsanalyse bestätigte ein minimales bzw. kein residuales Bias. In der Sekundärstudie, zeigten die Mediane der Fettgewebswerte aus dem Mann-Whitney Test keinen signifikanten Unterschied zwischen der BAA und nicht-BAA Gruppe.

Schlussfolgerung. Periaortales Fettgewebsvolumen und HU-Mittelwert zeigen eine minimale Variation zwischen arteriellen und nativen CTs und lassen sich in kontrastverstärkten Aorten-CTs sehr zuverlässig bestimmen. Der Fettgewebsmittelwert ist von der Präsenz anderer paraaortale Organe unabhängig. Gewisse Faktoren, z.B. nicht-zirkuläre aortalen Scheiben, histologische Grenzen des periaortalen Fettgewebes und seine Abhängigkeit vom Body Mass Index und anderen Fettgewebskompartimenten benötigen eine weitere Analyse.

2. INTRODUCTION

2.1 Background of the present study

Small (< 50 mm) abdominal aortic aneurysms (AAAs) can rupture while large AAAs (> 50 mm) may remain stable for the rest of the patient's life.¹ Consequently, basing the indication for AAA treatment on AAA size means that about 10 AAAs must be treated to prevent one rupture,¹ so that additional prognostic criteria could be beneficial to identify AAAs prone to rupture.^{1,2} Periaortic fat tissue (PaFT) has been implicated in AAA pathophysiology and has raised interest as a factor for AAA growth.³

The processes driving human AAA progression towards rupture are not fully understood yet. Recently, extensive adventitial fatty degeneration has been identified as a distinctive, yet so far ignored characteristic of AAA formation.³ Expansion of periaortic fat tissue depots and increased expression of adipocyte-related genes found in ruptured AAAs support a potential association between the amount of periaortic fat tissue and AAA rupture risk.³ This observation could be the reason for the failure of previous attempts to stabilize AAAs with medical (anti-inflammatory) therapies and may provide a lead for novel diagnostic approaches to identify AAAs prone to rupture.³

PaFT measurement, however, usually requires dedicated workstations limited to Radiology Departments. OsirixMD is a widely available FDA/CE-approved software for processing DICOM (Digital Imaging and Communications in Medicine) files for diagnostic purposes, with available tools for PaFT measurement already used for this purpose. Furthermore, existing research in PaFT quantification relies on unenhanced CTs, while AAA CT-diagnostics (outside of post-stenting imaging) is usually performed only with enhanced CTs. Intraluminal contrast medium, however, could interfere with the correct PaFT identification/ measurement, as it has been shown for aortic wall calcium quantification.⁴ For PaFT quantification specifically in enhanced CTs no data is published yet.

2.2 Pathophysiology of perivascular fat tissue

Effect of periarterial fat tissue on the arterial wall

Blood vessels are surrounded by adventitial perivascular fat tissue that may regulate vascular functions.⁵ Increased perivascular fat volume in animals is associated with pronounced inflammation, higher oxidative stress, and vascular smooth muscle cell proliferation.⁶⁻⁸ Similarly, PaFT adjacent to human atherosclerotic aortas is characterized by extensive macrophage infiltration and a shift in adipokine expression.^{9,10} Therefore, perivascular fat tissue seems to exert a local paracrine effect, potentially contributing to atherosclerotic alterations of the vessel wall.^{11,12} This, however, is not a one-way effect and a "crosstalk" between the perivascular adipose tissue and the vessel wall has been proposed.

“Crosstalk” between periarterial fat tissue and arterial wall

Inflammatory cells and fat tissue-derived stem cells can potentially migrate from perivascular adipose tissue into the vessel wall triggering inflammation, angiogenesis and neointimal formation.¹³

Perivascular adipocytes reside at the adventitial border of blood vessels and can function as endocrine cells able to respond to metabolic stimuli and then transfer signals to adjacent blood vessels. The mechanism of communication is assumed to consist of three key aspects: inflammation, vasoreactivity, and smooth muscle cell proliferation.¹³ The crosstalk theory consists of an “inside-out” model, where inflammation begins in the endothelium and radiates outwards, and an “outside-in” model, where perivascular adipose tissue is responsible for initiating inflammation.¹⁴ This model points to adipokines produced from fat cells as key regulators, acting on the vessel wall and inducing paracrine and autocrine effects, while also having systemic effects on remote tissues.^{14,15}

The role of perivascular adipocytes

Perivascular adipocytes come into direct contact with the outer vessel wall, since there is no barrier (fascia or elastic lamina) separating them from it, allowing them to penetrate into the outer adventitial layer.¹³ Consequently, any inflammatory mediators and adipokines excreted by adipocytes can directly act onto the vessel wall (paracrine effect).¹³⁻¹⁵ Mediators can also be transported to the inner layers of the vascular wall by the vasa vasorum, which in turn proliferate under the local inflammation.¹³

Enclosed within the PaFT, the vasa vasorum form a network of microscopic vessels within the adventitia of large arteries that provides oxygen and nutrients to the external layers of the arterial wall. Since periarterial fat tissue can interact closely with the adventitial vasa vasorum, proinflammatory adipokines derived from the PaFT likely contribute to the development of atherosclerosis and vascular remodeling.¹² Perivascular adipocytes also display a number of morphological differences compared to adipocytes from other fat depots. For instance, pericoronary fat cells feature more heterogeneous shapes, smaller sizes, lesser degrees of adipogenic differentiation and are also white-coloured compared to brown pericardial fat adipocytes.¹³ Similarly, adipocytes surrounding the thoracic aorta in mice are morphologically brown, while adipocytes from the infrarenal aorta are white coloured.¹³

Perivascular fat tissue promoting vascular wall inflammation

Cultured mice arteries show inflammatory factors secreted from the perivascular fat tissue that promote significant pro-oxidative and proinflammatory phenotypic alterations in the vascular wall.⁷ This points to a localized perivascular adipose tissue inflammation causing an exacerbation of vascular oxidative stress which leads to increased macrophage infiltration. The latter causes a significant proinflammatory shift in the cytokine/chemokine profile secreted from periarterial fat.⁷ Corroborating

magnetic resonance imaging evidence showed that excessive pericardial and thoracic periaortic fat may affect nearby tissues through locally secreted substances that exert negative effects on nearby endothelial and smooth muscle cells.¹¹ Certain stimuli cause an upregulation of the expression of proinflammatory genes and markers of immune cell proliferation in both PaFT and the aortic wall.¹⁶ The type/localisation of perivasular fat itself, however, could determine the vasoactive substances,¹⁷ since certain vasoactive factors are uniquely expressed in thoracic, brown fat tissue compared to white, abdominal periaortic fat.¹⁷

2.3 Clinical significance and histological characteristics of periaortic fat tissue

Periaortic fat tissue predictive of vascular disease and metabolic risk

PaFT has a local pathogenic effect on arteries associated with a higher prevalence of *arterial disease*.¹⁸ Most clinical research has involved thoracic PaFT, that has shown an association with cardiovascular disease (CVD).^{11,19} Furthermore, higher values for thoracic PaFT were shown in diabetics,²⁰ but not in cancer patients.²¹ This association of thoracic PaFT and CVD is independent of other fat depots, since high PaFT, even in the absence of increased visceral adipose tissue (VAT), is predictive of an adverse cardiometabolic profile.¹⁹ Functional²² and histological studies²³ showed an association of thoracic PaFT with microvascular function and large artery stiffness. Examining the effect of thoracic PaFT on different vascular beds, a relationship between thoracic PaFT volume and both coronary²⁴ and peripheral arterial disease¹⁸ was shown even after correction for VAT and Body Mass Index (BMI).

Studies on the association of various fat depots with *metabolic risk* profile showed positive associations between thoracic PaFT and circulating factors of higher metabolic risk.²⁵ The associations persist when eight different adipose tissue depots (abdominal subcutaneous, abdominal visceral, intramuscular, intrathoracic, pericardial, thoracic periaortic, intrahepatic and renal sinus adipose tissue) and multiple cardiometabolic risk factors were examined with CT.²⁶

An important question is whether PaFT affects the vessel wall directly (paracrine effect) or indirectly through excretion in the systemic circulation (exocrine effect). For instance, while epicardial adipose tissue and pericoronary adipose tissue are metabolically the same type of fat tissue, it is their different proximity to the coronary arteries that causes different pathophysiologic effects.²⁷ Research on the correlation between the various fat depots (pericoronary, epicardial, thoracic periaortic, extracardiac) and markers of inflammation independent of the presence of coronary artery disease points to a local effect of pericoronary fat on the manifestation of coronary artery disease.²⁷ It seems that adipokines, from pericoronary adipocytes, diffuse into the coronary artery wall and instigate the progression of atherosclerosis.²⁷ Moreover, this effect is separate from the impact of total body fat or systemic levels of inflammation.²⁷

Histological differences between abdominal and thoracic periaortic fat tissue

Thoracic PaFT shows histological differences from abdominal PaFT.^{13,17} There are several intrabdominal fat tissue-depots categorized on anatomic location. Subcutaneous fat tissue (SFT) lies underneath the skin, visceral fat tissue surrounds abdominal organs, mesenteric fat tissue (MFT) is lining the intestinal surface, omental fat tissue lies within the greater omentum and PaFT surrounds the abdominal aorta. These fat depots have different functions.²⁸ VAT is a highly active secretory organ, releasing adipokines into the portal vein and affecting hepatic metabolism. For instance, epidemiological studies show that abundance of VAT is related to diabetes and cardiovascular disease.²⁸ SFT is the least active fat tissue-depot, with weaker macrophage infiltration and adipokine secretion compared to visceral adipose tissue.²⁸ Abdominal PaFT is adjacent to the aortic adventitia, and can secrete adipokines, which diffuse into the aortic wall and contribute to aortic wall pathology.²⁸

Abdominal periaortic fat tissue as a distinct histological entity

Biopsies from four abdominal fat depots, subcutaneous, mesenteric, omental and PaFT, collected during aortic operations showed that PaFT was found to contain the smallest fat cells, the highest capillary density and produced high amounts of adipokines.²⁸ SFT was associated with the lowest number of macrophages and adipokines.²⁸ Mesenteric and omental fat tissue showed a similar inflammatory profile, with MFT inflammation most strongly related to metabolic complications of obesity.²⁸ The study underlined some important morphological characteristics of abdominal PaFT:

- abdominal PaFT was histologically the most active fat-tissue depot, showing the highest adipokine secretions involved in arteriosclerosis and implicated in the recruitment of immune cells to locations of inflammation, though morphological periaortic fat tissue characteristics were not related to systemic metabolic dysfunction. This supports a local effect of PaFT, directly affecting pathological processes in the vessel wall from outside-to-inside, without having systemic effects. The lack of systemic effects could, however, also be caused by the low amount of fat tissue mass in PaFT²⁸
- despite the close proximity of abdominal periaortic PaFT to other visceral fat tissues (mesenteric and omental fat tissue), PaFT was histologically separated and distinguished by relatively small adipocytes and a rich capillary network²⁸
- PaFT histological specimens were retrieved from sites adjacent to aortic aneurysms or occluded aortas, potentially contributing to the pronounced inflammatory state of PaFT.²⁸

When examining the association of PaFT with aortic calcification, another known marker of aortic wall inflammatory processes, thoracic periaortic fat was associated with coronary and abdominal aortic calcification but not thoracic aortic calcification.^{29,30}

2.4 Periaortic fat tissue and aortic aneurysm formation

Pathophysiology of AAA formation - Role of aortic wall inflammation

The aortic wall is formed by 3 layers: intima, media, and adventitia. The extracellular matrix consists mainly of elastin and collagen, which are primary constituents of the media (elastin) and adventitia (collagen). Elastin degradation seemingly plays a prominent role in AAA rupture. This degeneration of the aortic wall is considered to be mediated by inflammatory stimuli, with macrophages producing inflammatory cytokines found in perivascular fat tissues that are associated with atherosclerosis progression. Since aortic aneurysm formation is, at least partly, a chronic inflammatory process, macrophages can be assumed to play a significant role in the progression of aneurysmal dilatation.

Possible role of periaortic fat tissue in AAA pathophysiology - Role of periaortic macrophages

Examination of the role of PaFT-macrophage cells in aneurysm formation showed that suppression of macrophage infiltration into both aortic wall and PaFT suppresses aortic aneurysm formation and this is mediated by an anti-inflammatory effect in both the aortic and periaortic tissue.³¹ AAA has been considered a matrix degenerative disease. A number of proteases causing the degradation of aortic matrix proteins have been detected in both the aortic wall and the aortic intraluminal thrombus.^{32,33} Leukocytes are identified as sources of proteases degrading the aortic wall, leading to AAA formation. Usually, mobilization of immune cells and inflammation begins at the site of postcapillary venules. While the healthy human abdominal aorta does not have vasa vasorum, immune cell mobilization occurs via neovascularization, often seen in the adventitia of AAAs.^{34,35} Surrounding the adventitial layer of the aorta, fat tissue consisting in the abdominal aorta mostly of white fat, separates the aorta from the surrounding tissues. This PaFT varies with different disorders and is highly vascularized.³⁶

Possible role of periaortic fat tissue in AAA pathophysiology - Histological evidence

PaFT regulates aortic function through a large number of vasocrine molecules, like cytokines, which contribute to vascular inflammation in atherosclerosis, as well as adipokines, e.g. interleukin-6, whose plasma levels are increased in AAA patients.³⁷ Specimens from human AAAs, periaortic adipose tissue, and fat tissue surrounding peripheral arteries collected during AAA surgical repair were examined for necrotic adipocytes, type of infiltrating leukocytes and expression of proteases.³⁸ PaFT was found in AAAs to larger extent compared with control aortas from healthy organ donors and an increased presence of inflammatory cells was found in the PaFT of AAAs.³⁸ The findings included high numbers of neutrophils, macrophages, mast cells, and T-cells in PaFT around AAAs as well as close to necrotic fat tissue.³⁸

The AAA wall is typically strongly infiltrated by immune cells. Usually, high hemodynamic forces within the aortic lumen impede significant leukocyte adherence at the aortic luminal surface. Thusly, one possible portal for their entry into the aortic wall could be via capillary neovascularization, often seen in the adventitia of AAAs.³⁸ Another potential entry point could be post-capillary venules located in adjacent PaFT, followed by infiltration of the nearby AAA wall.³⁸ The pathogenetic process starts with adipocyte hypertrophy causing local hypoxia, which promotes infiltration by leukocytes. PaFT in turn is highly susceptible to inflammation, with the latter causing alterations of the aortic wall.³⁸

Leukocytes in PaFT excrete proteases causing damage to the aortic wall. Proteases like cathepsin K and S, implicated in AAA formation, are elevated in PaFT surrounding AAAs compared to their levels in control aortas.³⁸ Since cathepsin K and S are strongly expressed in the media layer of AAAs, their presence in PaFT may also be implicated in AAA formation.³⁸ Thus, PaFT around AAAs is characterized by adipocyte necrosis, sterile inflammation, and increased proteases activity, all participating in the damage to the adjacent AAA wall, and all beginning with periaortic adipocytes triggering the recruitment of leukocytes, which are attracted by adipocytes undergoing necrosis.³⁸

PaFT macrophage infiltration in experimental AAA formation models in mice showed that macrophage proinflammatory chemokines were more elevated in abdominal compared to thoracic PaFT.³⁹ Abdominal PaFT explants contained higher concentrations of Monocyte chemoattractant protein (MCP-1) and contained a higher macrophage infiltration than specimens from thoracic aortas, while hypertrophied white adipocytes surrounded abdominal aortas and brown adipocytes surrounded thoracic aortas.³⁹ These findings showed that increased macrophage concentration in abdominal PaFT is associated with increased AAA formation.³⁹ The earliest cellular change in AAA formation was medial accumulation of macrophages. Although it was unclear whether leukocytes infiltrate the aortic wall from the intimal or peri-adventitial spaces, macrophage concentration was also increased in the adventitia of suprarenal aortas with peri-adventitial penetration of leukocytes into the vascular wall.³⁹ This agrees with other studies demonstrating that perivascular adipocytes represent an integral part of the vascular wall since fat cells regularly invade the adventitia.³⁹ These results suggest that localized inflammation in abdominal PaFT could provide a macrophage-rich site enabling macrophage infiltration into the aortic media to further induce AAA formation.³⁹

2.5 Periaortic fat tissue measurement using computer tomography

The basic concept for PaFT quantification in non-enhanced MDCT was introduced by *Schlett* et al, who in 2009 quantified aortic and thoracic PaFT in 100 patients and showed that both abdominal and thoracic PaFT were correlated with both visceral and subcutaneous abdominal fat, waist circumference and BMI.⁴⁰ The authors concluded that “standardized semiautomatic CT-based volumetric quantification of PaFT is feasible and highly reproducible.”⁴⁰ The intra-observer agreement was excellent for abdominal and thoracic PaFT (Intraclass correlation coefficient-ICC= .970 and .986) as

was the inter-observer agreement (ICC= .968 and .983). The mean absolute and relative intra-observer differences were small for abdominal (-0.08cm^3 , 1.85%) and thoracic PaFT (0.55cm^3 , 3.56%), as was the inter-observer variability for abdominal (0.11cm^3 , 7.85%) and thoracic PaFT (-0.74cm^3 , -4.56%). 10 subjects were excluded from measurements of abdominal (10%, one AAA and 9 subjects with a non-circular aorta) and 3 of thoracic PaFT (3%, all 3 hiatal hernia). The mean abdominal PaFT volume was $6.38\pm 3.18\text{cm}^3$ and the mean thoracic PaFT volume was $16.34\pm 8.70\text{cm}^3$. Aortic and thoracic PaFT were highly correlated. Following *Schlett* et al, a number of studies involving quantification of PaFT in multi-detector CT (MDCT) (**Table 1**), and some in MRT,¹¹ were published.

Author (year)	sample/vessel	Method	Range	ROI	Software	CT-kV	Slice thickness
Schlett ⁴⁰ (2009)	100 thoracic /100 abdominal aortas (no AAAs) -non enhanced CT	Manual selection / segmentation	-45 to -195 HU	Schlett protocol	Aquarius 3D, TeraRecon	120	2.5 mm
Fox ¹⁸ (2010)	1205 subjects, throacic aorta -non enhanced CT	Manual selection and segmentation	-45 to -195 HU	Schlett protocol	Aquarius 3D, TeraRecon	120	2.5 mm
Lehman ²⁹ (2010)	1067 subjects, thoracic aortas -non enhanced CT	Manual selection and segmentation	-45 to -195 HU	Schlett protocol	Aquarius 3D, TeraRecon	120	2.5 mm
Britton ¹⁹ (2012)	3246 subjects, thoracic aorta -non enhanced CT	Manual selection/ segmentation	-45 to -195 HU	Schlett protocol	Aquarius 3D, TeraRecon	120	2.5 mm
Thanassoulis ³⁷ (2012)	3001 subjects, (for PAFT thoracic aorta) f(or AAA size (abdom. /thoracic aorta) -non enhanced CT	Manual selection and segmentation	-45 to -195 HU	Schlett protocol	Aquarius 3D, TeraRecon	120	2.5 mm
Akyürek ²⁰ (2014)	93 subjects, thoracic aorta	manual definition of ROIs	-200 to -450 HU	Schlett protocol	Volume Analysis Software, Siemens		
Efe ²⁴ (2014)	323 subjects, thoracic aorta	Manual selection and segmentation	-50 to -200 HU	Schlett protocol	Argus, Siemens	120	
Maurovich-Horvat ²⁷ (2015)	342 subjects, thoracic aorta	Manual selection and segmentation	-30 to -195 HU	Schlett protocol	Volume Viewer, Siemens	120	2.5 mm
Dias-Neto ⁴¹ (2018)	341 abdom. aortas 140: AAAs 104: stenotic aortas -enhanced CT 97: normal aortas -non enhanced CT	Manual selection and segmentation	-45 to -195 HU	Schlett protocol	OsirixMD	120	Thickness: variable 1-5mm Interval: 5-6mm

Table 1. Existing studies on PaFT quantification with computer tomography.

*Fox et al.*¹⁸ and *Lehman et al.*²⁹ quantified thoracic and abdominal PaFT. However, they cited technical limitations with abdominal PaFT measurement, like the dependence of PaFT volume on aortic size and the inability to visualize the separating retroperitoneal lining, as limiting their data interpretation. Hence, they did not include abdominal PaFT in their analysis. For thoracic PaFT, reproducibility was excellent for intra- and interobserver measurements (ICC= .99 and .98). *Britton et al.* applied the Schlett protocol in abdominal and thoracic PaFT quantification with the difference that abdominal MDCT images were reconstructed as 5.0 mm and not as 2.5 mm non-overlapping slices.¹⁹

Thanassoulis et al. applied the Schlett protocol in chest and abdominal CT imaging with 2.5 mm-thick, non-overlapping axial images for the thorax and a 5.0 mm thickness for the abdomen.³⁷ The authors also mention the difficulty of resolving the retroperitoneal lining and the dependence of abdominal PaFT volume from aortic size as limiting the reliability of abdominal PaFT quantification.³⁷ Subsequently, they considered abdominal PaFT measurement as secondary and applied thoracic PaFT as a substitute for abdominal PaFT in their primary analyses, thusly relating thoracic PaFT to abdominal aortic size.³⁷ However, since many studies have shown marked morphological and functional differences between abdominal and thoracic periaortic adipose tissue, this may have compromised the validity of their results. Reproducibility of PaFT volume was very high for intra- and interobserver measurements (intraclass correlation coefficients .99 and .98).³⁷

Akyürek et al. quantified thoracic PaFT using a threshold of -200 to -450 HU,²⁰ while *Efe et al.* defined PaFT as tissue with an attenuation range between ≤ -200 and ≤ -50 HU.²⁴ *Maurovich-Horvat et al.* measured thoracic PaFT in accordance with the Schlett protocol. They defined a volume of interest as a 7.0 cm vertical column of adipose tissue around the thoracic aorta extending from the pulmonary artery bifurcation to the diaphragm. PaFT was defined as voxels with HU values of -190 to -30 HU within the volume of interest.²⁷

All of the previous studies, however, involved unenhanced CT-scans and non-aneurysmatic aortas. *Dias-Neto et al.* applied the Schlett protocol for the first time in evaluating PaFT around abdominal aortic aneurysms (AAAs) and also for the first time in contrast-enhanced CT (CTAs) as well as unenhanced CTs.⁴¹ The authors conducted a multicentre study examining the distribution of abdominal adipose tissue depots (including PaFT) in AAA patients and compared it to patients with aortoiliac occlusive disease and patients without aortic disease. While they could not demonstrate a correlation between aortic size and PaFT volume, they found that in AAA subjects the PaFT density adjacent to the aneurysm sac was higher compared to the non-aneurysmatic infrarenal neck.⁴¹ Moreover, this intra-individual difference in PaFT density was positively associated with aortic volume, pointing to a potential contribution of PaFT to AAA pathophysiology by a local effect.⁴¹

2.6 Correlation of periaortic fat tissue and aortic diameter on computer tomography

Thanassoulis et al. used the Schlett protocol in 3001 individuals (mean age 50 ± 10 years, 49% women) and found that thoracic PaFT was positively associated with higher thoracic and abdominal aortic sizes.³⁷ Furthermore, this association was independent from age, sex, BMI and VAT volume. More specifically, each standard deviation increment in thoracic PaFT was associated with an 0.67 mm-increase in aortic size.³⁷ The authors concluded that thoracic PaFT volume positively correlated to both abdominal and thoracic aortic sizes independently from VAT, indicating that local fat depots in contact with the aorta contribute to aortic remodeling via local mechanisms.³⁷ A secondary study evaluated the association of abdominal periaortic fat with abdominal aortic dimensions with the same results. Importantly, the association between PaFT and aortic size was not mediated through circulating adipokines, confirming a potential local, rather than systemic, effect of PaFT.³⁷ However the results of the primary study were limited by the authors' use of thoracic PaFT, as a proxy for abdominal PaFT. Secondly, the authors could not relate PaFT to aortic aneurysms in this community-based population because of the very low prevalence of AAAs in their sample.³⁷

Dias Neto et al. quantified PaFT "density" (aortic size-adjusted volume) in patients with AAAs (n=140), compared to those with a non-dilated aorta (occlusive aortic disease, n=104 and no aortic pathology, n=97). The AAA group demonstrated higher intra-individual PaFT differences, namely higher PaFT densities adjacent to the aneurysm sac compared to the infrarenal non-aneurysmatic neck.⁴¹ More specifically, AAA presence increased intra-individual PaFT differences by 13.2 units.⁴¹ This result was independent from cardiovascular risk factors and other adipose tissue depots. Importantly, these intra-individual PaFT differences correlated highly to aortic volume, even after adjustment for other adipose tissue depots, BMI and sex/age, suggesting a relation between the deposition of PaFT and AAA pathophysiology.⁴¹ This means that in AAA patients, the larger the aortic diameter, the higher the PaFT density around the maximum aortic diameter. Lastly, the difference in PaFT densities was demonstrated within individual AAA patients providing a correction for inter-individual differences in PaFT densities.⁴¹

2.7 Objective of present study

The general hypothesis of the present study is that the quantification of abdominal periaortic fat tissue can be performed accurately in contrast enhanced CT scans of the abdominal aorta, retrospectively, using the commercially available DICOM post-processing software OsirixMD and one of its Plugins and that the results can be reliably converted into a baseline standard value that could have been acquired in unenhanced (native) aortic CT scans.

The specific hypothesis is that there is a high correlation between periaortic fat tissue Volume and mean HU values measured in enhanced CTAs with respective values measured in native CT scans, which allows linear regression models to produce a correction factor, who in turn will allow the reliable conversion of fat tissue values measured in enhanced CTAs into values measured in native CT scans, maintaining a high agreement between values obtained from corrected enhanced and those from native (unenhanced) aortic CT scans.

A conversion factor for PaFT Volume and PaFT Mean HU in CTAs is to be determined in a derivation cohort and the agreement between corrected PaFT values from CTAs with respective values from native CT scans is to be examined in a separate validation cohort. In a secondary study, the ability of the corrected PaFT values form CTAs to identify significant differences in fat tissue values between an AAA and a non-AAA group is to be compared to the same ability of PaFT values from native CTs.

3. MATERIALS AND METHODS

3.1 Existing PaFT quantification CT-protocols and their limitations

Protocol of Schlett et al. (2009)⁴⁰ - PaFT quantification in non-aneurysmatic aortas.

Image acquisition. Using an 8-slice MDCT scanner, non-gated CT scans of the abdomen and ECG-gated CT scans of the thorax were performed with a tube voltage of 120 kVp and tube current of 320 mA or 400 mA (BMI-dependent). Slices were obtained with 8×2.5 mm detector width and images were reconstructed with 2.5 mm thick, non-overlapping slices. PaFT volume was measured on an offline workstation (Aquarius 3D Workstation, TeraRecon®).

Exclusion criteria. For abdominal PaFT, data sets were excluded in the presence of a difference >5 mm between the transverse and anterior-posterior diameter, since non-circular aortas complicated a standardized definition of the PaFT cylinder. Data sets were also excluded if only a short aortic segment < 40 mm above the bifurcation was imaged on CT. For thoracic PaFT, subjects with hiatal hernia and intra-thoracic stomach were excluded.⁴⁰

Definition of PaFT attenuation values. Since CT-attenuation in absolute Hounsfield units (HU) corresponds to tissue properties, the authors selected an identification threshold for voxels containing fat tissue using a HU range of -195 to -45 HU.⁴⁰

Definition of PaFT ROI. For abdominal PaFT, the differentiation of periaortic from retroperitoneal fat and the standardization of measurements necessitated the definition of a ROI, in each axial image, in the form of a circle centered over the aorta with a diameter 10 mm larger than the anterior-posterior aortic diameter. This led to the definition of a cylinder of periaortic adipose tissue. The total PaFT volume was quantified from 16 contiguous slices, spanning 40 mm cranially to the aortic bifurcation. The measurement started with the first slice above the aortic bifurcation featuring a < 1 mm difference between transversal and anterior-posterior aortic diameters. Thoracic PaFT, contrary to abdominal PaFT, can be clearly separated from surrounding tissue. Thoracic PaFT was defined as “the area immediately surrounding the thoracic aorta anteriorly by a horizontal line through the esophagus, connected to the left costo-vertebral joint, posteriorly by the anterior edge of the vertebral body, and the right lateral border of the vertebral body.”⁴⁰

Adjustment of PaFT Volume for aortic size. To correct for the relationship between abdominal PaFT cylinder size and aortic size, all abdominal PaFT measurements were adjusted for aortic diameter (anterior-posterior diameter, first slice above the bifurcation).⁴⁰

Rationale for the 5 mm-wide PaFT ROI. While the identification of thoracic PaFT is straightforward, clearly separating abdominal PaFT from retroperitoneal adipose tissue represents a challenge. This is significant because the blood supply of PaFT drains directly into the vasa vasorum possibly causing local effects on the aortic wall. Here PaFT was measured in a cylinder of adipose tissue extending 5 mm around the aorta. This was based on histological examinations of pericoronary adipose tissue showing that cellular and molecular inflammatory responses post-angioplasty extended

beyond the adventitia of the injured arteries, with leukocytes and chemokines detected throughout the entire perivascular tissue extending several millimeters away from the injured arterial wall.⁴² Included among them were adipocytes, pericardial fibroblasts and myocardial capillary endothelial cells, with adipocytes and vasa vasorum endothelial cells within the periarterial tissue proliferating 3 to 7 days post-angioplasty.⁴² Additionally, measurements of epicardial fat surrounding coronary arteries also gave a mean fat tissue thickness of 5.3 mm.^{40,43}

Protocol of Dias-Neto et al. (2019)⁴¹ - PaFT quantification in aneurysmatic aortas (AAAs).

Image acquisition. CT/CTA imaging was performed with a 64-slice MDCT. Scan parameters were determined by the Right Dose indicated by manufacturer. Slice thickness varied between 1-5 mm and measurements were performed at intervals of 5-6 mm. PaFT was quantified with Osirix®.

Inclusion criteria. Included were AAA patients with available CTAs, patients with CTAs because of aortoiliac occlusive disease and controls >50 years with unenhanced CTs because of urinary stones. Thus, PaFT volumes from enhanced CTAs were compared to volumes from unenhanced CTs.

Exclusion criteria. Excluded were subjects with ruptured, symptomatic and inflammatory AAA, suspected aortic inflammation in CTA, previous aortic intervention and active neoplasia/infection.

Definition of PaFT attenuation values. Fat-containing tissue was identified within a HU range of -195 to -45 HU, concurring with Schlett et al.⁴⁰ Existing research demonstrated -107 ± 8 HU as the mean of the range where the attenuation borders of fat begin, varying up to +45 HU. Consequently, in the literature a “halfway method” has been applied. Whereas in early research (1988) a halfway upper boundary of -30 HU was applied as the cut-off point for fat tissue,⁴⁴ recent literature points to a value of -45 HU as the upper boundary.^{5,27} Pixels within this range were given a value of a “1”, while pixels outside this range were given a value of “0”. Subsequently, the fat tissue-containing pixels were summed up and quantified per cm^2 .⁴¹

Definition of PaFT ROI. PaFT measurements were based on the Schlett protocol.⁴⁰ Because of the relationship between abdominal PaFT volume and the aortic diameter, PaFT measurement was performed using concentric rings calibrated to the aortic diameter. To achieve that in a standardized manner, a region of interest (ROI) was defined in each slice, centered over the aorta and circumferential to the outer aortic contour. The periaortic ROIs, measuring a diameter of 10 mm larger than the aortic diameter, resulted in a hollow cylinder of aortic PaFT.⁴¹

PaFT Volume measurement. The aortic area, the area of the circumferential periaortic ring, and the number of adipose tissue pixels contained in that ring were measured in contiguous slices. The measurement began with the first slice below the lowest renal artery and concluded at the aortic bifurcation. Since analysis of ROIs in paraortic vertebrae and intervertebral discs confirmed these structures as being free from significant amounts of fat tissue, with values within the -195 to -45 HU range,⁴¹ these structures were not excluded from the PaFT ring.⁴¹

Adjustment of PaFT Volume for aortic size. The authors calculated a PaFT “density” in each axial image, defined as the ratio of the number of adipose tissue-containing pixels within the ring to the ring

area. The mean density of PaFT pixels from all axial images, namely the mean aortic PaFT density from AAA subjects was compared to the one of the subjects in the two control groups. Furthermore, the PaFT density was compared between two aortic segments of the same patient, namely the two most cranial axial images of the infrarenal aorta (aneurysm neck) were compared to the axial image containing the maximum aortic diameter in AAA patients or the mid-aortic segment in control subjects. This intra-individual PaFT measurement was carried out to examine regional differences in PaFT density within the same individuals by comparing aneurysmatic to healthy aortic segments. Subjects with short (< 1 cm) infrarenal necks were excluded from the analysis.⁴¹

Methodological considerations. The authors here addressed the aforementioned concerns about the retroperitoneal lining and the relationship between abdominal aortic diameter and abdominal PaFT volume. These concerns were aggravated by the necessity of volumetric measurements in a population (AAA patients) with inherent large variation in aortic size. To counter this, they applied a “density” approach to quantifying abdominal aortic PaFT, by measuring the ratio of the fat-containing pixels to the area of a ring extending 10 mm from the outer aortic contour, in each axial image, thus, adjusting the PaFT quantity to the aortic disc area. Moreover, since PaFT densities were quantified in two separate regions of the aorta in the same patient, this self-matching helped control for factors that vary among individuals, like BMI, quantity of visceral abdominal fat tissue and established comorbidities. One consideration mentioned by the authors was that the root of the mesentery, also consisting of adipose tissue, can be partly located within the periaortic PaFT hollow measurement cylinder. This omental fat, however, is separated from PaFT and the aortic adventitia by a dual layer of peritoneum, which impedes paracrine signaling. Furthermore, with this HU detection range for fat tissue (-195 to -45 HU), inflamed adipose tissue could not be identified.⁴¹

Remaining unanswered issues. A number of questions about abdominal PaFT quantification remain unanswered. *Dias-Neto* et al. did not address the issue of exclusion of non-circular aortic discs, as *Schlett* et al. did, but simply commented that by applying the concept of PaFT “density” adjusted to aortic size “...previously reported measurement problems because of differences between transverse and anteroposterior diameter were not a problem in the protocol...”⁴¹ Another issue is that *Dias-Neto* et al. compared PaFT measurements made in contrast-enhanced CTAs (AAA group and aortoiliac, occlusive disease control group) with ones made in unenhanced abdomen CTs (control group with urinary stones). Since previous experience is based on unenhanced CT scans, it is not known, whether the presence of intraluminal contrast medium can affect the HU values of PaFT, as it has been shown to increase the HU intensity of adjacent intramural calcifications.⁴ The HU intensity of PaFT could be altered in contrast-enhanced scans through artefacts. Furthermore, histological examinations of abdominal PaFT consistently show a very rich vascularization of the adipose tissue^{28,36} that could lead to an early enhancement of PaFT in enhanced CT scans.

3.2 Methodological considerations for the present study

3.2.1 Impact of patient and CT-scanner variability on tissue attenuation values

Examinations on the effect of scanner and patient variability on tissue (i.e. calcium) attenuation values in CT-images showed that the mean CT-attenuation values of a calibration phantom showed significant variability dependent on scanner and participant BMI. More specifically, mean CT-attenuation values were lowest for Siemens MDCT scanners, followed by GE-Imatron electronbeam and GE LightSpeed MDCT scanners.⁴⁵ Attenuation values were also lower for morbidly obese (BMI > or =40 kg/m²) subjects, followed by obese (BMI 30- 39.9 kg/m²), overweight (BMI 25-29.9 kg/m²), and normal-weight or underweight (BMI <25 kg/m²) subjects.⁴⁵ Since these differences apply to patients scanned with different scanners and to different scans of a single patient over time, they can affect studies seeking standardization of PaFT quantification methods but not the present study where patients were scanned with scanners from one manufacturer and the paired scan sets were performed during one examination run.

Another issue arises in the presence of high image noise, because it can be misinterpreted by the automatic detection software as non-adipose tissue. This led to the exclusion of enhanced scans with high noise, as indicated by intraortic attenuations with a standard deviation above SD >35.⁴⁶ High noise over the entirety of the scan is usually not an issue with modern CT scanners but individual axial images can be affected by it. Consequently, CT scans with high image noise (SD > 35 HU) throughout the examination volume were excluded from the present study.

3.2.2 Impact of CT-tube voltage on tissue attenuation values

The CT-voltage is of interest because different voltage values can lead to different tissue attenuation values as well as different levels of noise. The reason for this is that the tube voltage determines the energy of individual X-ray photons. As they pass through the patient's body, different energy photons are liable to differential absorption leading to a different attenuation value. Generally, lower tube voltages result in more absorption of photons and thus higher attenuation values. For instance, CTA examinations performed with a CT-voltage of 100 kV result in higher signal intensity and a higher image noise compared with the standard of 120 kV,⁴⁷ since a voltage reduction from 120 to 100 kV causes a signal intensity increase for both contrast medium and tissue attenuation values.^{48,49} The reason for this is, that increasing the x-ray tube potential from 80 kVp to 140 kVp increases the mean photon energy from about 52 keV to about 72 keV and increases the contrast-to-noise ratio by a factor of 2.6 for muscle tissue and by a factor of 1.4 for iodine.⁴⁸ Comparing tube voltages of 120 and 100 kV in coronary calcium scoring, the mean image noise was significantly lower with the higher voltage,

20 ± 5 and 27 ± 7 for 120 and 100 kV, respectively and the use of 100 kV tube voltage compared with 120 kV led to significant overestimation of calcium attenuation values.⁵⁰

In the present study, in order to completely exclude this confounding factor, only paired sets of scans performed with the same CT voltage (100, 120 or 130 kV) in the unenhanced and enhanced phase were included. To examine the potential effect of voltage on the definition of the conversion factor, the CT voltage was included as a coefficient in the multivariate regression model comparing unenhanced and enhanced scores, to test if different voltages necessitate different conversion factors.

3.2.3 Impact of CT-tube current on tissue attenuation values

Unlike CT tube voltage, tube current, usually expressed as the effective tube current-time product (mAs), does not affect tissue attenuation values, since CT current affects the total number of X-ray photons but not the energy of individual ones. Variable CT current values are typical in modern protocols for dose reduction purposes⁵¹ and tube current modulation was applied in all of the examined scans. Although tube current does affect image noise, this issue has already been addressed above.

3.2.4 Impact of slice thickness and increment on volume reconstructions

The total PaFT Volume is calculated from a 3D reconstruction of all the ROIs containing voxels with values -195 to -45 HU. Since some interpolation of slices is applied, the result of the reconstruction could be dependent on slice thickness/increment. Turning to the experience from measuring Calcium Volume scores, because of the similar volume reconstructions, suggests that slice thickness can, indeed, have multiple effects on quantified calcium, both when identifying individual calcified lesions as well as when summing scores from different axial images.⁴⁹ Generally, thinner slices lead to significantly higher calcium scores,⁵¹⁻⁵⁴ as well as lower variability of results, so that a thinner slice thickness further enhances reproducibility.⁵² To compensate for these effects, the use of overlapping slice reconstruction has been recommended.⁵¹ However, the use of interslice interpolation, which theoretically plays a significant role because it verifiably reduces intra- and interobserver variability, is rendered negligible nowadays, since currently applied CTA protocols all implement a collimation of 0.625 mm and apply very low pitches so that a maximum slice overlapping is usually obtained. That is why slice differences become less relevant in enhanced CTA scan protocols,⁵⁵ compared to the standard Agatston protocol used in calcium scoring that necessitates non-overlapping slices.

In this study, the slice thickness as a confounding factor was excluded altogether by only including paired data sets with identical slice thickness/increment. However, paired data sets of different slice thicknesses were included and tested for their effect in the multivariate regression analysis.

3.3 Applied Method

3.3.1 General considerations

Ethical approval. The study was deemed by the Institutional Ethics Review Board not to require ethical approval. Additionally, the Ethics Committee of the Medical Association of the local federal state approved the study without further requirements for written patient consent retrieval, based on the use of retrospective, post-processed, anonymised radiological data and the fact that patients did not undergo any additional investigations. This was in agreement with similar published research.⁵⁶

Sample size. The retrospective nature of the study did not necessitate an a priori calculation of a sample size, since the statistical significance of the results can be determined by the confidence levels of the resulting outcomes. To empirically place some constraints on the sample size, a literature review was performed. For PaFT quantification, no comparison study for unenhanced vs. enhanced CT scans was found. Based on the Schlett protocol, a sample size of about 100/50 data sets was selected,⁴⁰ that should result in about 300 PaFT measurements (200 in the derivation and 100 in the validation cohort). Although it became obvious during the course of the study that a very high statistical significance ($p < .0001$) of the results for PaFT quantification could be achieved with a much lower sample size, the need to derive a conversion factor from the regression model with as much precision as possible led to the completion of the study up to the predetermined sample size.

Data acquisition. The data collection carried out was entirely retrospective. Consecutive CT scans of the abdomen or thorax/abdomen performed in the Radiology Department of our institution between 05.12.2018 - 04.07.2019 (for the derivation study) and 01.01.2020 – 30.03.2020 (for the validation study) were reviewed on a Web Pacs workstation. Studies deemed relevant were then examined more closely on an Intelispace Portal (Philips) workstation for potential inclusion in the study.

Inclusion criteria. The following inclusion criteria were applied:

- CT examinations containing imaging of the abdominal aorta or entire aorta with at least one native (unenhanced) and one strictly arterial (enhanced) phase. The presence of only a late arterial or venous phase made the study ineligible for inclusion.
- No constraints were placed on the clinical indication of the reviewed CT examinations. The reason for that was to test the applicability of the method with different imaging protocols and because the detection of AAAs is often performed in CT scans examining aother pathologies.
- A complete acquisition of the entire infrarenal aorta from the level of the renal arteries to the aortic bifurcation.
- Identical slice thickness and increment as well as identical CT tube-voltage for the enhanced and unenhanced series.
- CT tube current-exposure time product (mAs) was not considered since tissue attenuation values are independent from it.

Exclusion criteria. The following exclusion criteria were applied:

- Previously treated aortas either surgically or endovascularly.
- Presence of foreign bodies within the lumen or wall of the aorta or adjacent to it (stents, coils, embolising factors, cava filters).
- Inadequate imaging of the aorta (extended artefacts by spinal osteosynthesis material, very high signal to noise ratio). For the arterial phase specifically an intraluminal standard deviation of > 35 HU, as proposed in the literature,⁴⁶ throughout the examined volume rendered the scan ineligible for inclusion.
- Different slice thickness or CT tube voltage between unenhanced and enhanced series.
- Radiographic signs of inflammatory processes in the aortic wall, (aortitis, inflammatory AAAs).
- Ruptured AAAs.

Imaging protocol. Images were obtained using a 256-detector (Philips, Brilliance iCT) and a 64-detector (Philips, Ingenuity) multiscanner with $2 \times 128 \times 0.625$ mm and 64×0.625 mm detector collimation and 0.27 sec and 0.42 sec gantry rotation time, respectively. Protocols for both the abdominal aorta only and the entire aorta were included. The image slice and thickness were identical between phases, most of the examination pairs had a slice thickness of 3 mm and a slice increment of 2 mm. Examination-pairs with a slice thickness of 5 mm and a slice increment of 4 mm were also included. The examinations were also paired in the kilovoltage setting with most being at 120 kV for both phases. Paired examinations with 100 kV and 130 kV were also included. Tube current modulation was applied to all examinations. For the CTA, 100 ml contrast medium (Accupaque 350) was delivered at 4 ml/sec by an automated injection driver system, triggered when a threshold of 150 HU was reached in the center of the aorta. A sharp (C) reconstruction kernel was used for both phases.

Processing protocol: Unenhanced phase and contrast-enhanced arterial phase images from a single examination were transferred to an Apple, Mac Book Pro 15'' (2019) laptop computer with an Intel octacore processor operating the OsirixMD Software platform (v.10.0.5). This version of OsirixMD is FDA and CE approved for radiological diagnosis. For PaFT quantification, the freely available third-party Global Thresholding Plug-In was also used, after validation. Images were viewed on a 27'', 5K Monitor (Ultrafine, LG), and examined under magnifications between 1800-3200%. Similar methods with observer selected calcium areas on axial CT images with adjacent volume reconstruction (Syngo) have shown minimal interobserver variability.⁵⁷ The first image immediately distal to the ostium of the distal renal artery was selected as the proximal initial point and the last image with a still circular aorta proximal to the aortic bifurcation was selected as the distal point for the evaluated aortic segment.⁵⁷ The maximal aortic diameter was selected as the short axis of the larger circular /elliptical aortic ROI. A maximum diameter of ≥ 30 mm was considered aneurysmatic.

Data collection. All values resulting from the processing of the images according to the study protocol were stored on Microsoft Excel spreadsheets (Microsoft Office 2010 and 2021).

OsirixMD and its software tools. The choice of OsirixMD was based on its many advantages like: increasing popularity, proven performance, open architecture, built-in segmentation tools and exportable segmentation volumes. The software tool was introduced in 2005 as an open-source Mac-based DICOM viewing and post-processing software. It has two main versions: a 32-bit light, free non-FDA/CE approved version and a 64-bit FDA/CE approved version called OsirixMD (used in the study). The GlobalThresholding Plugin is a freely available third-party Plugin (Rene Laqua. (2016). Global Thresholding v1.0 OsiriX Plugin [Software]. Zenodo. <http://doi.org/10.5281/zenodo.208170>). The software tools and processing parameters were selected and tested by the author.

Independent Validation of the GlobalThresholding Plugin. Before application in the study, the freely available, third-party GlobalThresholding Plugin, was independently validated. To do that, a periaortic ROI was set in both native and enhanced axial images using the OsirixMD basic platform and then the GlobalThresholding Plugin was applied in the same ROI, set with the same pixel HU value range that was measured by OsirixMD. As demonstrated in **Figure 1**, both the basic values (ROI area in cm^2 , Mean HU Values and their SD) and more importantly their histograms were identical for both the original OsirixMD-ROI and the ROI created by summing all voxels using the Plugin. This provided independent validation of the correct function of the GlobalThresholding Plugin and its ability to correctly identify all pixels within a given HU range and allocate their respective HU values.

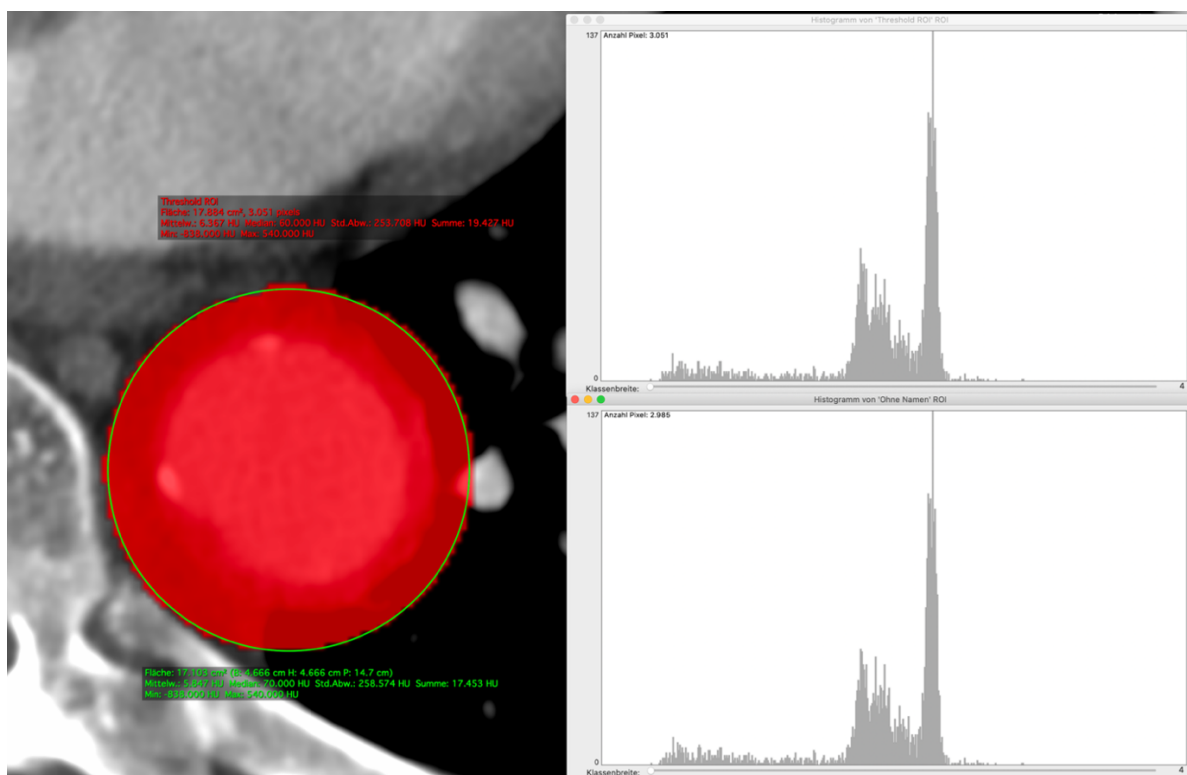


Figure 1. Validation of the GlobalThresholding Plugin. This was achieved, by comparing the summary values (left image) and histograms (right image) of a standard periaortic ROI set with the basic OsirixMD software (green ROI) and a ROI resulting from the addition of all pixels in the same HU range created with the Plugin (red ROI). Both the total pixel areas, Mean HU values and their SD and the resulting histograms were identical for both ROIs, providing independent validation of the Plugin. Very small differences in the summary values were due to differences between Osirix and the Plugin when allocating pixels on the very boundary of the ROI.

3.2.2 Method for PaFT quantification

Step 1. Selection of aortic and periaortic ROI (Figure 2). Based on the two published protocols of Schlett et al. and Dias-Neto et al., the present study also measured periaortic fat tissue within a 5 mm-wide circular ring adjacent to the aortic wall.^{40,41} To achieve that, firstly a circular region-of-interest (ROI), co-centered with the aortic disc, was introduced in the first axial non-enhanced infrarenal image of the aorta and modified to match the circumference of the outer layer of the aorta. This step was repeated on every axial image of aorta beginning distally to the lowest renal artery and ending with the last image of a circular aorta proximally to the aortic bifurcation. For non-circular aortic discs, an oval aortic ROI was introduced following the aortic contour as closely as possible and then this aortic ROI was extended by 10 mm in both diameters.

Once the aortic ROIs were established in all unenhanced axial images of the infrarenal aorta, the periaortic ROIs were then established, simply by extending the aortic ROIs by 10 mm concentrically in both axes (**Figure 2**). After that, the individual periaortic ROIs were saved and transferred to the arterial phase images, in order to ensure an identical and directly comparable periaortic cylinder in both phases.

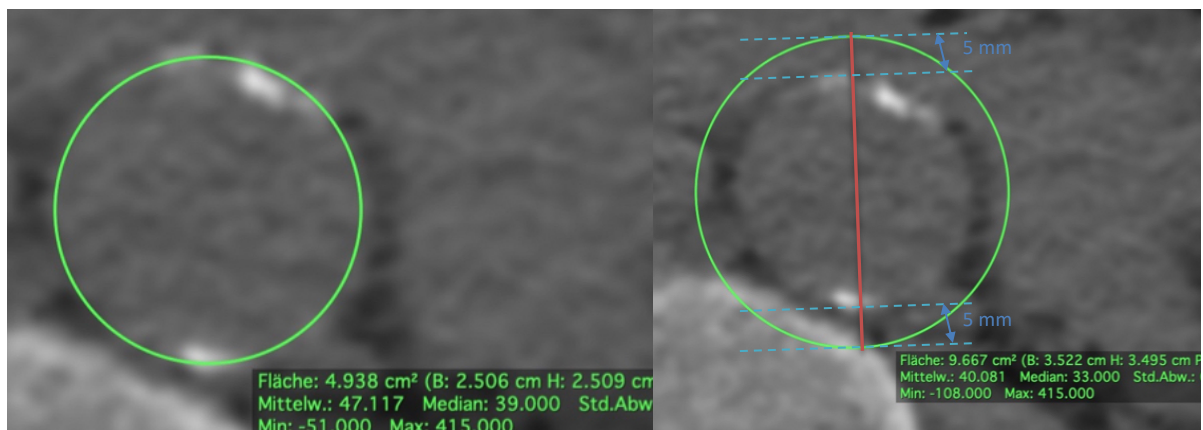


Figure 2. Selection of aortic (left) and periaortic (right) ROIs for PaFT measurement. By extending the diameter of the aortic ROIs concentrically by 10 mm, the periaortic ROIs defined a disc extending 5 mm from the outer boundary of the aortic wall. Subtracting the aortic ROI from the periaortic ROI results in a 5 mm wide periaortic ring. PaFT is then quantified within this 5 mm periaortic ring.

Step 2. Calculation of aortic volume and periaortic volume (Figure 3). Using the OsirixMD function, the Aortic Volume (**AVol**) was measured from reconstruction of all the aortic ROIs in the unenhanced series. After that, the Periaortic Volume (**PaVol**) was also measured from reconstruction of all periaortic ROIs in both the enhanced and unenhanced series, confirming that PaVol was identical in both phases. Lastly, the Periaortic Ring Volume (**PaRVol**), equal to the volume belonging to periaortic tissue within 5 mm of the aortic wall, was calculated by subtracting the AVol from the PaVol. The PaRVol was used then to adjust the PaFT Volume for the size of the aorta by dividing the PaFT Volume by the PaRVol, in order to calculate a PaFT-„ratio“.

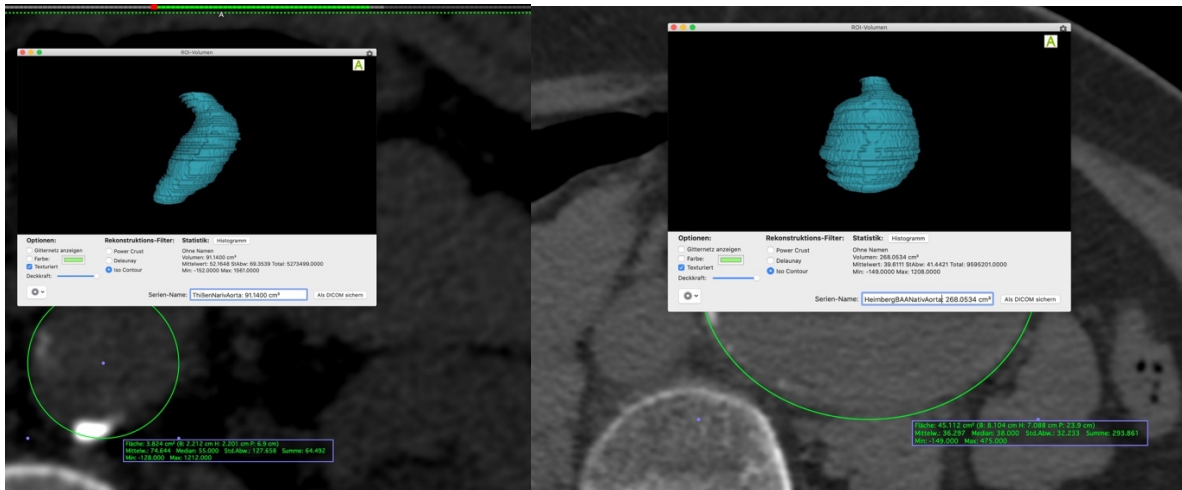


Figure 3. Calculation of the aortic volume (AVol) based on the aortic ROIs in OsiriXMD.

Step 3. Selection of fat tissue density range. A review of previous experience with PaFT measurement (**Table 1**) shows that, with one exception (-200 to -450 HU),²⁰ all studies used a HU attenuation range of -195 to -45 HU or very close to that. The three most relevant studies in the infrarenal aorta all applied the range of -195 to -45 HU.^{37, 40, 41} Consequently, the same density range was adopted for this study. This range of attenuation values has to be inputted into the setting of the GlobalThresholding Plugin.

Step 4. Setting all voxels outside the periaortic ROI to zero (Figure 4). This is necessary because the GlobalThresholding Plugin cannot be restricted by pre-existing ROIs. So, if the voxels outside the periaortic ROI are not nullified, all voxels in the axial image with HU values between -45 and -195 HU will automatically be included in the measurement.

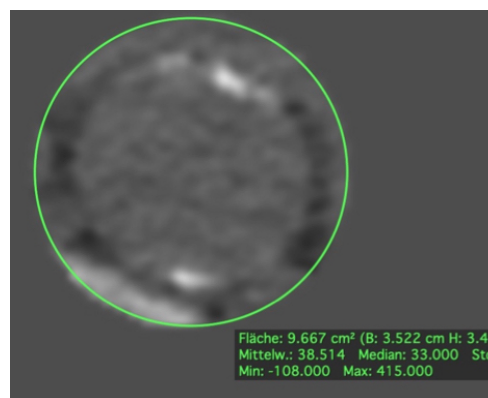


Figure 4. Setting all voxels outside the periaortic ROI to a value of zero. This is necessary to ensure that voxels with the range of -45 to -195 HU will be included only from within the periaortic ROI and not from within the entire axial image.

Step 5. Selection of periaortic fat tissue and PaFT Volume calculation (Figures 5,6,7,8). Using the GlobalThresholding Plugin of OsiriXMD, all voxels with a signal density of -195 to -45 HU within the periaortic ROIs were selected in the unenhanced and enhanced (arterial) phase. This Plugin creates a separate ROI in every axial image (marked in red), that includes all voxels with signal densities in the

selected range. These ROIs were then used by the Volume Reconstruction function to reconstruct the total volume of voxels with HU values in the -195 to -45 HU range in both the unenhanced and arterial phases.

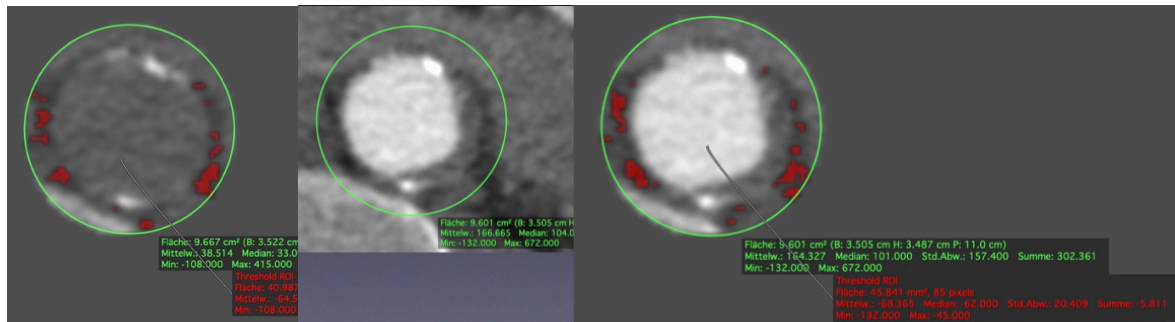


Figure 5. Selection of voxels with values -45 to -195 HU using the Global Thresholding Plugin in OsirixMD in the native (left image) and arterial phase (middle and right image).

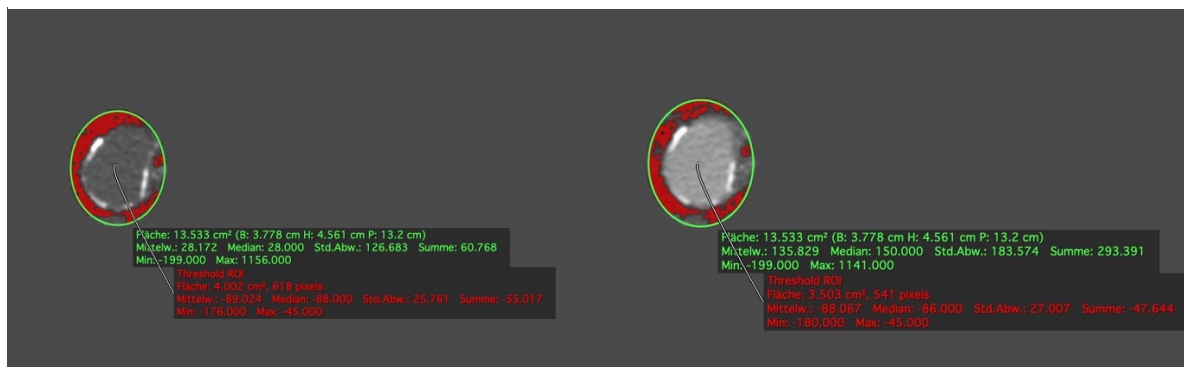


Figure 6. Selection of pixels with attenuation values of -45 to -195 leads to the creation of a ROI (red color) that contains pixels with attenuation values within this range. From the parameters of this ROI provided by the software (number of pixels, area in mm² and Mean HU value of the pixels with values -45 to -195 HU) two were included in this study: the area in mm² which was used to reconstruct a total PaFT Volume in mm³ or cm³, and the Mean HU value of the PaFT pixels. Typically, the number of pixels and the area of PaFT invariably decreases in the arterial phase compared to the native scan, whereas the Mean HU of PaFT remains nearly constant.



Figure 7. The selection of pixels with HU values -45 to -195 is made in identical axial images of the native (left image) and arterial (right image) phase. The periaortic ROI (green colour) is drawn in the native scan by concentrically extending the aortic ROI by 10 mm and is then copied into the arterial phase as well. The inset images show the same native scan image with selected calcium ROIs for calcium scoring, which can be performed simultaneously.

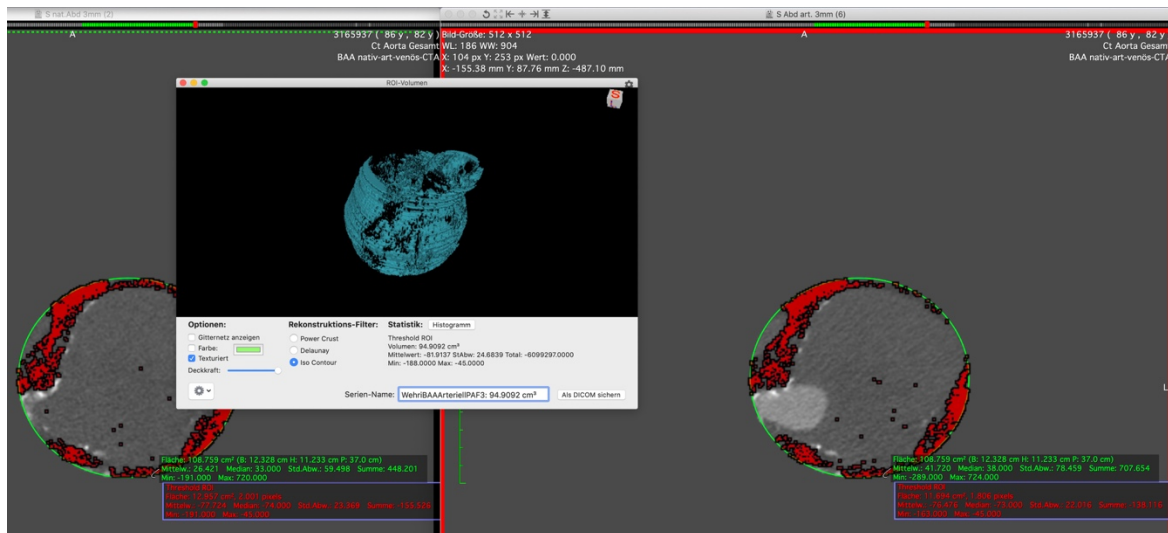


Figure 8. Selection of periaortic fat containing pixels in a large AAA and reconstruction of the total volume of periaortic fat containing pixels (inset image). The same principles are applied in large AAAs. In this case with high noise (not included in the study) there is a small number of pixels with values between -45 and -195 HU within the intraluminal AAA thrombus in both native and arterial phases.

This approach assumes that all relevant voxels (-195 to -45 HU) in the periaortic ROI are strictly located only within the 5 mm-wide periaortic ring volume and not within the aortic disc. One way to ensure this would be by interposing both aortic and periaortic ROIs on every axial image and applying the selection of -195 to -45 HU voxels only in the ring space between the two ROIs. The disadvantage of this approach is that by excluding the volume within the aortic ROI, which can not perfectly match the outer contour of the aortic wall, one risks excluding voxels that are in direct contact to the wall and thus very relevant for the measurement of PaFT. Experience with the method showed that no voxels within the -195 to -45 HU range were encountered in the aortic ROI of the enhanced (arterial) phase and very few/isolated, if any, such voxels were detected within the aortic disc in the unenhanced phase, so that by selecting the desired HU range within the periaortic ROI of both phases, one can safely assume that practically all -195 to -45 HU voxels are located within the 5 mm-wide periaortic ring space (**Figures 9,10**). This assumption was further examined in the present study.

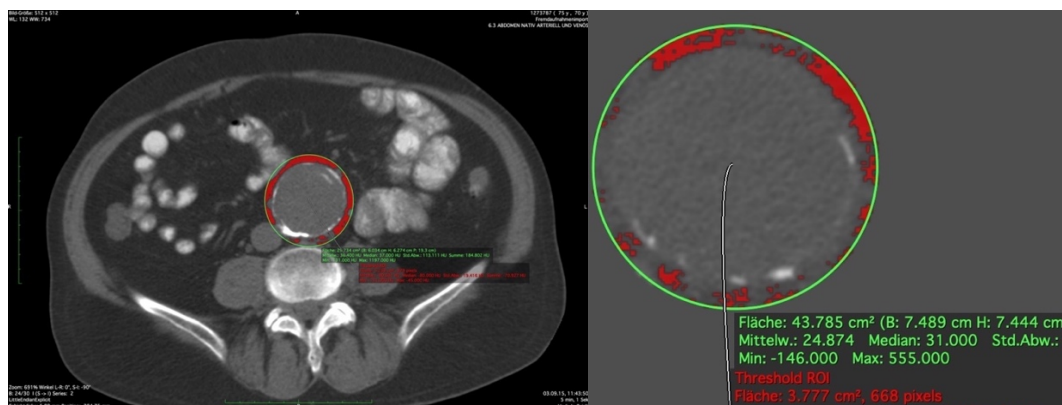


Figure 9. Frequency of intraluminal pixels with values -45 to -195 HU. Even in the case of large AAAs only isolated pixels with fat tissue values are found in the unenhanced lumen (left image, one intraluminal pixel). Usually, the unenhanced aortic lumen is free from pixels with fat tissue values (right image, 6,5 cm AAA with no intraluminal pixels within the -45 to -195 HU range).

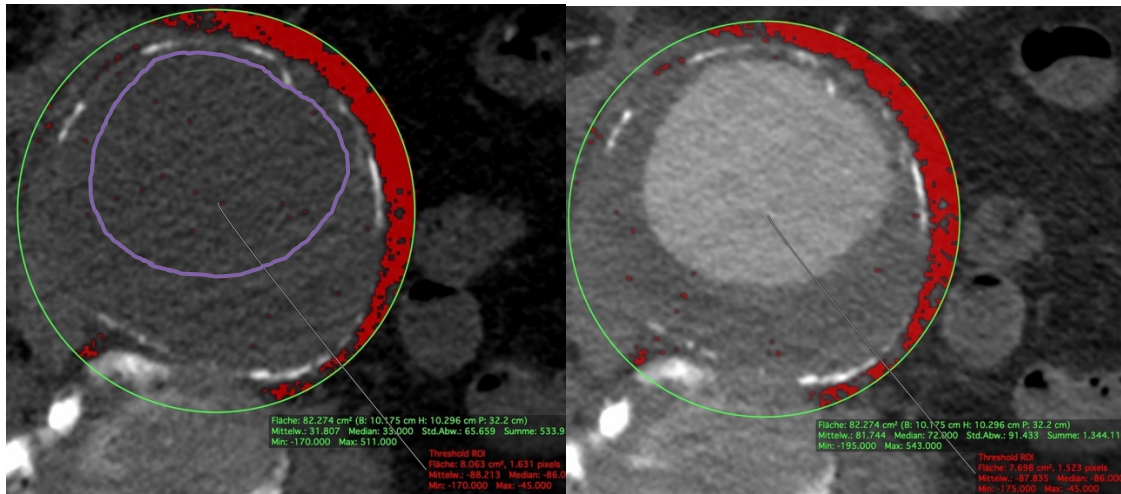


Figure 10. Frequency of intraluminal pixels with values -45 to -195 HU. Intraluminal pixels with fat tissue HU values can be encountered in images with high noise, like in this case of a ruptured AAA. Even in this case most pixels with values -45 to -195 HU are found within the intraluminal thrombus in similar numbers in both unenhanced and enhanced images with very few pixels found solely in the unenhanced aortic lumen. Thus, taking additional measures to exclude the aortic lumen when measuring fat tissue-containing pixels within the unenhanced periaortic ROI is not warranted.

Step 6. Calculation of maximum aortic diameter. Calculation of the maximum aortic diameter has been carried out with different methodologies in the literature. Since this value is of secondary significance in this study and used only for classification purposes (normal, ectatic or aneurysmatic aorta), the maximum aortic diameter was defined as the length of the shorter axis of the largest aortic disc within the examined area.

Step 7. Determination of PaFT-„ratio“. Since the amount of PaFT depends on the amount of total periaortic volume and the latter depends on the size of the aortic volume and thus the aorta, different PaFT amounts are to be expected around different size aortas. To rectify this situation the PaFT Volume has to be adjusted for the size of the periaortic volume. To achieve this, the resulting total PaFT Volume of the aortic segment was divided by the volume of the 5 mm-wide periaortic ring volume (**PaRVol**) to calculate a PaFT- „ratio“ [**PaFTVol**]. The value of PaFT „ratio“ was then applied to compare PaFT in aneurysmatic and non aneurysmatic aortas in the secondary study.

Step 8. Measurement of intraluminal contrast mean HU value and SD. The impact of intraluminal contrast medium was examined by setting an intraluminal sample ROI in enhanced scans and measuring the mean contrast HU value and its standard deviation. To examine the impact of lateral contrast dispersion, three different sample ROI-sizes were applied (8, 10 and 12 mm). To account for longitudinal contrast dispersion, an average contrast mean HU value was calculated from three measurements (infrarenal, mid-aortic and bifurcation level) and a longitudinal contrast variability was defined as: (maximum contrast HU) – (minimum contrast HU)/ (average contrast mean HU value) and examined in multi-regression analysis. To examine the effect of aortic wall calcification, a modified Agatston score was measured (using the Calcium Score Plugin in the unenhanced series with a

calcium detection threshold at 130 HU). A preliminary analysis showed that lateral contrast dispersion would not be an issue, whereas longitudinal variability in larger AAAs ($>100 \text{ cm}^3$) could be significant. As a result, a subgroup analysis excluding larger AAAs ($> 55 \text{ mm}$) was also performed.

Step 9. Data collection. For every patient the following values were measured and documented:

Native (unenhanced) series.

- Aortic Volume (**AVol**) of the examined infrarenal segment. Measured from the reconstruction of the aortic ROIs.
- Periaortic Volume (**PaVol**) of the examined aortic segment extended to 5 mm around the aortic wall. Measured after reconstruction of the periaortic ROIs.
- Periaortic fat tissue Volume (**PaFTVol**) around the examined infrarenal aortic segment within 5 mm from the aortic wall. Measured by Volume reconstruction of the axial PaFT ROIs as determined by the Global Thresholding Plugin.
- Periaortic fat tissue Mean HU attenuation value (**PaFTmeanHU**) and its standard deviation (**SD**). Measured by the Global Thresholding Plugin within the ROI with values of -45 to -195 HU.

Arterial (enhanced) series.

- Periaortic Volume (**PaVol**) of the examined aortic segment extended to 5 mm around the aortic wall. Measured after reconstruction of the periaortic ROIs.
- Periaortic fat tissue Volume (**PaFTVol**) around the examined infrarenal aortic segment within 5 mm from the aortic wall. Measured from reconstruction of the PaFT ROIs as determined by the Global Thresholding Plugin.
- Periaortic fat tissue Mean HU attenuation value (**PaFTmeanHU**) and its standard deviation (**SD**). Measured by the Global Thresholding Plugin within the ROI with values of -45 to -195 HU.

Additional parameters calculated.

- Difference of Periaortic fat tissue Volume between the native and arterial images in absolute and percentage values.
- Periaortic Ring Volume (**PaRVol**) as the volume of a 5 mm wide ring surrounding the examined aortic segment. Calculated as the difference between the Periaortic Volume (**PaVol**) and Aortic volume (**AVol**): **PaRVol = PaVol - AVol**
- Periaortic fat tissue “ratio” or “density” defined as the Periaortic fat tissue Volume adjusted for aortic size [**PaFTVol**]. Defined as the Periaortic fat tissue Volume divided by the Periaortic Ring Volume: **[PaFTVol] = PaFTVol / PaRvol**

Throughout this text, PaFT Volume and PaFT Mean HU, written with capital letters will refer to the specific quantities of the present study as defined above, whereas PaFT volume and mean HU, written with small letters, will refer to their general definitions.

All aforementioned measurements were performed by the author for a total of 296 PaFT measurements (148 in native and 148 in enhanced CT-scans, from those n=101 from the derivation and n=47 from the validation cohort for each CT phase). All axial images with periaortic ROIs and PaFT-ROIs of both unenhanced and arterial phases were saved as DICOM files. The Volume Reconstruction Images containing the AoVol, PaVol in both phases as well as the PaFT Volumes for both phases were saved as JPG. files. All measured values were entered in a Microsoft Excel spreadsheet for every individual patient. After the completion of data collection, all data was transferred to a single Microsoft Excel spreadsheet for statistical processing.

Using the postprocessing software. Reconstructed axial images of the unenhanced and arterial phase were transferred as DICOM files and imported into the OsirixMD software platform running on an Apple, MacBook Pro 15'' (2017) with an octacore Intel Processor and 64 MB RAM connected to an LG Ultrafine 5K 27'' Monitor and viewed with a magnification of 1500-2600 %. PaFT voxel selection was performed using the GlobalThresholding Plugin (**Figures 11, 12, 13**).

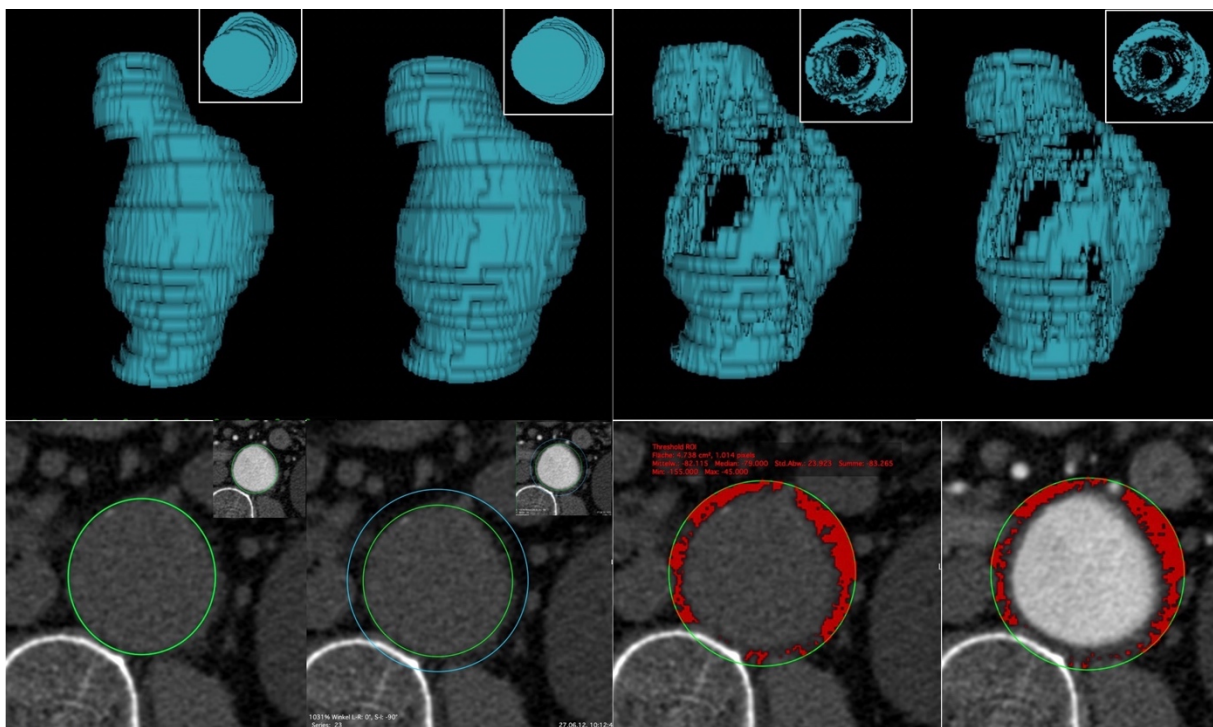


Figure 11. Summary of Volume measurements. The top images show the reconstructed Volumes measured (from left to right: aortic Volume, Periaortic Volume, native PaFT Volume, arterial PaFT Volume.) The bottom images show the respective ROIs used for the reconstructed Volumes (from left to right: native aortic Volume, native and aortic periaortic Volumes, native PaFT Volume, arterial PaFT Volume). Note that the top views of the 3D reconstructed PaFT volumes show the inside of the cylinder containing different aortic contours and not fat-containing voxels within the aortic disc.

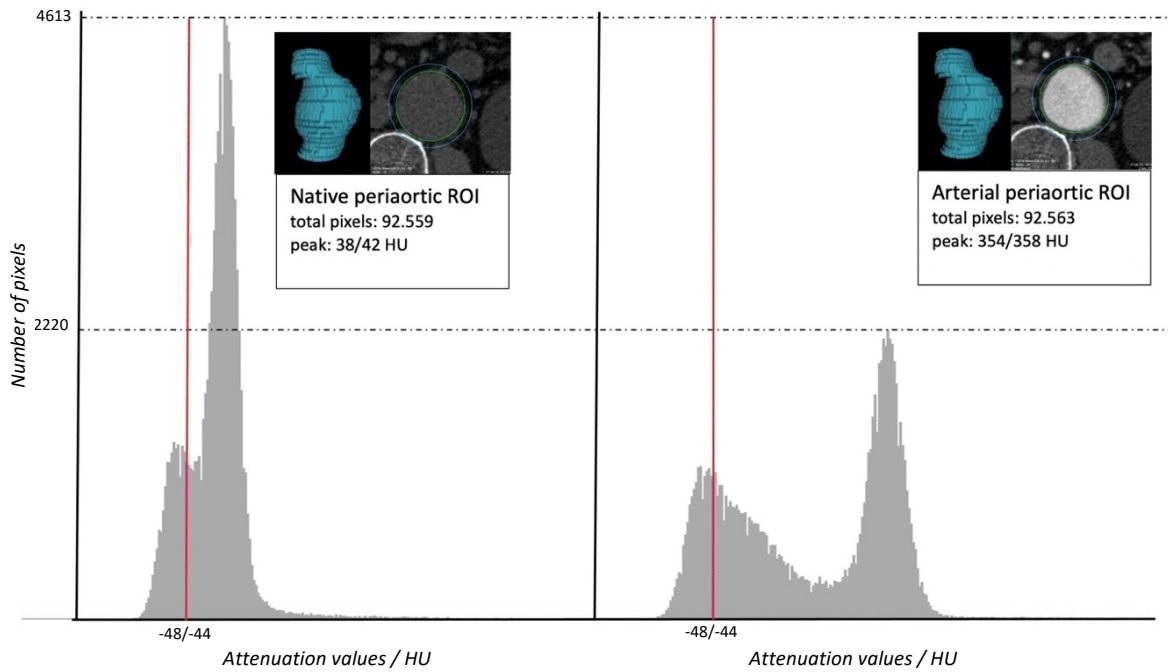


Figure 12. Distribution of pixel HU values within the periaortic ROI in the native and arterial scans (red line represents the threshold for the fat containing pixels with values -45 to -195 HU). In the native phase pixel HU values peak in the 38-42 HU value range. In the arterial phase pixel values within the identical periaortic ROI peak in the 354- 358 HU range. The distribution of pixels with values < -45 HU shows few changes. (numbers given as --/-- represent groups of values in the histogram presenting the distribution of pixel HU values)

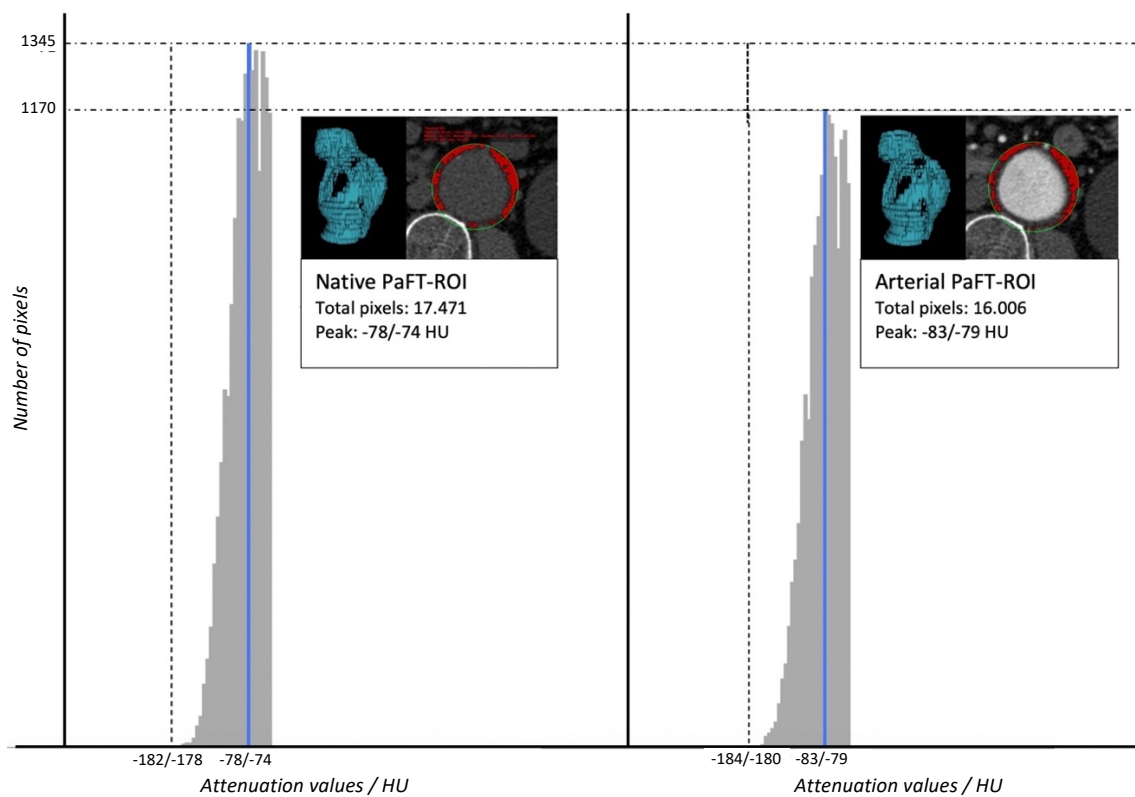


Figure 13. Distribution of pixel HU values within the PaFT-ROI in the native and arterial scans (the blue line indicates the range of HU values containing the peak HU value). The distribution of HU value frequencies changes slightly between the native and arterial phase. The total number of fat tissue containing pixels are slightly reduced (from 17471 in the native to 16006 in the arterial phase) and so does the total Volume of ROIs with pixels with values -45 to -195 HU. The Mean HU value of the PaFT -ROIs remains nearly constant. The objective of the present study is to further examine these relationships in a statistically significant sample.

3.3 Statistical analysis

3.3.1 Normality of distribution

Continuous variables were assessed using the Kolmogorov-Smirnov and Shapiro-Wilks tests, histograms, and normal quantile-quantile plots (QQ plots) to test for normality. Continuous variables were expressed as mean (\pm standard deviation, SD) [range], if normally distributed and as medians (intraquartile range) [range] if not normally distributed (although means were also mentioned here). Continuous variables were compared with a Student's t-test if normally distributed, a Wilcoxon test if non-normally distributed and paired and a Mann-Whitney test if not paired. A P value of $< .05$ was considered statistically significant. Statistical analysis was carried out using commercially available software (MedCalc® Statistical Software version 20.011, MedCalc Software Ltd, Ostend, Belgium, <https://www.medcalc.org>; 2021), which has been used in similar studies.⁵⁸

3.3.2 PaFT quantification

Derivation study. Firstly, the correlation between total PaFT Volume scores in the unenhanced and arterial phase was determined. Subsequently, a single linear regression in the patients of the derivation cohort allowed the determination of a conversion factor. In this context, comparing either total PaFT Volumes or aortic size-adjusted PaFT- „ratios“ [PaFTVol] yields the same result, since the latter are equal to the former divided by the PaRVol, which is identical in both unenhanced and arterial phases. Correlation between PaFT volumes and mean HU values in unenhanced and arterial phases was measured with a correlation coefficient. To determine the influence of various parameters, a multivariate linear regression model was carried out. CT voltage (as dummy variables, 1=100 kV, 2=120 kV, 3=130 kV), slice thickness (as dummy variables, 1=3 mm, 2=5mm), intraluminal sample-ROI size (as dummy variables, 1=8 mm, 2=10mm, 3=12 mm), mean intraluminal contrast medium intensity, aortic calcification, maximum aortic diameter, longitudinal dispersion of intraluminal intensity and image noise (defined as the intraluminal SD in the enhanced phase) were examined as potential confounding factors. Variables were introduced in the model if statistically relevant ($p < .05$). From the multivariate regression model a conversion factor for PaFT volume and mean HU value measurement in enhanced CTs was determined. This conversion factor was then applied in the validation study to adjust PaFT Volume scores and mean HU values from enhanced CTs and compare them to native CTs. The residuals of the linear regression were also examined for bias.

Validation study. The agreement between corrected enhanced PaFT Volumes/mean HU values and raw unenhanced PaFT Volumes/mean HU values was then examined with Bland-Altman scatter plots and Passing-Bablok regression in the validation cohort. The residuals of both tests were examined for bias.

Secondary study. By pooling the data from both studies, a sample size of 148 total infrarenal aortas was created. Aortas were stratified according to maximal diameter in one AAA group (> 30 mm) and one non-AAA group (<30 mm). Since the secondary study compared aortas of different sizes, the median size-adjusted PaFT Volume ([PaFTVolume]) or PaFT-“ratio” and the median PaFT-Mean HU in the unenhanced phase was determined for both groups. The same was calculated for the corrected median PaFT-“ratio” and corrected median PaFT-Mean HU measured in the arterial phase. Any differences between groups detected by the unenhanced PaFT ratios and PaFT-mean HU values were compared to differences detected by the corrected enhanced scores using the Mann-Whitney test. The latter was used because of the unpaired nature of the data (uneven groups, with the AAA-group being also small).

Reproducibility study. To test the reproducibility of the method, 20 data sets were reloaded in OsirixMD one year later and all ROIs were retraced again. Thereafter, Aortic Volumes, PaFT Volumes and PaFT Mean HU values were measured again. The Intraclass correlation coefficients (ICC) for the three values were then measured (two-way model with the same rater for all subjects, tested for absolute agreement). Data collection, post-processing and statistical analysis was performed by the author.

4. RESULTS

4.1 Normality of distribution

PaFT Volume. Applying the normality tests to the size-adjusted periaortic fat tissue Volume [PaFTVolume], the normality of sample (coefficient of skewness -0.1554 and coefficient of kurtosis -0.7912) was accepted by both Shapiro-Wilks ($W=0.9760$; $P= .0624$) and Kolmogorov-Smirnov ($D=0.0730$; $P> .10$) tests and demonstrated in a histogram (Figure 14) and QQ plot (Figure 15).

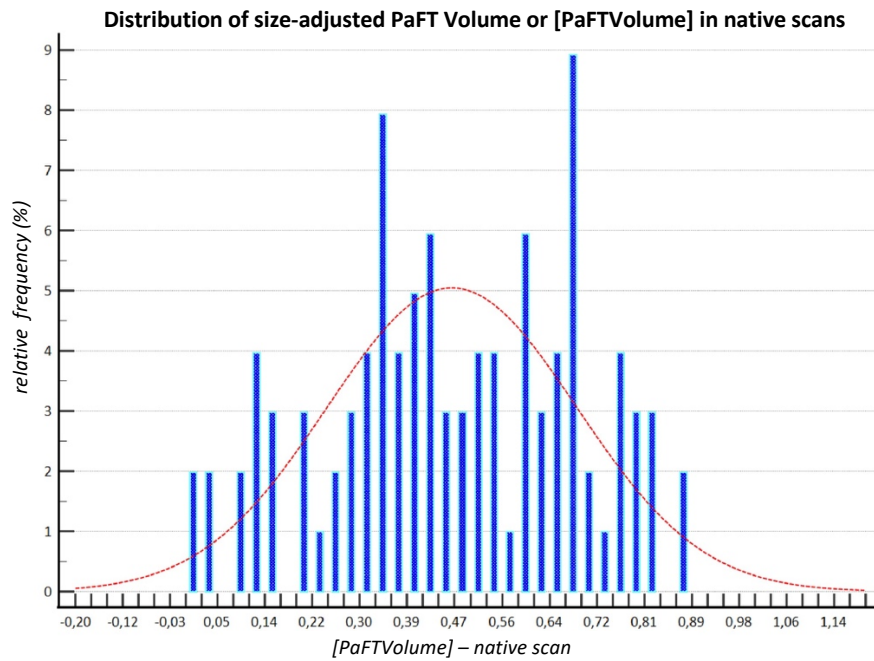


Figure 14. Histogram of the normal distribution of size-adjusted periaortic fat tissue Volume [PaFTVol] or PaFT “density” in native scans.

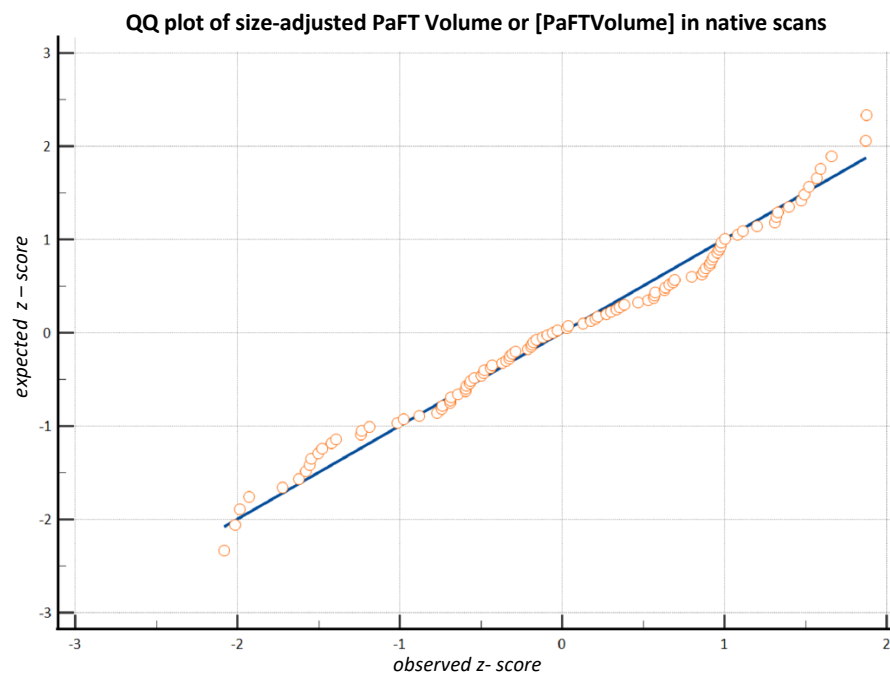


Figure 15. QQ plot of the normal distribution of size-adjusted periaortic fat tissue Volume [PaFTVol] or PaFT “density” in native scans.

PaFT Mean HU. Likewise, for the periaortic fat tissue Mean HU value, the normality of the sample (coefficient of skewness +0.3950 and coefficient of kurtosis +0.6990) was also confirmed by both Shapiro-Wilks ($W=0.9836$; $P= .2434$) and Kolmogorov-Smirnov ($D=0.0615$; $P> .10$) tests and demonstrated in a histogram (**Figure 16**) and a QQ plot (**Figure 17**).

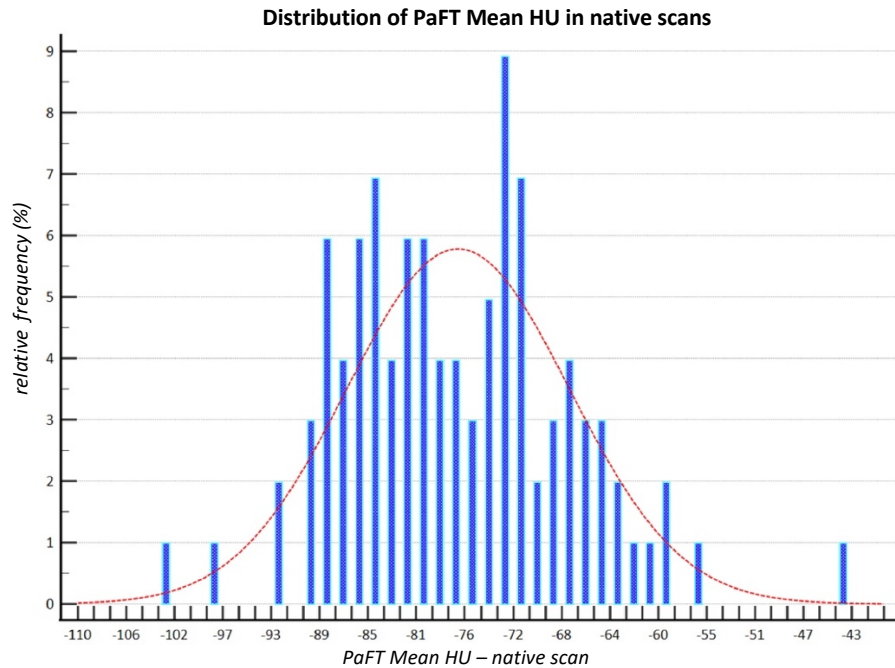


Figure 16. Histogram of the normal distribution of periaortic Mean HU values in native scans.

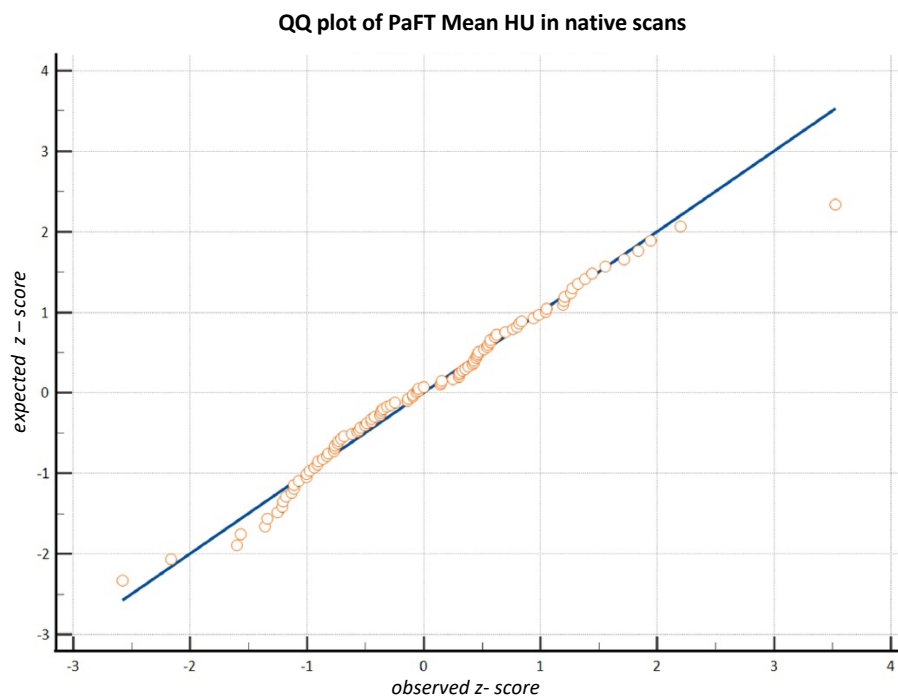


Figure 17. QQ plot of the normal distribution of periaortic Mean HU values in native scans.

4.2 Derivation Study

Initially, 114 data sets from the selection time period were found to be eligible for inclusion according to the inclusion criteria and their image sets (DICOM files) were transferred to the OsirixMD database. During post-processing, another 13 data sets were found to be incompatible with further processing for the following reasons: slice mismatch between native and arterial phase (n=1), incomplete imaging of the abdominal aorta (n=1), uneven slice thickness within a CT-phase detected by Osirix as precluding volume reconstruction (n=11). Finally, 101 paired data sets of one native and one arterial phase with identical slice thickness/increment and CT kilovoltage were included in the statistical analysis of periaortic fat tissue.

Demographic data and various parameters measured in the derivation study are depicted in **Table 2**.

Mean age / years		71.8 (\pm 10.6) [48-94]
Sex -male (%)		62 (61.4)
Mean intraluminal attenuation, arterial phase / HU		315.9 (\pm 82.3) [195-612]
Size of intraluminal sample-ROI / mm		8 mm, n=41 10 mm, n=39 12 mm, n=21
Slice thickness / mm		3 mm, n=96 5 mm, n=5
CT tube kilovoltage / kV		100 kV, n= 14 120 kV, n= 86 130 kV, n= 1
Mean aortic diameter / mm -total	n=101	26.9 (\pm 14.6) [15.6-110.5]
	-non-AAAs (<30 mm) n=83	22.3 (\pm 2.7) [15.6-29.4]
	-AAAs (>30 mm) n=14	54.2 (\pm 24.3) [31-110.5]
Median aortic volume / <i>mean</i> / cm ³		27.2 (14.5) [10.9 – 749.3] / 48.9

Table 2. Imaging and protocol parameters of the derivation study. (n=101)

The various parameters measured in the derivation study of PaFT are depicted in **Table 3**.

Median aortic volume / mean / cm ³	27.2 (14) [10.9 – 749] / 48.9
Median periaortic volume / mean / cm ³	62.1 (22.4) [29.9- 906.1] / 86.7
Median periaortic Ring volume / mean / cm ³	33.8 (9.2) [18.2 -156.8] / 37.8
Mean difference arterial PaFTVol-native PaFTVol/ cm ³	-1.96 (±1.65) [-10.3 to 0.4]
Mean difference arterial PaFTVol-native PaFTVol / %	-12.56 (±11) [-40.7 to 59.3]
Median longitudinal intraluminal attenuation variability / %	4.46 (4.1) [5.2 – 82.6] / 6.1
Median intraluminal SD, arterial phase / mean / HU	21.7 (5.1) [13.8 -38.7] / 22.2

Table 3. Parameters measured in the derivation study of PaFT.

The derivation study resulted in PaFT Volume and Mean HU values demonstrated in **Table 4**.

	Mean PaFT Volume/ cm ³	Mean [PaFTVolume]*	Mean of PaFT-mean HU
Native	17.6 (±13.68)[0.34-105.25]	0.467 (±0.221)[0.006-0.882]	-76.99 (±9.66) [-101.9 to -42.9]
Arterial	15.65 (±12.66)[0.33 -94.9]	0.414 (±0.211)[0.006- 0.829]	-76.77 (±10.18)[-104.08 to-29.76]

*[] is the PaFT Volume adjusted for periaortic Ring Volume: [PaFTVolume]= PaFTVolume / Periaortic Ring Volume

Table 4. Mean values (standard deviation) [range] of PaFT Volume and PaFT mean HU.

4.2.1 Correlation of periaortic fat tissue values between arterial and native scans

4.2.1.1 Periaortic fat tissue Volume

The correlation of arterial PaFT Volume to native PaFT Volume is shown in Table 5 and Figures 18, 19. The Pearson correlation coefficient was applied because of the normally distributed sample.

	PaFTVolume (with large AAAs)	PaFTVolume (without large AAAs)
Pearson	r= .9951 (p< .0001) [.9927 to .9967]	r= .9933 (p< .0001) [.9900 to .9956]

Table 5. Pearson correlation coefficient for PaFT Volume in arterial CT scans to native CT scans.

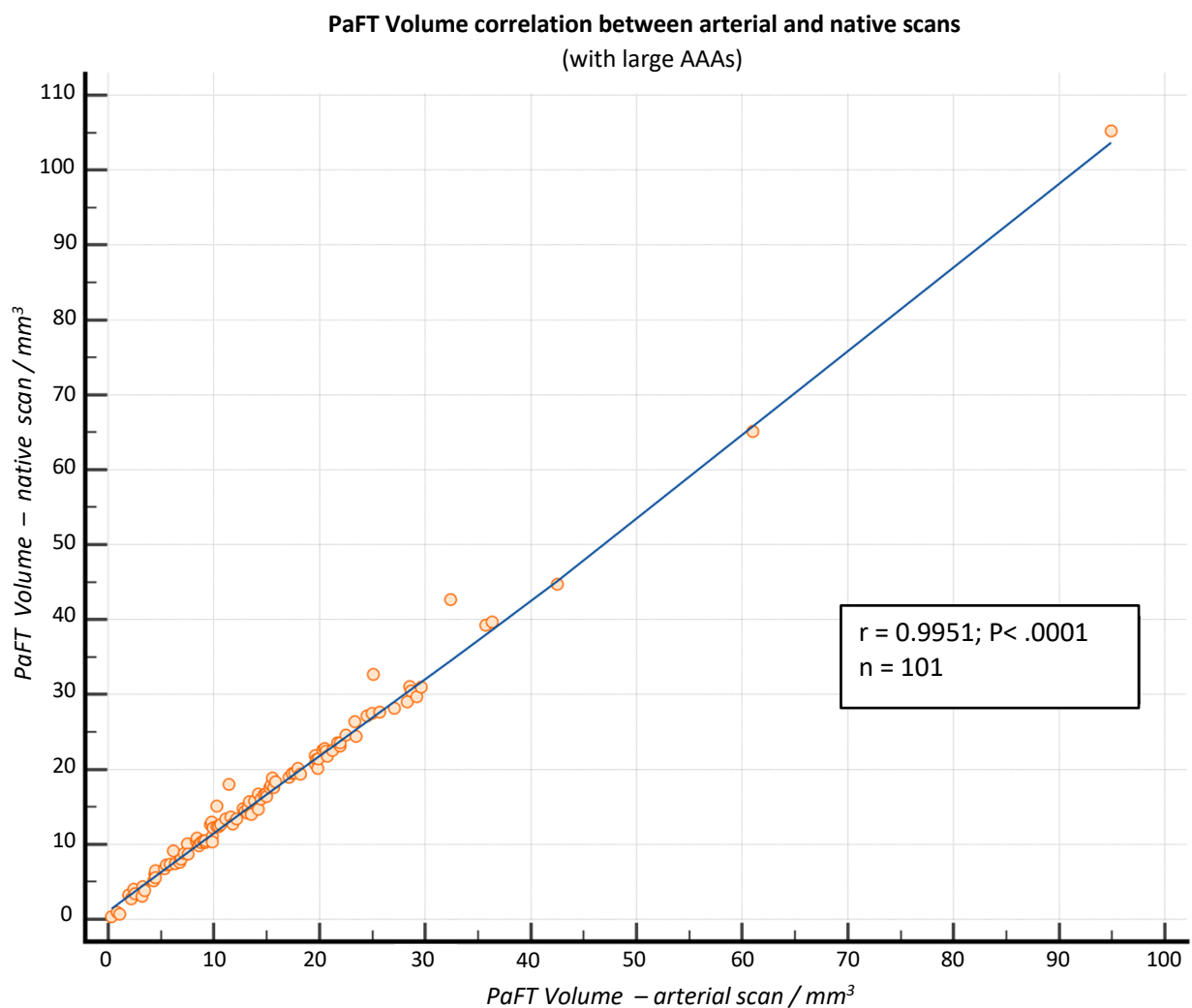


Figure 18. Correlation of PaFT Volumes including large (> 50 mm) AAAs.

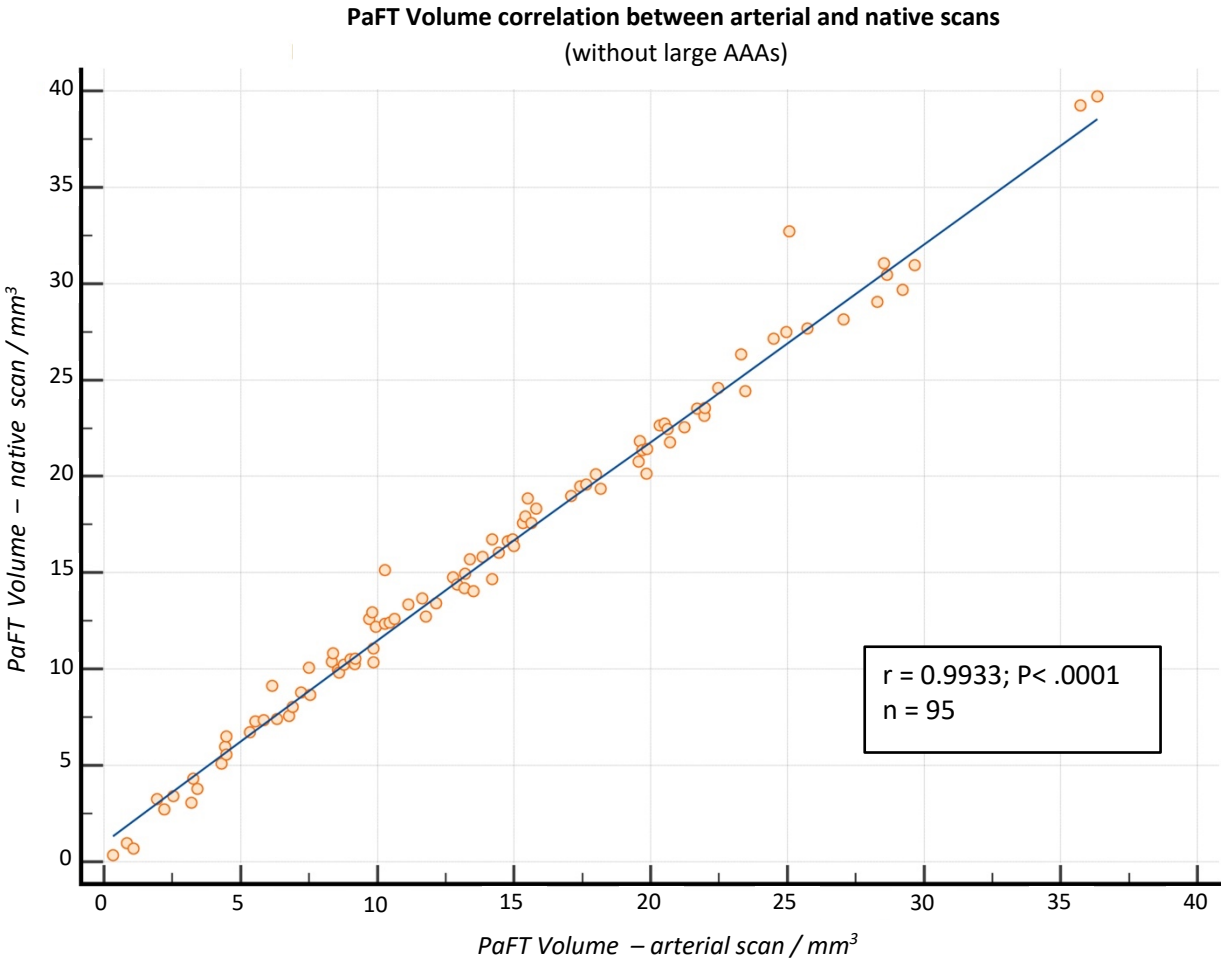


Figure 19. Correlation of PaFT Volumes excluding large (> 50 mm) AAAs.

4.2.1.2 Periaortic fat tissue Mean HU

The correlation of the arterial periaortic Mean HU value to the native PaFT Mean HU value is shown in Table 6 and in Figures 20, 21.

	PaFTMeanHU (with large AAAs)	PaFTMeanHU (without large AAAs)
Pearson	r= .9522 (p< .0001) (.9297 to .9675)	r= .9529 (p< .0001) (.9300 to .9685)

Table 6. Pearson correlation coefficient for PaFT Mean HU value in arterial CT scans to native CT scans.

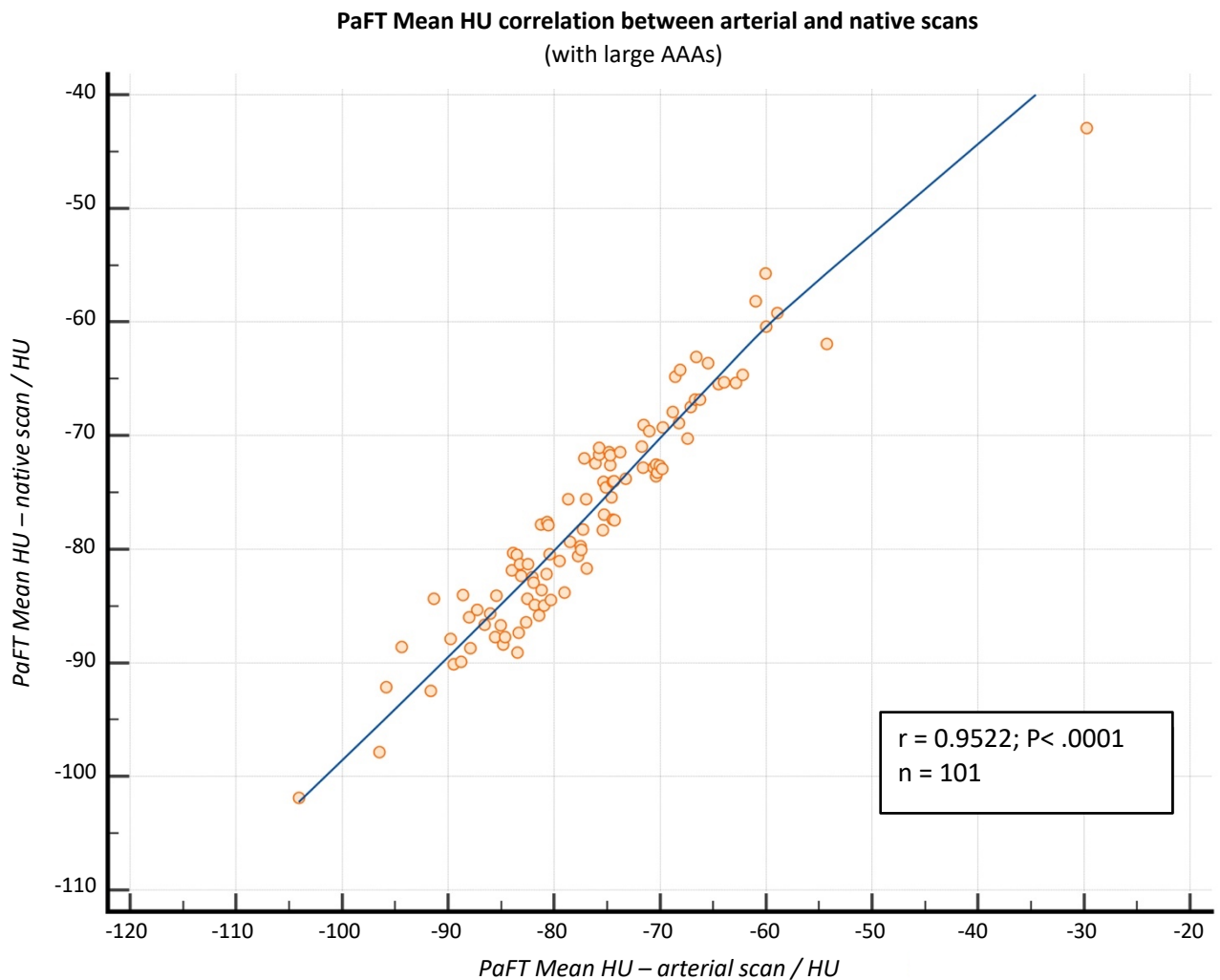


Figure 20. Correlation of PaFT mean HU values including large (>50 mm) AAAs.

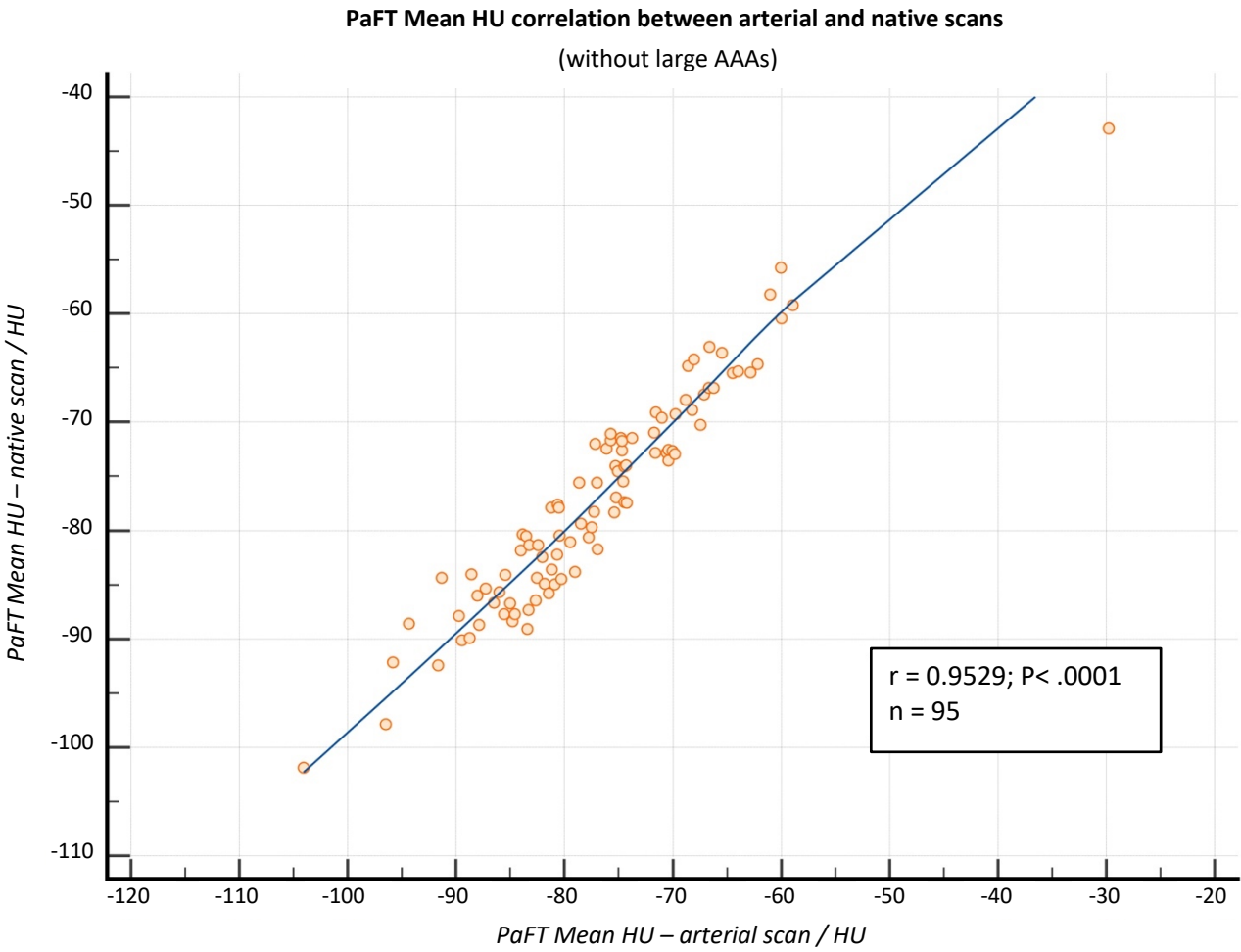


Figure 21. Correlation of PaFT mean HU values excluding large (>50 mm) AAAs.

4.2.2 Linear Regression of periaortic fat tissue values in arterial and native scans

4.2.2.1 Periaortic fat tissue Volume

The univariate linear regression analysis of arterial and native PaFT Volumes is shown in **Table 7** and in **Figures 22, 23**.

	PaFTVolume (with large AAAs)	PaFTVolume (without large AAAs)
Sample size	101	95
Equation	$y = 1.1057 x$	$y = 1.1029 x$
Coefficient	1.1057	1.1029
Stand.error	0.007136	0.007138
95% CI	1.0916 to 1.1199	1.0887 to 1.1171
T	154.9503	154.5169
P	< .0001	< .0001
F-ratio	24009.6103 P< .0001	23875.4738 P< .0001

Table 7. Univariate linear regression of PaFT Volume in arterial CT and native CT scans.

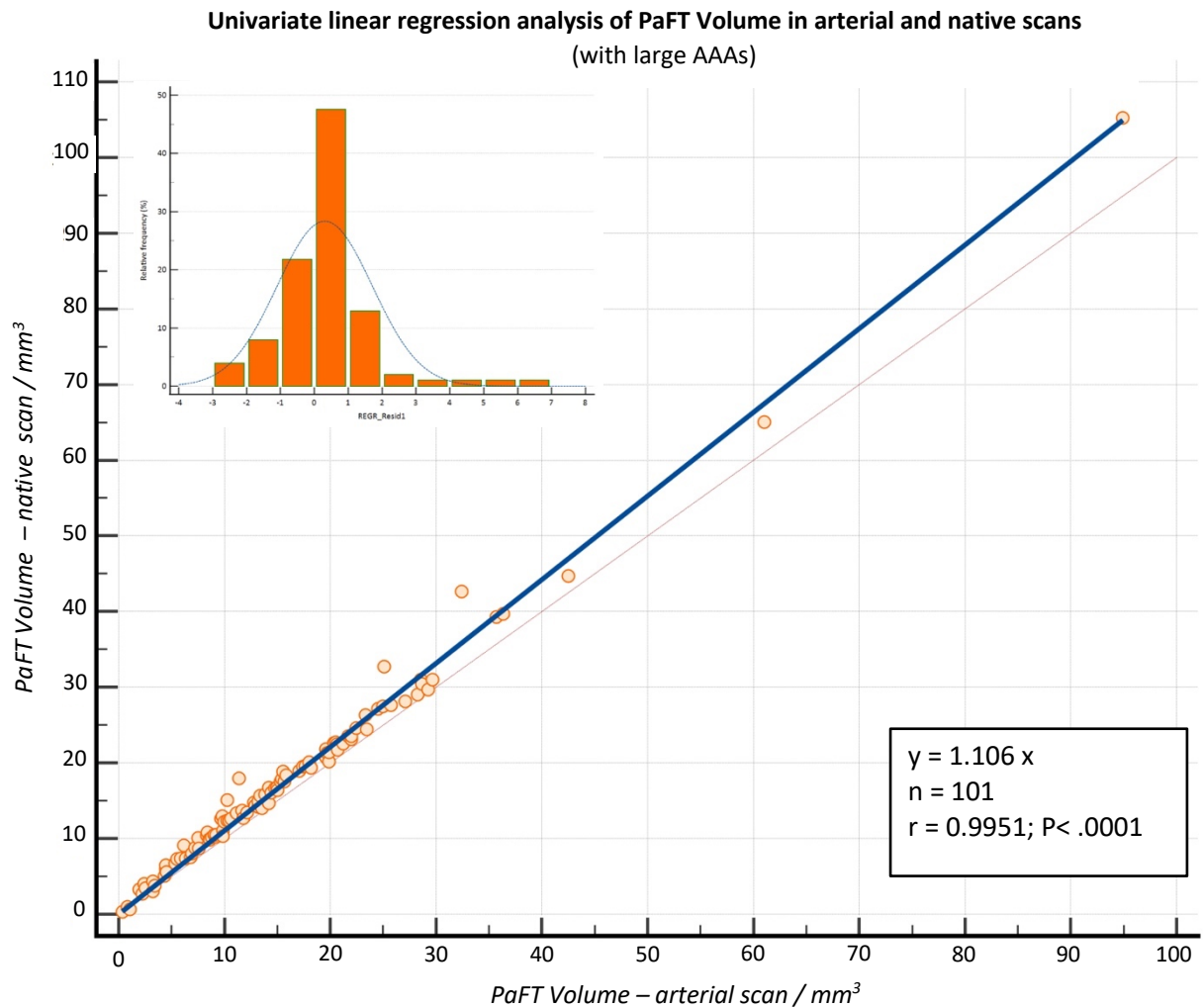


Figure 22. Univariate linear regression of PaFT Volumes including large AAAs. (Inset figure: Distribution of residuals resulting from the regression model: near normal distribution indicative of lack of bias).

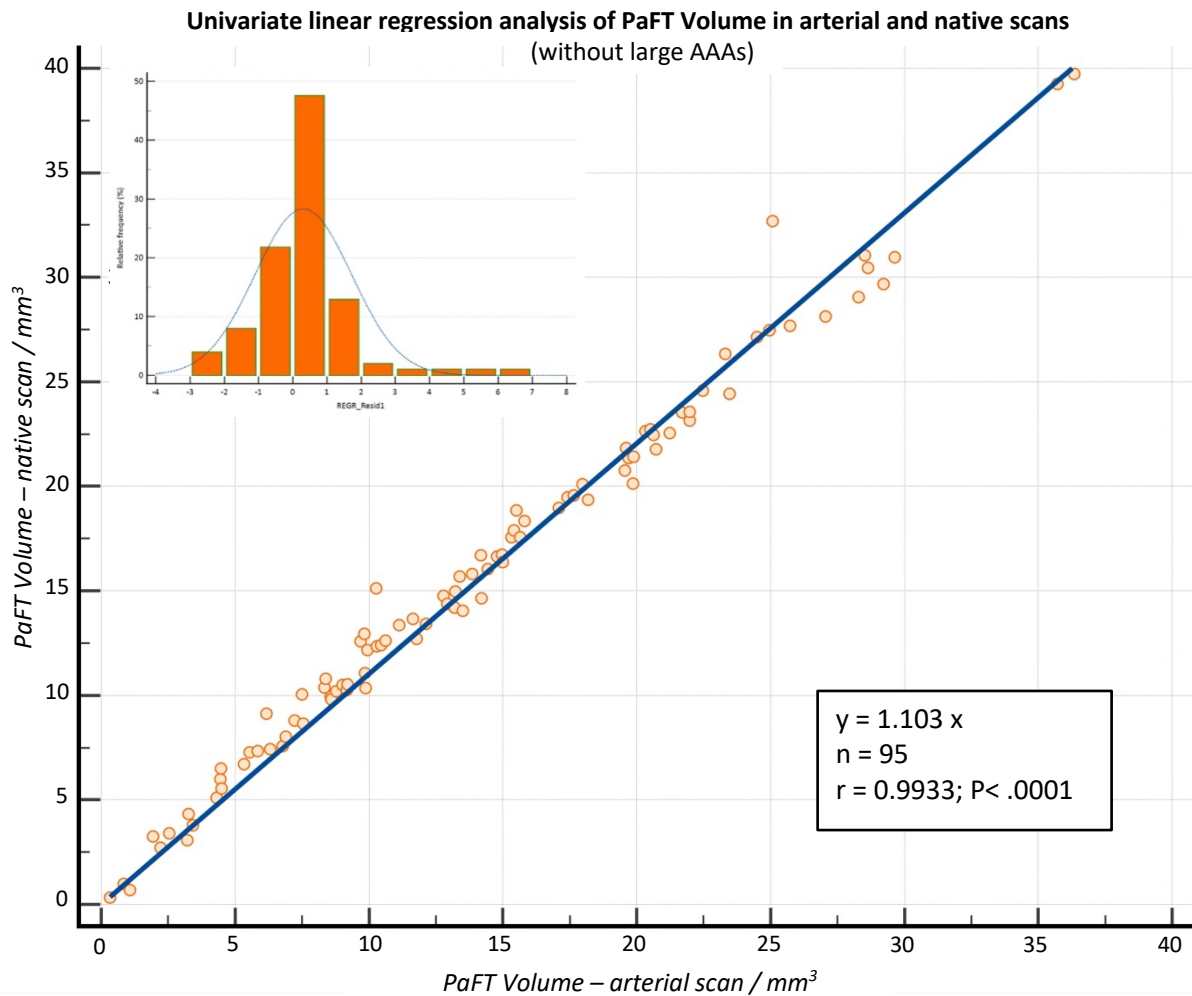


Figure 23. Univariate linear regression of PaFT Volumes excluding large AAAs. (Inset figure: Distribution of residuals resulting from the regression model: near normal distribution indicative of lack of bias).

The multivariate regression analysis of arterial and native PaFT Volumes is shown in **Table 8**.

	PaFTVolume (with large AAAs)	PaFTVolume (without large AAAs)
Sample size	101	95
r²	.9921	.9882
multiple r	.9961	.9941
Independent variables		
Arterial PaFT Volume	P< .0001	P< .0001
Agatston score	P= .0816	P= .1089
Mean contrast HU value	P= .1573	P= .5946
Aortic Diameter	P= .1431	P= .09122
Size of contrast sample-ROI	P= .7243	P= .6669
Slice thickness	P= .0882	P= .8372
Kilovoltage	P= .7509	P= .6270
Mean intraluminal SD, arterial phase	P= .7612	P= .4936
Longitudinal contrast variation	P= .1315	P= .100

Table 8. Multivariate linear regression of PaFT Volumes including (left) and excluding (right) large AAAs.

Of the nine independent variables included in the model, only the arterial PaFT Volume was significantly related to the native PaFTVolume. The resulting regression equation was:

corrected PaFTVolume = 1.1057 x arterial PaFTVolume.

4.2.2.2 Periaortic fat tissue Mean HU

The univariate linear regression analysis of arterial and native periaortic Mean HU values is shown in Table 9 and Figures 24, 25.

	PaFTMeanHU (with large AAAs)	PaFTMeanHU (without large AAAs)
Sample size	101	95
Equation	$y = 1.0011 x$	$y = 0.9996 x$
Coefficient	1.0011	0.9996
Stand.error	0.004008	0.004081
95% CI	0.9932 to 1.0091	0.9915 to 1.0077
T	249.7950	244.9658
P	< .0001	< .0001
F-ratio	62397.53436 P< .0001	60008.23198 P< .0001

Table 9. Univariate linear regression of PaFT Volume in arterial CT and native CT scans.

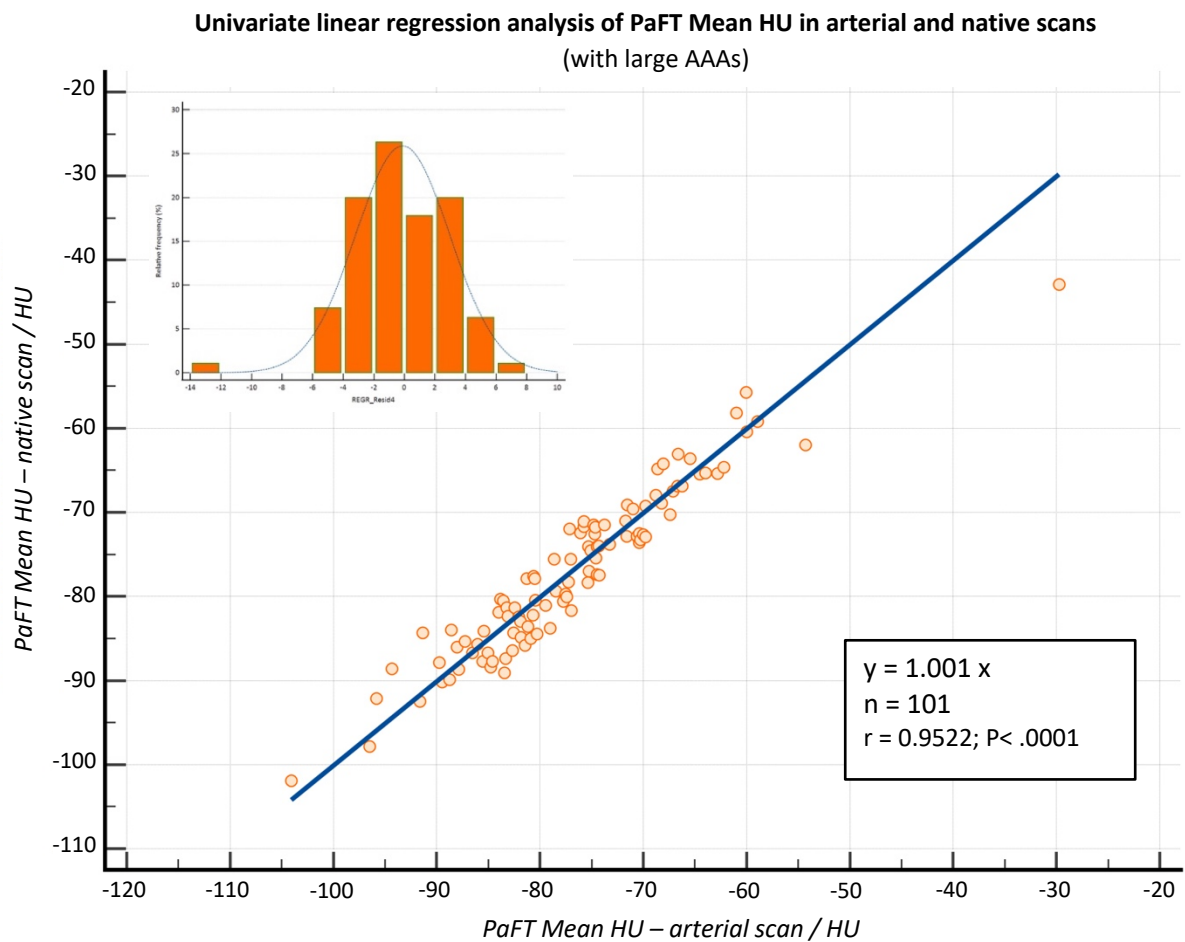


Figure 24. Univariate linear regression of PaFT Mean HU values including large AAAs. (Inset figure: Distribution of residuals resulting from the regression model: near normal distribution)

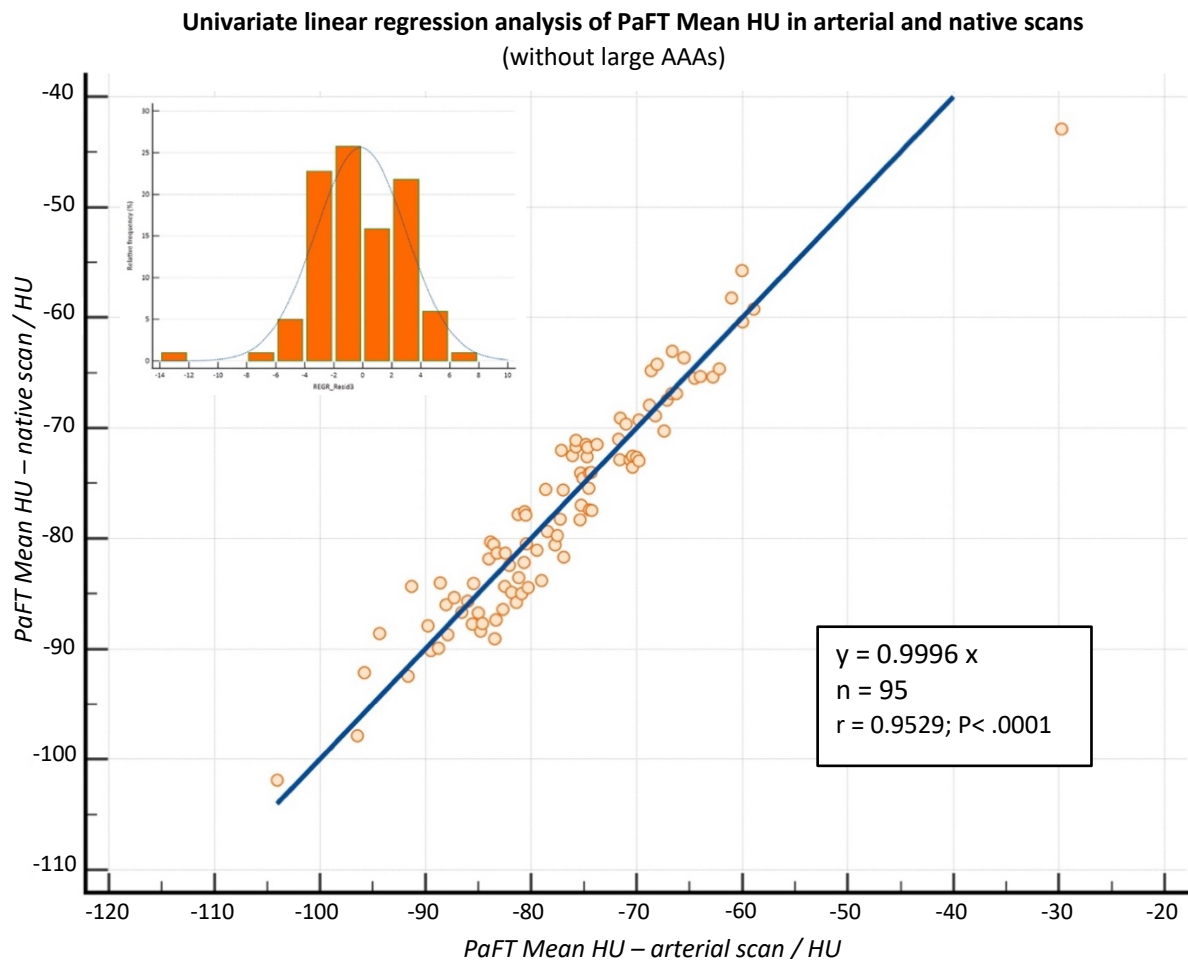


Figure 25. Univariate linear regression of PaFT mean HU values without large AAAs. (Inset images: distribution of residuals)

The multivariate regression analysis of arterial and native PaFT mean HU values is shown in **Table 10**

	PaFTMeanHU (with large AAAs)	PaFTMeanHU (without large AAAs)
Sample size	101	95
r^2	.9409	.9449
multiple r	.9700	.9721
Independent variables		
Arterial PaFT mean HU value	$P < .0001$	$P < .0001$
Agatston score	$P = .2020$	$P = .053$
Mean contrast HU value	$P = .2903$	$P = .1556$
Aortic Volume	$P = .7971$	$P = .0927$
Size of contrast sample-ROI	$P = .2670$	$P = .4380$
Slice thickness	$P = .4580$	$P = .0969$
Kilovoltage	$P = .0901$	$P = .1603$
Mean intraluminal SD, arterial phase	$P = .0716$	$P = .0613$
Periaortic Ring Volume	$P = .4246$	$P = .3552$
Longitudinal contrast variation	$P = .7602$	$P = .1249$

Table 10. Multivariate linear regression of PaFT mean HU values with (left) and without (right) large AAAs.

Of the nine independent variables included in the model, only the arterial PaFT MeanHU was significantly related to the native PaFT MeanHU. The resulting regression equation was:
corrected PaFT MeanHU = 1.0011 x arterial PaFT MeanHU.

4.3 Validation Study

Initially, 53 data sets from the selection time period were found to be eligible for inclusion according to the inclusion criteria and their data sets (DICOM files) were transferred to the OsiriXMD database. During post-processing, another 6 data sets were found to be incompatible with further processing for the following reasons: slice mismatch between native and arterial phase (n=1), incomplete imaging of the abdominal aorta in at least one phase (n=2), uneven slice thickness precluding volume reconstruction (n=3). Finally, 47 paired data sets of one native and one arterial phase with identical slice thickness/increment and CT kilovoltage were included in the statistical analysis of both calcium scoring and periaortic fat tissue (**Table 11**).

Table 11. Demographic data of the validation cohort (n=47).

Mean age / years	71.4 (± 10.65) [range, 48 -93]
Sex – male (%)	29 (61.7)

Table 11. Demographic data of the validation cohort (n=47).

The values of various protocol parameters are shown in **Table 12**.

Table 12. Imaging and protocol parameters of the validation cohort. (n=47)

Mean intraluminal attenuation, arterial phase / HU		312.67 (± 98.59) [127.48-605.49]
Size of intraluminal sample-ROI / mm		8 mm, n= 47
Slice thickness / mm		3 mm, n=41 5 mm, n=6
CT tube kilovoltage / kV		100 kV, n= 1 120 kV, n= 42 130 kV, n= 4
Mean aortic diameter / mm – total	n=47	25.8 (± 12.1) [18.4 – 90.7]
- non-AAAs (<30 mm)	n=39	21.84 (± 2.48) [18.4 – 28.8]
- AAAs (>30 mm)	n=8	45.4 (± 20.16) [30.4-90.7]
Median aortic volume / mean / cm ³		25.1 (15.1) [15.8-510.5] / 42.9

Table 12. Imaging and protocol parameters of the validation cohort (n=47).

Three outlier values were found in the PaFT cohort (**Figure 26**). All three had normal levels of noise in the native and in most of the arterial phase but had very high noise levels in some segments of the arterial phase (SD of 41, 83 and 124 HU). This resulted in abnormally low values of PaFT Volume, all close to zero (0.3379, 0.4732 and 0.2668 cm³) and abnormally high periaortic Mean HU values (-46 HU, -59 HU, -45 HU) in the respective segments of the arterial phase. These cases were thus excluded from further validation.

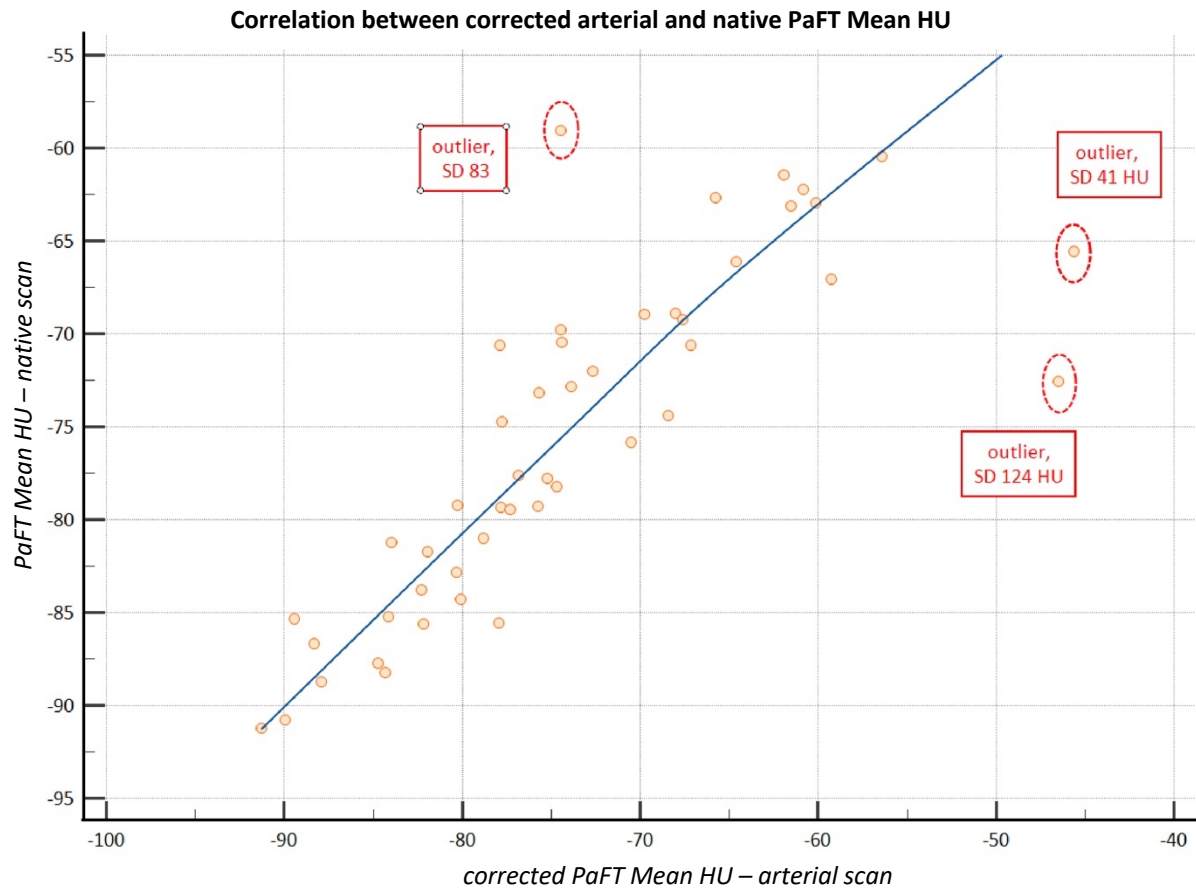


Figure 26. Outliers in the PaFT validation cohort.

The measured parameters of the validation study are shown in **Table 13** and PaFT values in **Table 14**.

Table 13. Parameters measured in the validation study of PaFT

Median aortic volume / mean / cm ³	25.1 (15.1) [15.8-510.5] / 42.9
Median periaortic volume / mean / cm ³	56.3 (24.2) [37.8-646.97] / 78.3
Median periaortic Ring volume / mean / cm ³	31.3 (9.8) [21.98-136.5] / 35.5
Median difference arterial PaFTVol-native PaFTVol/ cm ³	-1.49 (1.65) [-10.97 to 0.92] / -1.92
Median difference arterial PaFTVol-native PaFTVol / %	-13.4 (12.89) [-65.85 to 5.84] / -16.2
Median intraluminal SD, arterial phase / mean / HU	22.16 (5.55) [9.5-124.4] / 24.9

Table 13. Imaging and protocol parameters of the validation cohort (n=47).

Table 14. Mean values and (standard deviation) [range] of PaFT Volume/ mean HU (validation cohort)

	Mean PaFT Volume/ cm ³	Mean [PaFTVolume]*	Mean of PaFT-mean HU
Native	15.2 (±11.7) [0.3 – 56.4]	0.413 (0.241) [0.02-0.906]	-75.64 (±9.0) [-91.0 to -59.1]
Arterial	13.3 (±10.4) [0.26 -45.4]	0.361 (±0.223) [0.01-0.854]	-73.98 (±10.56) [-91.0 to -45.6]

*[] is the PaFT Volume adjusted for periaortic Ring Volume: [PaFTVolume]= PaFTVolume / Periaortic Ring Volume

Table 14. Imaging and protocol parameters of the validation cohort (n=47).

4.3.1 Periaortic fat tissue Volume

Corrected arterial PaFT Volume compared to native PaFT Volume.

The Bland-Altman analysis resulted in a mean difference between native and corrected arterial values of 0.3589 with a 95% confidence level including the zero value [-0.01407 to 0.7320] indicative of no significant residual bias. The hypothesis of agreement (H_0 : Mean=0) was accepted ($P= .0589$) (**Figure 27**). This was further explored with a Passing-Bablok regression model that showed no proportional bias (slope $B= 0.9631$ with 95% CI including 1 [0.9233 to 1.0086]) and only minimal systematic bias (intercept $A= 0.8168$ with 95% CI just outside 0 [0.2169 to 1.2948]) (**Figure 28**). Mean values of PaFT Volume were 14.3998 cm^3 for the native and 14.0408 cm^3 for the corrected arterial cohort.

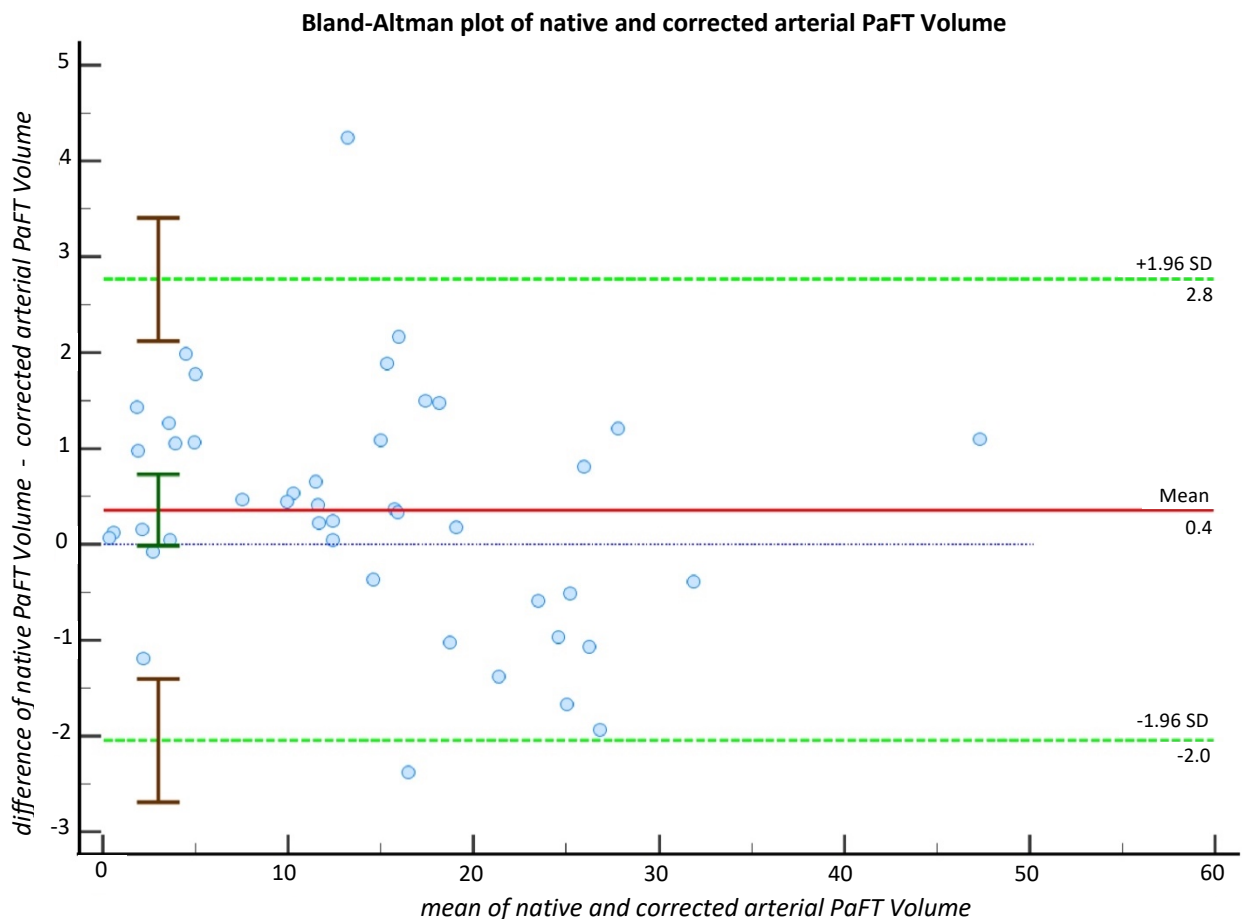


Figure 27. Comparison of corrected arterial PaFT Volume and native PaFT Volume with a Bland-Altman plot. The Bland-Altman plot (mean difference 0.3589 [-0.01407 to 0.7320], limits of agreement -2.0458 [-2.6882 to -1.4035] and 2.7637 [2.1213 to 3.4061]) after removal of three outliers shows a good dispersion of values with only one value outside the LoA. The blue line of zero difference is inside the green bar representing the 95% confidence interval (CI) of the mean difference.

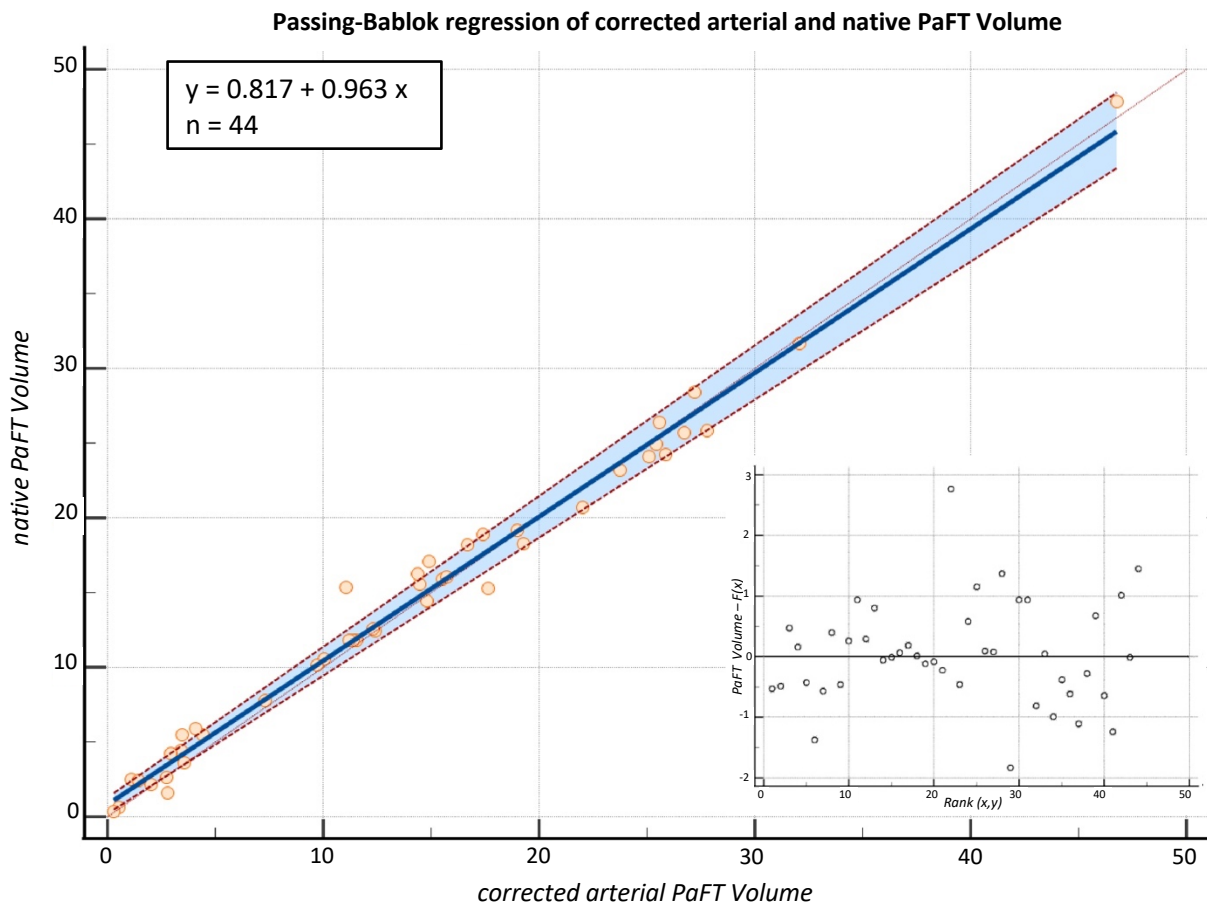


Figure 28. Comparison of corrected arterial PaFT Volume and native PaFT Volume with a Passing-Bablok regression. The Passing-Bablok plot (with residuals distribution in the inset) showed only minimal systematic bias. The Cusum test ($P = .59$) and Spearman coefficient ($r = .983$, $p < .0001$) showed no significant deviation from linearity.

4.3.2 Periaortic fat tissue Mean HU

Corrected arterial periaortic Mean HU compared to native PaFT Mean HU

Bland-Altman analysis resulted in a mean difference between native and corrected arterial values of -0.8347 with a confidence level including the zero value $[-1.7750$ to $0.1056]$ indicative of no significant residual bias. The hypothesis of agreement ($H_0: \text{Mean} = 0$) was accepted ($P = .0804$) (**Figure 29**). This was further explored with a Passing-Bablok regression model that showed no proportional bias (slope $B = 0.9962$ with CI including 1 [0.8899 to 1.1176]) and no systematic bias (intercept $A = -1.6142$ with CI including 0 [-9.4201 to 7.6662]) (**Figure 30**). Mean values for PaFT Mean HU were -76.5380 HU for the native and -75.7033 HU for the corrected arterial cohort.

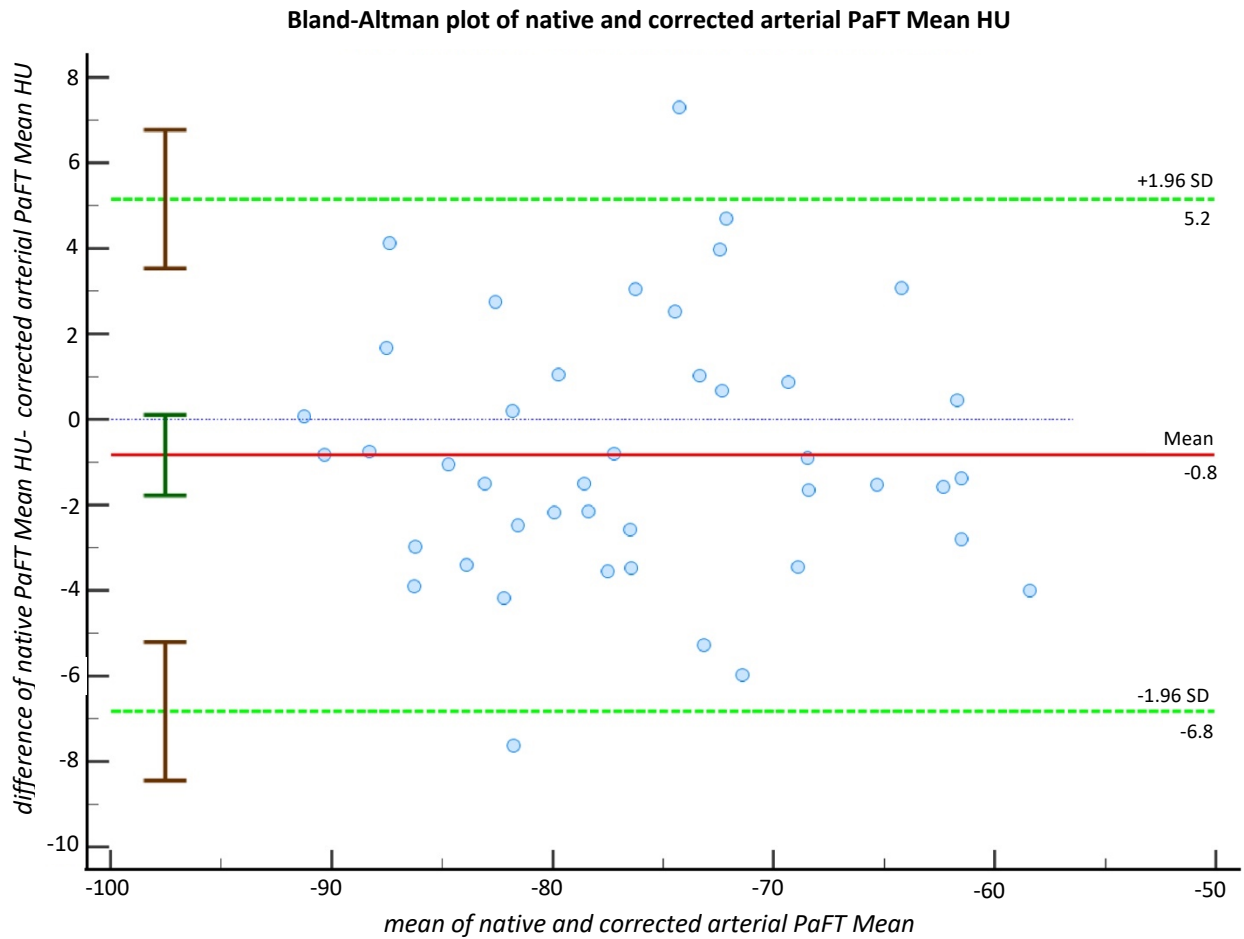


Figure 29. Comparison of corrected arterial PaFT mean HU value and native PaFT mean HU value with a Bland-Altman plot. The Bland-Altman plot (mean difference -0.8347 [-1.7750 to 0.1056], limits of agreement -6.8232 [-8.4428 to -5.2037] and 5.1538 [3.5343 to 6.7734]) after removal of three outliers shows a good dispersion of values with only one value outside the LoA. The blue line of zero difference is inside the green bar indicating the confidence interval (CI) of the mean difference.

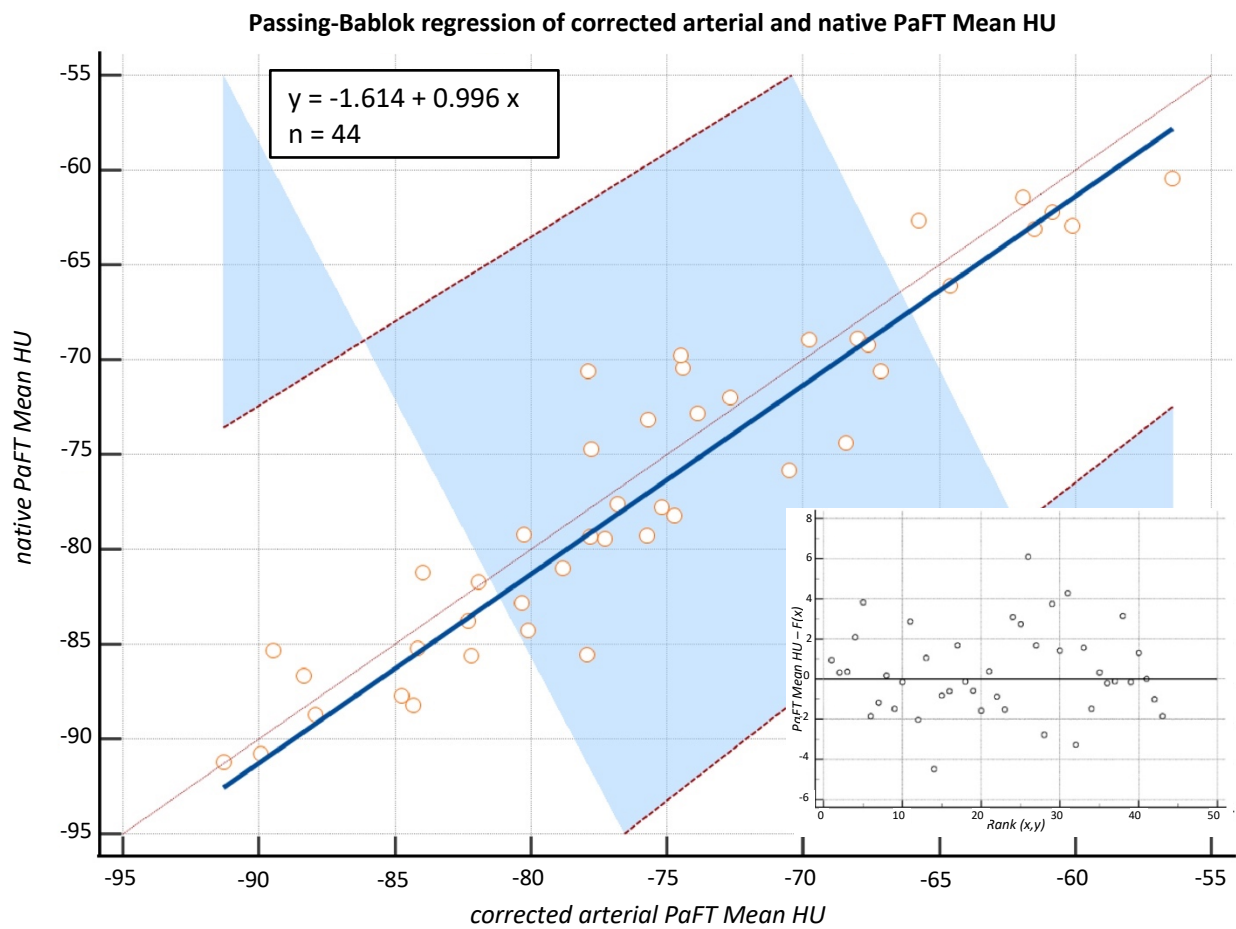


Figure 30. Comparison of corrected arterial PaFT mean HU value and native PaFT mean HU value with a Passing-Bablok regression. The Passing-Bablok plot (with residuals distribution in the inset) showed no significant proportional or systemic bias. The Cusum test ($P = .56$) and Spearman coefficient ($r = .943$, $p < .0001$) showed no significant deviation from linearity.

4.4 Secondary study

When comparing PaFT-,ratios“ [PaFTVol] and mean PaFT HU values in the pooled non-AAA and AAA groups in both native and arterial phases, the Mann-Whitney test showed on average higher PaFT “ratios” and lower Mean HU values in the AAA group. This difference, however, did not reach statistical significance, considering that this study was not meant to answer this question. The *median of native [PaFT Volumes]*, in the non-AAA and AAA group was 0.4618 (95% CI [0.4051 – 0.5426]) and 0.5125 (95% CI [0.3918 – 0.5767]) respectively, corresponding to a Hodges-Lehmann median difference of -0.001476 (95% CI [-0.1155 to 0.1020]), which was not significant ($n_{\text{nonAAA}}=122$, $n_{\text{AAA}}=19$, $U = 1\ 154$, $P = .9759$). The *median of corrected arterial [PaFT Volumes]* in the non-AAA and AAA group was 0.4491 (95% CI [0.394 – 0.52]) and 0.5149 (95% CI [0.3432 – 0.5795]) respectively, corresponding to a Hodges-Lehmann median difference of -0.0101 (95% CI [-0.1279 to 0.1050]), which was not significant ($n_{\text{nonAAA}}=122$, $n_{\text{AAA}}=19$, $U = 1\ 124$, $P = .8326$).

The median of native PaFT mean HU values in the non-AAA and AAA group was -77.74 (95% CI [-79.91 to -74.08]) and -80.04 (95% CI [-83.01 to -73.68]) respectively, corresponding to a Hodges-Lehmann median difference of -0.334 (95% CI [-4.53 to 4.06]), which was not significant ($n_{\text{nonAAA}}=122$, $n_{\text{AAA}}=19$, $U= 1\ 137$, $P= .8943$). The median of corrected arterial mean PaFT HU values in the non-AAA and AAA group was -77.07 (95% CI [-79.69 to -75.21]) and -77.84 (95% CI [-80.46 to -72.08]) respectively, corresponding to a Hodges-Lehmann median difference of 1.617 (95% CI [-2.7 to 5.56]), which was not significant ($n_{\text{nonAAA}}=122$, $n_{\text{AAA}}=19$, $U= 1034$, $P= .4504$) (**Figure 31**).

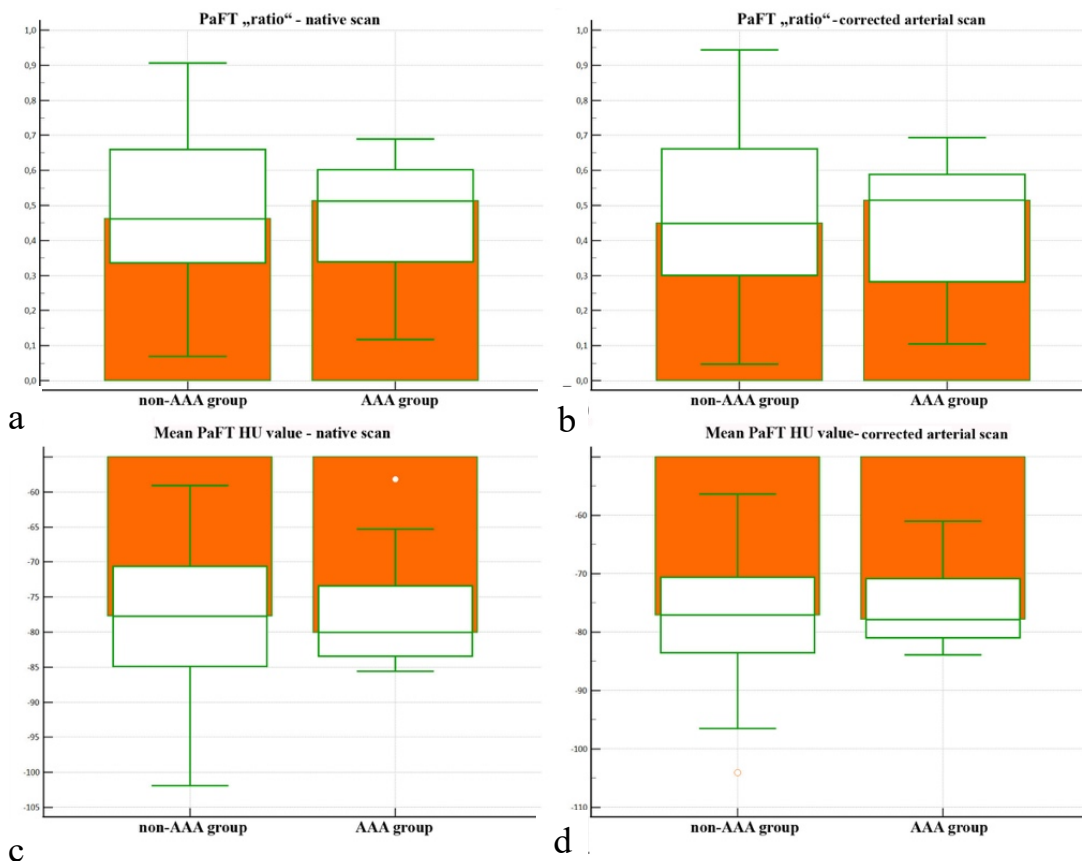


Figure 31. Secondary study results. Box-Whisker plots for PaFT “densities” (or “ratios”) [PaFT volumes] in the non-AAA vs. AAA groups measured in native (**a**) and corrected arterial (**b**) scans, as well as for mean PaFT HU values in the native (**c**) and corrected arterial (**d**) scans. Corrected arterial values were almost identical to the values from native CTs. No significant difference was found between the non-AAA and AAA groups. The indication in the non-AAA group were: pancreas diagnosis in 17/122, kidney or urinary tract diagnosis in 22/122, hematoma detection in 25/122, abdominal ache in 37/122, abdominal/colorectal/gynecological complications 21/122.

4.5 Reproducibility study

For the Aortic Volumes, the Intraclass correlation coefficient (ICC) was .9963 (95% CI [.9907 – 0.9985]) (**Figures 32, 33**). This was expected, since the tracing of the Aortic/Periaortic ROIs with zoom factors > 2000% allows a precision of < 0.5 cm, which is below the voxel size. For the PaFT Volumes, the ICC was .9911 (95% CI [.9780 – .9964]) (**Figures 34, 35**) and for the PaFT mean HU values the ICC was .998 (95% CI [.995 – .9992]) (**Figures 36, 37**).

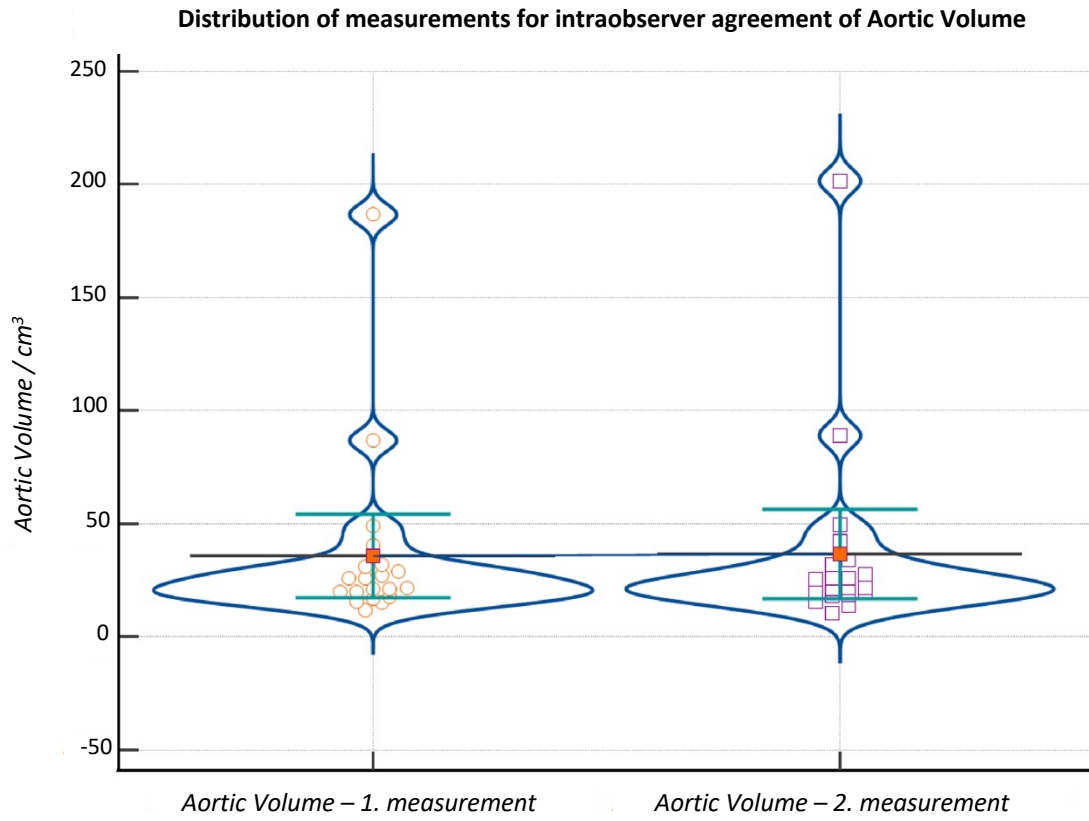


Figure 32. Distribution of measurements of Aortic Volume in the reproducibility study (n=20).

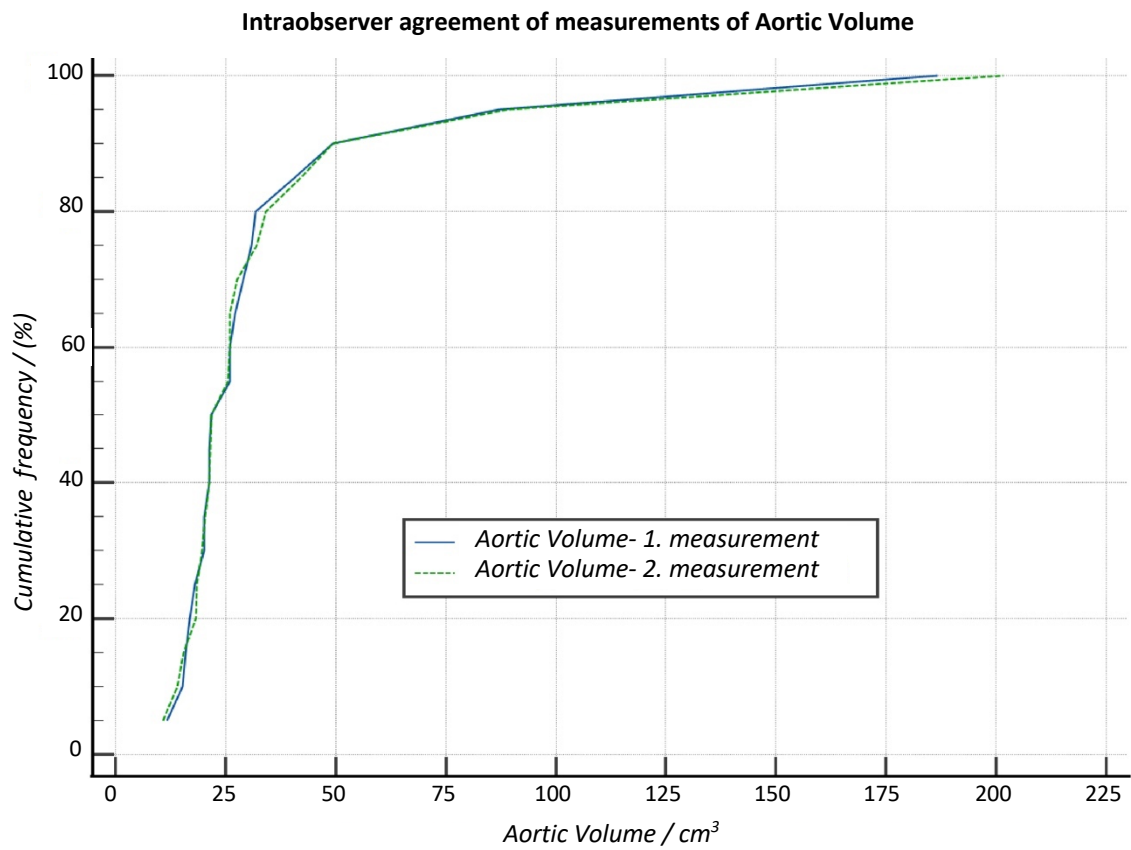


Figure 33. Intraobserver agreement of measurements of Aortic Volume in the reproducibility study(n=20)

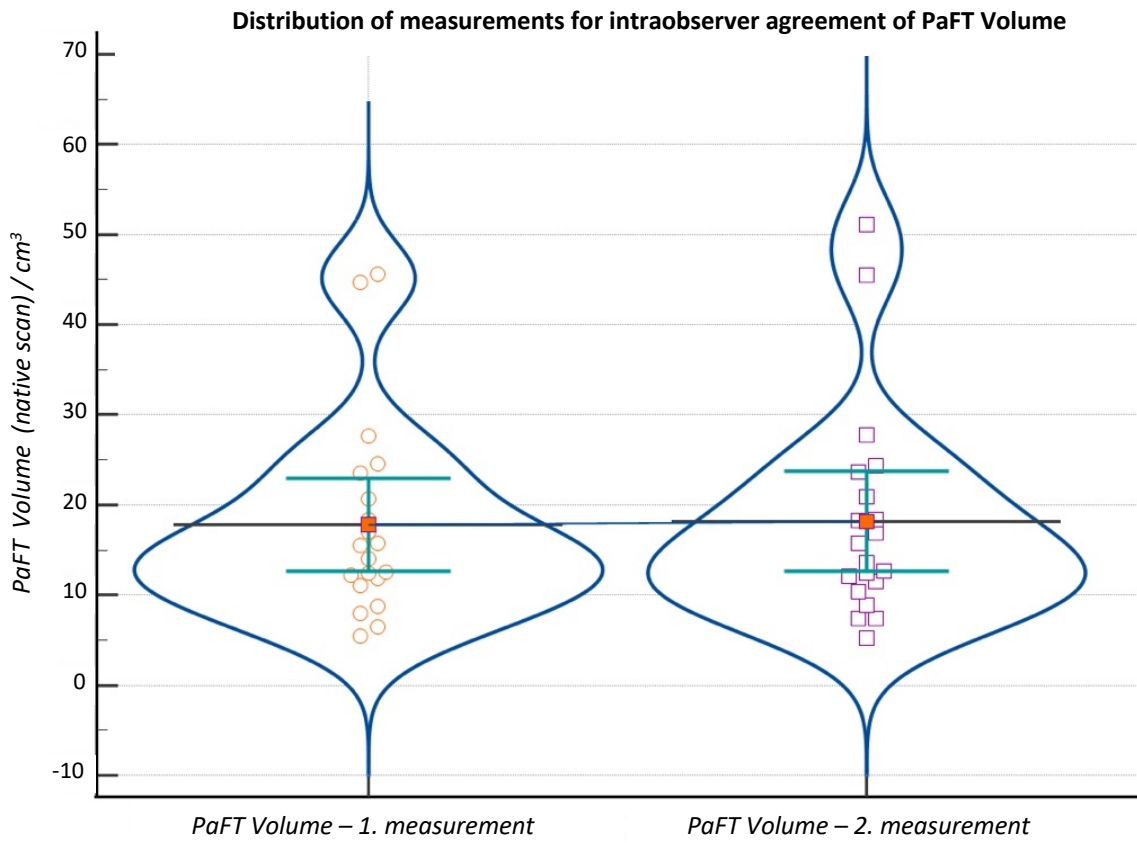


Figure 34. Distribution of measurements of PaFT Volume in the reproducibility study (n=20).

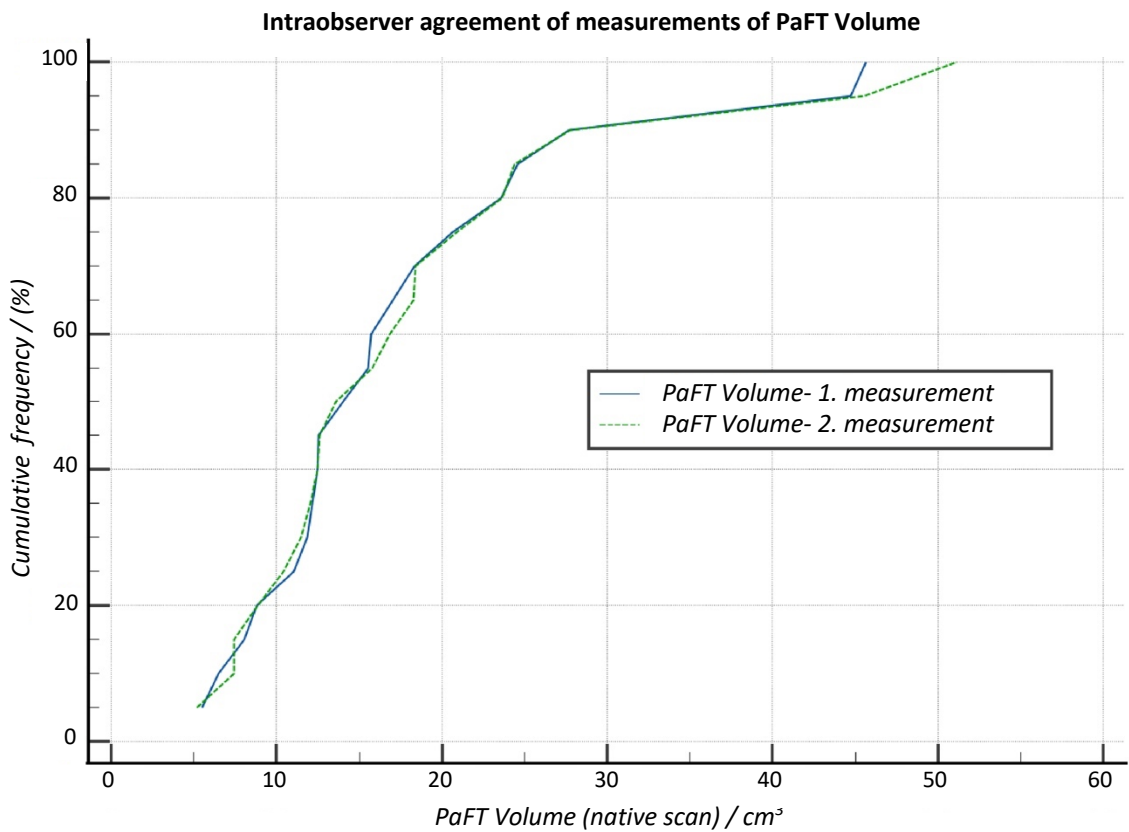


Figure 35. Intraobserver agreement of measurements of PaFT Volume (native scans) in the reproducibility study (n=20).

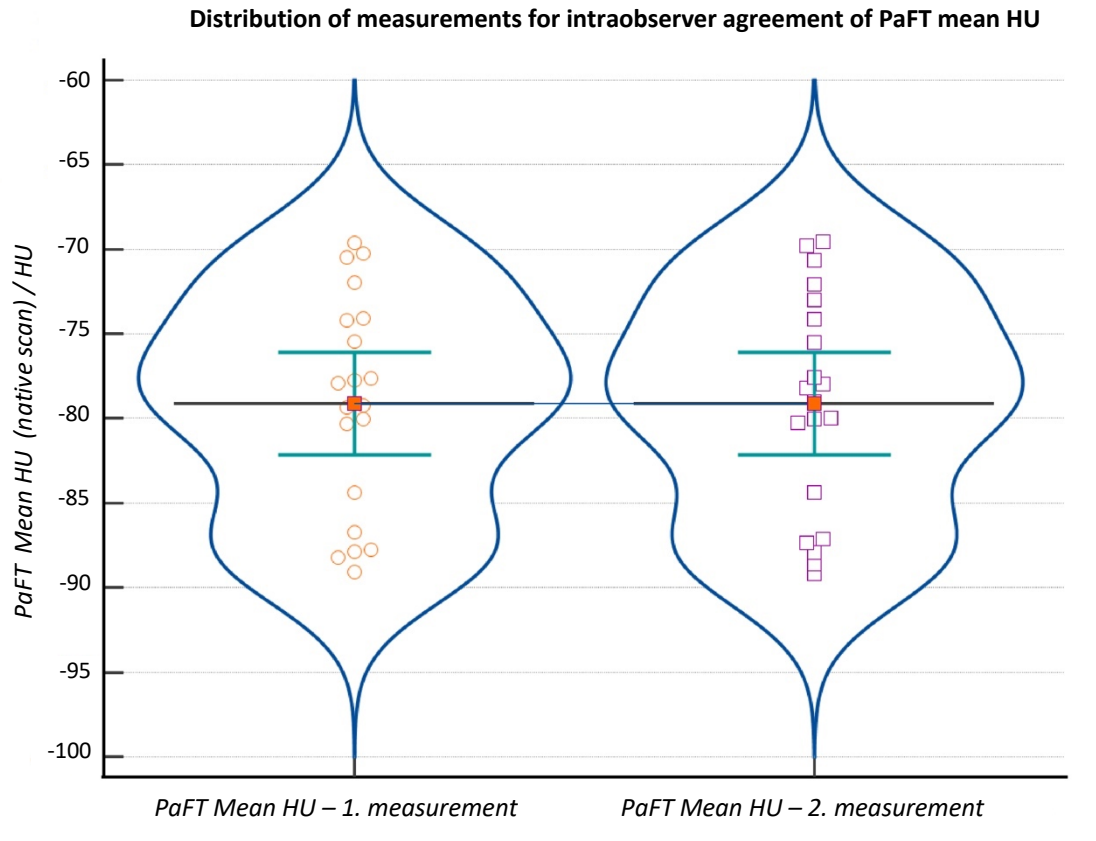


Figure 36. Distribution of measurements of PaFT mean HU values (native scans) in the reproducibility study (n=20).

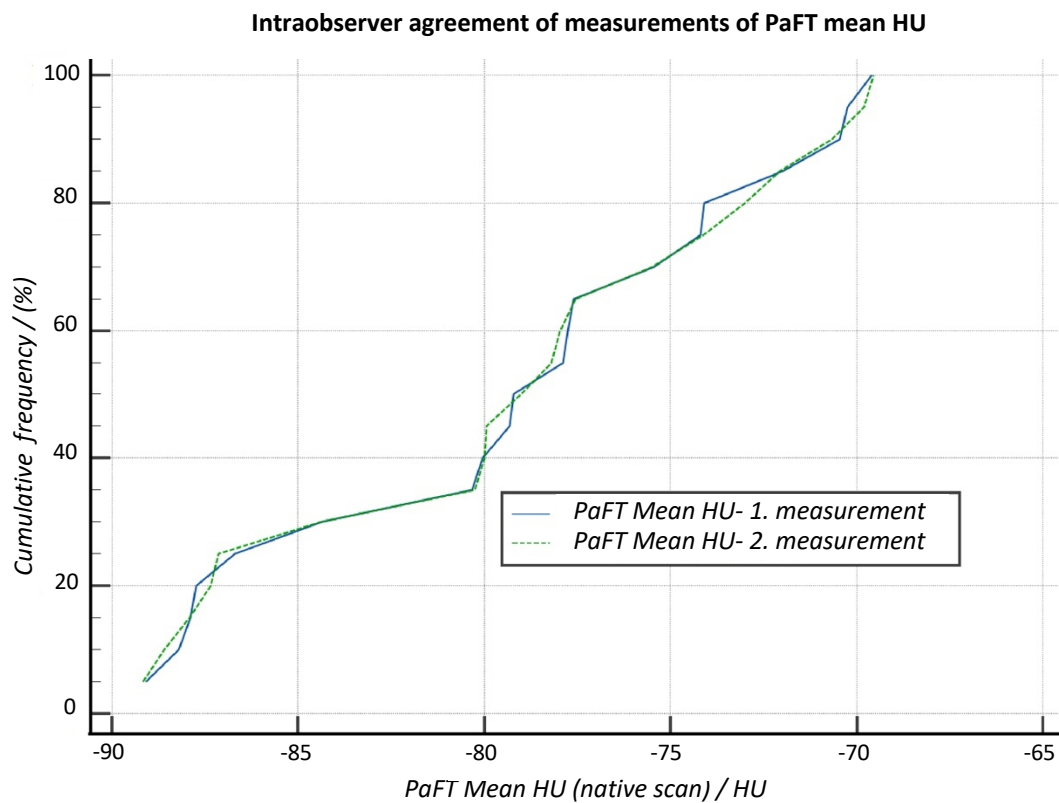


Figure 37. Intraobserver agreement of measurements of PaFT mean HU values (native scans) in the reproducibility study (n=20).

5. DISCUSSION

5.1 Discussion of study background

Origins of the study

Extensive literature has demonstrated the critical role inflammation plays in the pathophysiology of AAA.⁵⁹ A multitude of immune cells, like mast cells, macrophages, neutrophils and lymphocytes as well as adventitial fibroblasts, excrete cytokines and enzymes, which in turn promote an inflammatory reaction, extracellular matrix degradation, and neovascularization. Enzymes secreted cause medial degeneration, smooth muscle cell apoptosis and adventitial collagen degradation, promoting abdominal aortic aneurysm rupture. Chemokines cause recruitment and proliferation of inflammatory cells, whereas cytokines promote neoangiogenesis.⁶⁰

Recent evidence is pointing to the periadventitial adipose layer's role as a functional fourth layer of the blood vessel. This role is performed by the fat cells (adipocytes) of this layer secreting, often pro-inflammatory, vasoactive substances.¹⁷ Since inflammatory processes are not limited within the aortic wall but extend beyond it into the periaortic tissue, the relationship between inflammatory processes in periaortic tissue and AAA formation attracted interest as well. Histological evidence from both mouse AAA-models^{31,39} and human periaortic tissue obtained during aortic surgery for AAA repair³⁸ demonstrated increased number of inflammatory cells in periaortic tissue surrounding AAAs. Additionally, biopsies of human periaortic tissues showed that periaortic tissue histologically is a distinct entity from retroperitoneal tissue, comprising small, white, dense adipocytes with a distinct, rich vascular bed.²⁸ Furthermore, PaFT shows adventitial encroachment into the adjacent vessel, and is interspersed with vasa vasorum.^{61,62} Both these facts make PaFT a good candidate for paracrine signaling. There is already ample evidence for "outside in" signaling involving PaFT from studies on atherosclerosis pathophysiology¹⁴ or even for bidirectional communication between adipose tissue and the vessel wall.¹⁵

Adipose tissue surrounding the aorta could have similar effects on aortic wall remodeling and AAA progression caused by inflammatory "crosstalk". This fact, coupled with research indicating a more pronounced adipogenic potential of AAA adventitial mesenchymal cells and increased expression of adipocyte-related genes in tissue from ruptured AAAs, potentially implicates adipose adventitial degeneration as a factor for AAA rupture.³ It seems that the pronounced adipose tissue degeneration within the aortic adventitia is a distinctive AAA feature and the finding of enrichment of adipocyte genesis and adipocyte-related genes in ruptured AAAs points to an association between the amount of adventitial adipose tissue degeneration and AAA rupture.³ Therefore, the quantification of PaFT has been recognized as a potential prognostic target to better differentiate AAAs at higher risk for rupture.

The principles of PaFT quantification with computer tomography

In this regard, increased **PaFT Volume** is considered to represent a higher concentration of periaortic adipocytes and, thus, a greater inflammatory effect. Another possibility is that higher PaFT density may be partially caused by a locally increased number of fat pixels in the aortic wall itself.⁴¹ Further histological evidence reveals abundant adventitial adipocyte-aggregates to be an exclusive phenomenon of AAAs.³ Additionally to PaFT volume, the **PaFT mean HU value** is also significant. Since adipocyte lipid content is the main component of PaFT, larger and more numerous adipocytes have a higher proportion of lipid phase (adipocytes) compared to the aqueous phase (extracellular space) of PaFT, leading to more negative attenuation values of PaFT.⁶³ These assumptions were confirmed recently, whereby the histological and clinical (inflammatory effect) properties of perivascular fat tissue were directly correlated to its morphological characteristics (attenuation value) in CT imaging.⁶³

The need for PaFT quantification in enhanced CT angiography

The existing literature on the subject pertains almost exclusively to PaFT measurement in non-enhanced CT-scans. Thereby PaFT is usually correlated with either clinically manifested atherosclerotic vascular disease (coronary or peripheral arteries) or with metabolic risk.^{5,18,19,24,27,29} The present study, however, originates from the more recent attempts to correlate PaFT with the pathophysiology of AAAs. This introduces two issues concerning PaFT measurement in CT-scans.

The first issue is that CTAs in AAA patients routinely omit the non-enhanced phase for exposure reduction reasons. This issue has been already encountered by other authors. *Buijs et al.* encountered the same issue when attempting to quantify aortic wall calcification in AAA patients and remarked that: "However, in the Netherlands the pre-operative anatomical assessment of the AAA is performed solely with CT angiography."⁶⁴ Similarly, in Germany, AAA patients, usually initially identified with ultrasound, are routinely examined only with enhanced CT-scans preoperatively (omitting the non-enhanced phase), whereas post-EVAR controls always include a non-enhanced phase for endoleak detection. Indeed, one of the issues the execution of the study was confronted with was the low number of AAAs included, because of the lack of non-enhanced CT-scans containing AAAs.

The second issue arises when including both enhanced and non-enhanced CT scans in clinical studies, as the one carried out by *Dias-Neto et al.*, whereby they compared an AAA group (all CTAs) to a control group of patients with atherosclerotic aortic disease (all CTAs) and a second control group of patients with CT-scans with other indications, like kidney stones (all unenhanced CT-scans).⁴¹

5.2 Discussion of study results

5.2.1 Study results- PaFT volume

The derivation study demonstrated that PaFT Volume can be measured in enhanced aortic CT-scans with very high reliability. PaFT volumes from the arterial phase correlated almost perfectly ($r > .99$) with PaFT volumes from the native phase, as it was expected. PaFT volumes measured in the arterial phase were uniformly lower than PaFT volumes measured in the native phase by a factor very close to 1.1 or 10%. None of the eight potential confounding factors (intraluminal contrast intensity, aortic wall calcification, aortic diameter, longitudinal variation in contrast intensities, size of intraaortic sample ROI, CT kilovoltage, slice thickness and image noise) significantly affected the correlation of PaFT volumes. Corrected PaFT volumes from enhanced CT-scans in both the validation and secondary studies showed very high agreement with PaFT volumes from native CT-scans, confirming the reliability of the method.

The very high correlation of PaFT volumes was expected and is actually indicative of the correctness of the hypothesis. Similar studies on the interference of contrast medium on tissue attenuation values, like calcium, all show similarly very high correlation factors.⁴⁶ The main finding, namely, was the conversion factor derived from the regression analysis and not the high correlation. The high correlation is however indicative that the differences of PaFT volume are not random. It must also be pointed out, that the PaFT rings are not identical, since the PaFT rings of the arterial phase universally contained fewer fat-containing voxels compared to the PaFT rings of the native phase.

Effect of intraluminal contrast medium on PaFT Volume

The reason for this very constant, slight underestimation of PaFT volumes in arterial scans could be either a very early enhancement of this tissue compartment, which is histologically characterized by an exceptionally rich vascularization^{28,36} or attenuation artifacts caused by the presence of intraluminal contrast medium. Since intraluminal contrast medium is strongly attenuating in CT-scans, its presence may induce severe artifacts, like the ones caused by metal or calcium.⁶⁵ These artifacts usually manifest as hypo- and hyperdense regions adjacent to the strongly attenuating source. Artifacts from strongly attenuating materials can result from the following mechanisms: i) beam-hardening (selective absorption of only low energy photons), ii) photon starvation (total absorption of all photons), and iii) scatter artifacts (originating from pronounced attenuation differences, for instance between soft tissue and iodine contrast medium).⁶⁵ In particular, “streak artefacts” (beam hardening artefacts) cause dark streaks through structures in the vicinity of strongly-attenuating materials (beam-hardening effect) and can be caused by vessels filled with high iodine concentration.⁶⁶

Since the severity of the artefacts depends on the attenuation of the contrast medium, they are expected to be more severe in the arterial phase. Consequently, they can impair the assessment of adjacent perivascular tissues, like muscle, lymphatic and fat tissue as well as nearby arterial vessels.⁶⁵

Furthermore, the issue is clinically relevant and serious enough to prompt attempts aimed at reducing the effects of contrast medium-induced attenuation artefacts.⁶⁷⁻⁶⁹

Lastly, because of the current CT-scanner resolution (about 600 microns), there are voxels adjacent to the wall containing both aortic wall and periaortic tissue, so that contrast enhancement of the aortic wall itself can also cause the average pixel HU value to exceed the -45 HU limit (partial volume effect). This could be a third mechanism for the loss of PaFT-containing voxels in enhanced CT-scans.

Comparison with studies on PaFT Volume

Schlett et al. were the first to measure abdominal PaFT volume within a volume defined by 5 mm-wide coaxial periaortic rings.⁴⁰ Interestingly, the mean PaFT volume from the native CT-scans of the present study (17.6 cm³) was in line with the measurement of *Schlett* et al. (6.38 cm³),⁴⁰ considering that they measured PaFT in 40 mm long aortic segments, whereas the present study measured PaFT along the entire infrarenal aorta (mean length 102 mm). In contrast to the present study, however, the authors applied their method only to unenhanced CT scans and non-aneurysmatic aortas.

After that, a number of authors applied the *Schlett* protocol to quantify PaFT in epidemiological studies (non-AAA related) and only in the thoracic aorta, citing considerations like the variable PaFT volume and the inability to locate the retroperitoneal lining, that are limiting its use in the abdominal aorta.^{18-20,24,27,29}

Thanassoulis et al. were the first to apply the *Schlett* protocol to examine the correlation between PaFT and aortic dimensions of the abdominal and thoracic aorta. They actually found that higher PaFT volumes correlate with larger aortic diameters.³⁷ But they primarily correlated abdominal aortic dimensions with thoracic PaFT volume as a proxy for abdominal PaFT to find a positive correlation. This was a confounding factor since thoracic PaFT has been shown to be histologically distinct from abdominal PaFT. The authors confirmed their results, when they correlated abdominal PaFT with abdominal aortic dimensions. However, they considered PaFT quantification in the abdominal aorta as less reliable.³⁷ They also only examined non-enhanced CT scans, unlike the present study, and their results were hampered by an underrepresentation of aortic aneurysms in their sample cohort.³⁷

Dias -Neto et al. were the first to apply the *Schlett* protocol to correlate PaFT around AAAs with aortic dimensions as well as examine intra-individual PaFT differences in different aortic segments.⁴¹ To address the limitations of abdominal PaFT quantification, they adjusted the PaFT volume to the

aortic area. This was a concept already implemented by Schlett in their original article. They compared, however, PaFT measurements of AAAs in enhanced CTA scans with unenhanced abdomen CT scans of the control group without any previous consideration about the validity and the agreement of PaFT measurements made with and without the presence of intraluminal contrast medium.⁴¹ *Dias-Neto* et al. found no correlation of PaFT Volume with aortic diameter, although they found higher PaFT densities around the AAA maximum diameter compared to the non-aneurysmatic infrarenal neck.⁴¹ Overall, this research field is characterized by very few and contradictory studies, underlining the need for a standardized and easily available method for PaFT quantification.

Adjustment of PaFT volume to aortic size

Regarding the issue of the relation of PaFT volume to aortic size, the simple solution is the adjustment of PaFT volume for aortic size. This was done by *Dias-Neto* et al. in every axial image by determining the ratio of number of fat voxels to the total area of the aortic disc.⁴¹ *Schlett* et al. also adjusted their PaFT measurements by aortic disc diameter.⁴⁰ While this approach is methodologically correct, it is painstakingly long, since it requires measurements of PaFT and aortic disc areas in every single axial CT image. In the present study, the advantageous functionality of the GlobalThresholding Plugin was used to measure a total volume of the combined fat containing voxels and then divide it with the total volume of the periaortic ring extending 5 mm from the outer aortic wall, greatly simplifying this step of the process.

Regarding the different lengths of examined aortic segments, it has to be pointed out that they are only relevant when comparing volumes between different subjects. The primary study investigating the effect of contrast medium on PaFT Volume und HU values was, thusly, not influenced by the variable aortic segment lengths, since it compared PaFT Volumes und Mean HU values in identical aortic segments of the same length in the same patient during the same examination run with the only difference being the addition of contrast medium in the arterial phase. For this reason, in the primary study, the original, non-size-adjusted PaFT volumes were compared. In the secondary study, comparing PaFT Volumes between different subjects, the aortic size-adjusted PaFT Volumes or [PaFTVolumes] were compared, instead of the original PaFT Volumes. Since the PaFT Volumes here were given per unit of aortic volume, the difference in aortic length was compensated for.

5.2.2 Study results- PaFT mean HU value

The derivation study demonstrated the same points for the Mean HU value of the PaFT-ROI. PaFT Mean HU values measured in the arterial phase showed a very high correlation ($r > .95$) with respective values measured in the native phase. Furthermore, the Mean HU value of PaFT seemed to

remain constant (regression coefficient very close to 1.0) suggesting that the presence of intraluminal contrast medium does not significantly affect the Mean HU value of PaFT at all. This relation remained unaffected by all eight potential confounding factors in the multivariate regression model. When the correction factor (1.0011) was applied on PaFT Mean HU values measured in arterial scans, the agreement with respective values in native scans in both validation and secondary studies was almost perfect.

Effect of contrast medium on PaFT mean HU value

Although no systematic study examined the effect of contrast medium on periaortic fat attenuation values, *Antonopoulos et al.* addressed the subject in two cohorts of their study on the inflammatory effect of pericoronary fat tissue, one cohort examining pericoronary fat and one epicardial fat tissue.

In a sample of 30 subjects from cohort 3, the authors examined the mean attenuation value of pericoronary fat tissue (defined as the “fat attenuation index”, or FAI), measured within a pericoronary area equal to the coronary artery diameter. However, the authors did not compare the FAI between CT scans with and without contrast medium, since all patients in this group received CTAs, but looked for any correlation between the volume of contrast medium /intraluminal attenuation and the FAI. The authors observed no association between the average attenuation or the volume of the luminal contrast and the fat attenuation index.⁶³ This result agrees with the one of the present study.

In cohort 1, comprising samples of epicardial fat tissue but no samples of pericoronary (PVAT) tissue, the fat attenuation index (FAI) of epicardial fat was compared between scans without and with contrast medium. The authors found a strong linear association between the FAI of epicardial fat tissue obtained from images with and without contrast agent administration.⁶³ This strong linear association agrees with the correlation in the present study.

These results agree with the findings of the present study pertaining to the lack of effect of intraluminal contrast medium attenuation on the difference of the PaFT mean HU between the enhanced and unenhanced phase. However, the authors did not examine here the effects of the presence or not of contrast medium on the pericoronary FAI but the effects of the contrast medium volume/attenuation on pericoronary FAI.

The differences to the present study can be surmised as: i) The authors examined pericoronary fat tissue within a pericoronary area equal to the coronary diameter and not periaortic fat tissue (PaFT) within 5 mm of the aortic wall. The effect of contrast medium can be different considering the different dispersion of contrast in the large aortic lumen both laterally and longitudinally compared to the coronary arteries. The perfusion of PaFT can also be different, due to anatomical differences of the vasa vasorum. ii) The methodology was different since for pericoronary fat tissue they did not

compare unenhanced to enhanced CT scans but examined the effect of the presence of different volumes/attenuations of contrast medium on pericoronary FAI. The comparison between CT and CTA was performed only for epicardial fat tissue and here a strong correlation was found. iii) Their sample of 30 patients was much smaller. iv) They only considered the average HU value of PaFT (as the FAI) but did not report on PaFT volumes. This is important since the present study also found no effect of contrast medium on the PaFT mean HU values but did find a systematic underestimation of PaFT volume.⁶³

Comparison with studies on PaFT Mean HU value

A recent study measuring the fat attenuation index, defined as the mean attenuation of abdominal periaortic fat volume, found that the PaFT mean HU value or FAI was the most predictive for metabolic syndrome among other abdominal fat depots.⁷⁰ Both *Antonopoulos et al.*⁶³ and *Lee et al.*⁷⁰ applied a fat attenuation index defined as the average (mean) HU value of fat voxels within the column of interest (-190 to -30 HU). This is in complete agreement with the second parameter examined in the present study, which was also the mean HU value of the PaFT containing voxels (-195 to -45 HU). Both studies found a correlation between pericoronary inflammation⁶³ and metabolic risk⁷⁰ with lower (more negative) FAIs (perivascular fat mean HU values).

The PaFT Mean HU value is independent of the presence of any periaortic not-fat containing tissue (like blood in ruptured AAAs). The latter would displace PaFT, altering the PaFT Volume but would not alter the PaFT mean HU, which is measured only within the PaFT containing periaortic space. Overall, the mean PaFT HU value, defined as the fat attenuation index in studies, seems to offer three distinct methodological advantages: it is unaffected by contrast medium and the presence of non-fatty periaortic tissue and does not require aortic size adjustment. It is unknown, however, which PaFT value (mean HU or Volume) is more representative of PaFT properties.

5.2.3 Study results- Secondary study

The purpose of the secondary study was to examine whether corrected PaFT values from enhanced CT-scans, measured as the average value of a group or cohort, agreed with the average cohort values measured in native CT-scans. This was demonstrated with the corrected arterial PaFT median values being almost identical to the native median values. As for the direct comparison of PaFT values between the AAA and non-AAA groups, a trend for higher PaFT Volumes and more negative PaFT HU values in the AAA group was shown, although it was not statistically significant. This finding

would agree with the results by Dias-Neto et al., who also found no correlation between AAA presence and higher PaFT -“densities” (size corrected PaFT volumes).⁴¹

5.2.4 Study results- Reproducibility study

The very high reproducibility of the results, repeated one year later, was also to be expected, since the tracing of the Aortic/Periaortic ROIs with zoom factors > 2000% allows a tracing precision of < 0.5 mm, which is below the voxel size.

5.2.5 Study results- Sample size

The retrospective nature of the study did not necessitate an a priori calculation of a sample size, since the statistical significance of the results can be determined by the confidence levels of the resulting outcomes. The sample size was determined based on existing literature. No dedicated studies comparing PaFT quantification in enhanced and non-enhanced CTs were found in the literature. There are however quite a few similar studies examining the interference of contrast medium in the quantification of arterial wall calcium scores in enhanced and non-enhanced CTs. While the factors influencing contrast medium interference in wall calcium and PaFT may not be identical, we assessed these studies as indicative for our sample size (same methodology with derivation and validation cohorts and similar r values of .99 and .96) with derivation/validation cohorts of 90/120⁴⁶ and 92/47.⁷¹ The landmark study of PaFT quantification by Schlett et al. also included 100 subjects.⁴⁰

5.2.6 Study results- Potential confounding factors

Among factors that could potentially influence the quantification of PaFT in enhanced CT-scans, **aortic wall calcification** was examined since high calcium densities can cause blooming artefacts affecting the adjacent periadventitial tissue. **The longitudinal variation in contrast intensities** was examined because the severity of contrast medium attenuation artefacts depends on the attenuation values of contrast medium, and the attenuation values of contrast medium can vary substantially in large AAAs in the longitudinal axis. The limit of 55 mm for the subgroup analysis was considered because of the clinical implication that these AAAs would not require a PaFT measurement as a prognostic marker, since the decision of whether they are surgically treated or not should be already made at the critical diameter. **The lateral variation in contrast intensities** was examined by including 3 different intraluminal sample ROIs in the enhanced scans (diameters of 8 mm, 10 mm, 12 mm).

CT-kilovoltage can affect attenuation values and **slice/increment thickness** can affect the volume reconstructions. Therefore, they were taken into consideration in comparing paired enhanced with unenhanced CT-scans. Additionally, both factors were examined as confounding factors potentially influencing the conversion of PaFT values from enhanced to those from unenhanced CT scans.

None of the aforementioned factors influenced the PaFT quantification.

Regarding **image noise**, the formal definition of high image noise in the aortic phase is usually defined by placing an intraaortic ROI and measuring the standard deviation (SD) of the mean attenuation value.⁶⁶ The limits for high noise are usually set at $SD > 30 \text{ HU}$ ⁶⁶ or $SD > 35 \text{ HU}$.⁴⁶ In the present study, a SD of 35 HU was defined as indicative of very high image noise.

High image noise interfered by registering positive HU values within the periaortic space, where negative values are usually measured. Indeed, in the 3 high image noise scans of the present study, the mean PaFT HU values were abnormally higher than usual and the PaFT Volumes were abnormally low, all close to zero.

Other possible confounding factors included the **non-gated CT-scans**. Since the enhanced and unenhanced-CT were not ECG-gated, some underestimation of PaFT volume could be attributed to the fact that the PaFT ring measured in diastole and then applied to the same axial cut in systole could exclude some fat voxels that were before inside the ring leading to underestimation of fat volume.

Although such a mechanism could be conceivable, it did not affect the results of the study. Since both phases were not-gated, this mechanism would result in a completely random over- and underestimation of PaFT in the enhanced and unenhanced phases, resulting in a completely random variation of PaFT values between the two phases. The high correlation and the fact that there was a universal underestimation of PaFT values in the arterial phase excluded any significant systematic effect of sustained PaFT underestimation only in the arterial phase. Simply put, this mechanism would cause a completely random effect compensated within the sample size and not a systematic (bias) effect showing a consistent underestimation of enhanced PaFT volumes, as shown in the study, since there is no reason why only the arterial scans would be captured during systole.

The issue of PaFT exact localization and its histological limits

A number of previously reported issues with quantification of abdominal PaFT had to be considered in this study. Regarding separating PaFT from retroperitoneal tissue, despite the close proximity of abdominal periaortic PaFT to other visceral fat tissues (mesenteric and omental fat tissue), PaFT is histologically clearly separated and distinguished by relatively small adipocytes and a rich capillary network.²⁸ So, periaortic fat tissue is morphologically and functionally a distinct entity, different from adjacent visceral fat. There are two considerations here: the first is where does PaFT end and where visceral adipose tissue begins. For instance, *Dias-Neto et al.* considered the confounding presence of

mesenteric adipose tissue in the fat cylinder defined for PaFT measurement. As explained by *Schlett et al.*, existing histological evidence indicates that vascular wall inflammation extends to at least several mm from the wall⁴² and pericardial fat around coronary arteries has a mean thickness of about 5 mm.^{30,40} So, it seems reasonable to assume that PaFT extends to at least 5 mm from the aortic wall.

The second question is the location of the retroperitoneal lining, because adipose tissue on the other side of it can be included in the fat cylinder without having an effect on the aortic wall because the two-fold membrane does not allow diffusion of secreted substances. These issues are, however, important only when defining a model for measuring PaFT and are, thus, not relevant for the present primary study that seeks to determine the effect of intraluminal contrast medium on the HU density of periaortic tissue within 5 mm from the aortic wall, a distance that includes most of the adipose tissue involved in periaortic inflammation processes. The objective of this study, namely, is not to determine whether 5 mm of periaortic tissue coincide with PaFT but to determine whether contrast enhancement alters the measured number of fat-containing voxels within that area.

5.2.7 Study results- Study limitations

Study limitations included the low number of AAAs included, although the statistical analysis showed that the results were not affected by aortic size. The correction factors obtained in this retrospective, single center study should also be tested in a multi-center setting utilizing different scanners with different imaging and processing parameters.

One of these parameters would be the contrast medium amount and injection rate. The amount of contrast medium and the injection rate was the same for all subjects included in the study, as this was the protocol at the time of the examinations. The effects of the amount of contrast medium or injection rate on the attenuation of the aortic lumen were indirectly included in the results (the mean intraluminal attenuation value as well as both the lateral and longitudinal dispersion of intraluminal contrast medium were independently examined and also evaluated as possible confounding factors in the multiple regression analysis). The effects of the contrast medium or injection rate on the PaFT Volume or HU could not be examined because of the imaging protocol.

Unlike most existing studies, this study focused on the abdominal aorta, because of its clinical significance (as the location of the majority of abdominal aneurysms) and the specific methodological challenges it poses for PaFT quantification. Excluded data sets were caused mostly by issues with the already reconstructed data sets (with no longer available raw data) and should be perceived as a limitation of the retrospective nature of the study and not the method itself.

Whereas our results were limited to the arterial phase, they are indicative of a constant effect of contrast medium on PaFT Volume and no effect on PaFT Mean HU value, which could also be the case for other non-arterial enhanced CT-phases as well.

5.3 Methodological considerations

A number of potential methodological considerations, concerning the application of the method to AAAs, in the presence of non-circular aortic discs or the interference from paraaortic organs/tissues were examined.

Lateral CM dispersion in AAAs. The lateral dispersion of contrast medium in AAAs does not lead to any significant variation in intraluminal attenuation values (mean HU density and SD) (**Figure 38**).

This result is irrespective of the level of image noise. Thus, the lateral variation of intraluminal attenuation values does not preclude the application of the method to AAAs, at least to those with about <50 mm of perfused lumen.

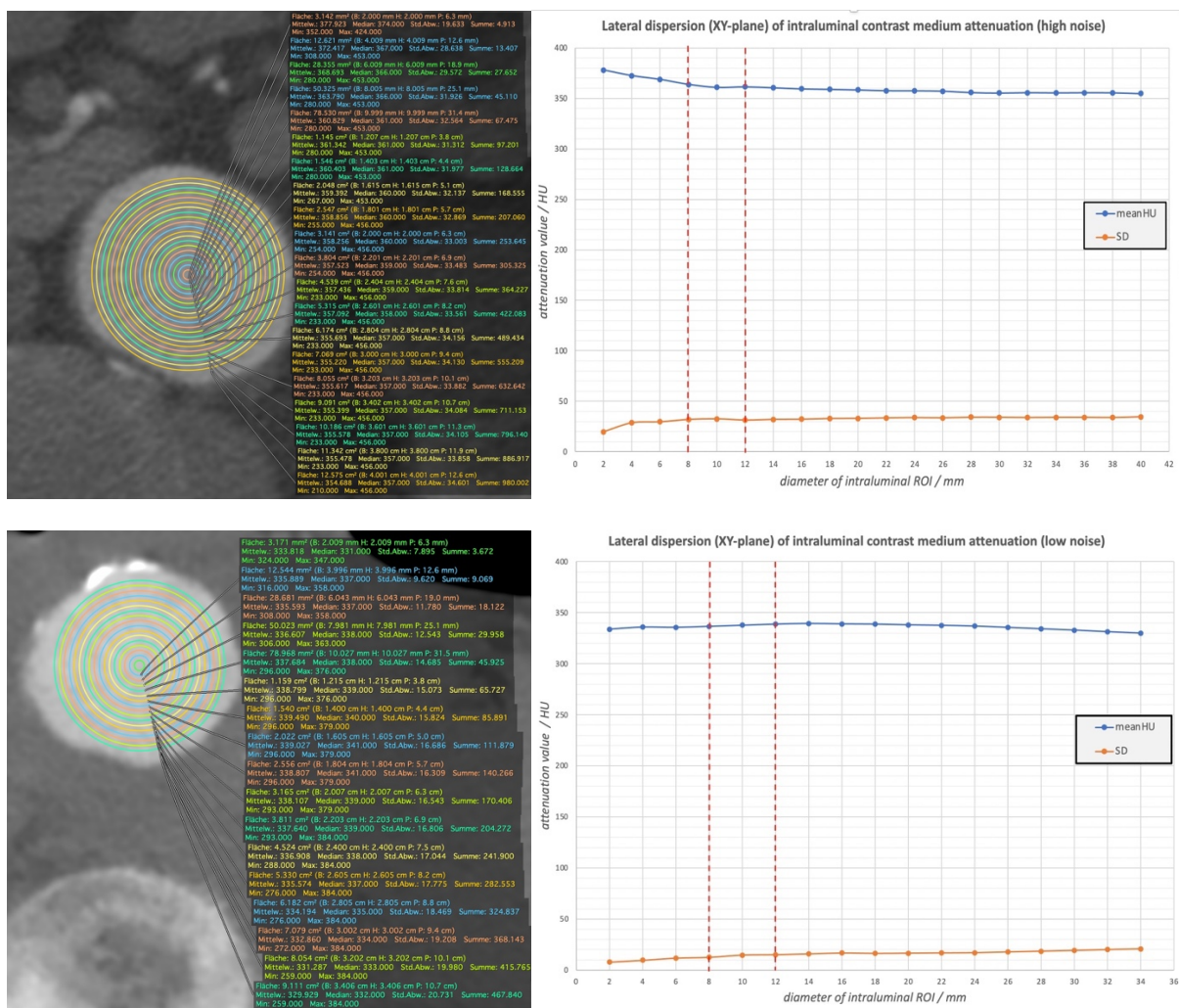


Figure 38. Lateral dispersion of contrast medium and the resulting variation of attenuation values within the lumen of two AAAs in the presence of high (top image) and low (bottom image) image noise. In both instances, both the mean intraluminal attenuation as well as the SD remain quite constant all the way to the periphery of the aortic disc. The two red lines in each image signify the position of the smaller (8 mm) and larger (12 mm) sample ROI used in the study.

Longitudinal contrast medium dispersion in AAAs. The longitudinal variation in intraluminal attenuation values remains within low levels for AAAs up to a volume of 100 cm³, after which it increases abruptly. Although it does not pose a problem for the application of the method in AAAs with a maximum diameter < 55 mm (**Figure 39**), it could conceivably be an issue in large AAAs. The current study, however, found no measureable impact of longitudinal CM dispersion in large AAAs.

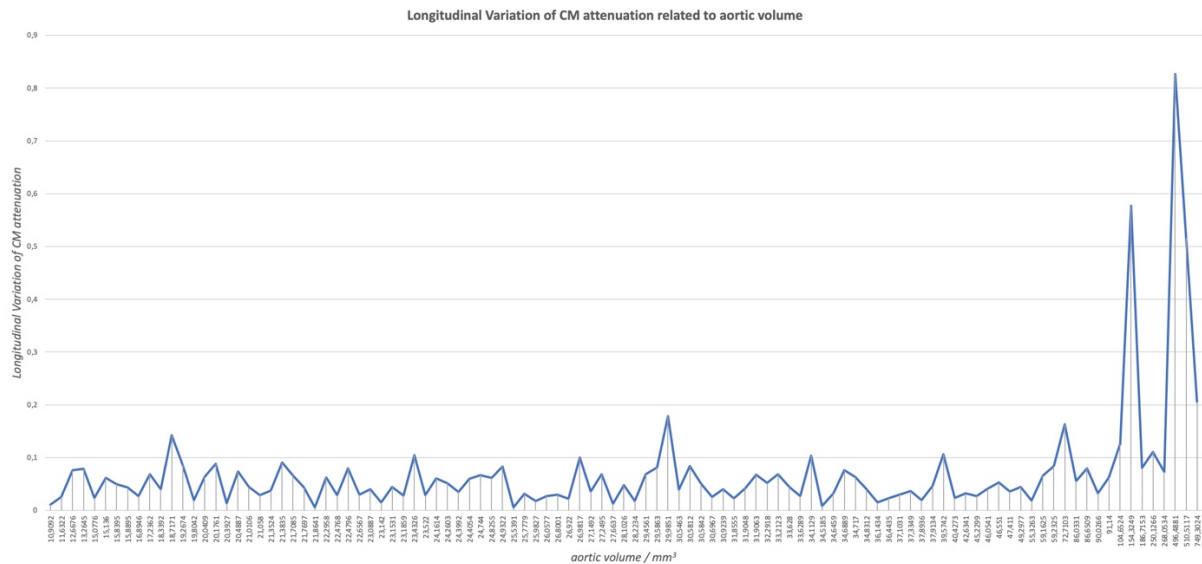


Figure 39. Longitudinal variation of mean intraluminal HU attenuation with increasing aortic volume.

Intraluminal voxels with values -45 to -195 HU. Although no pixels with attenuation values in the -45 to -195 HU range are seen in the contrast enhanced aortic lumen in CTA scans, isolated such pixels can be very rarely seen within the aortic lumen in the native phase. The main cause for their existence is high image noise or artifacts, for instance metal/high-density foreign material artifacts (**Figure 40**).

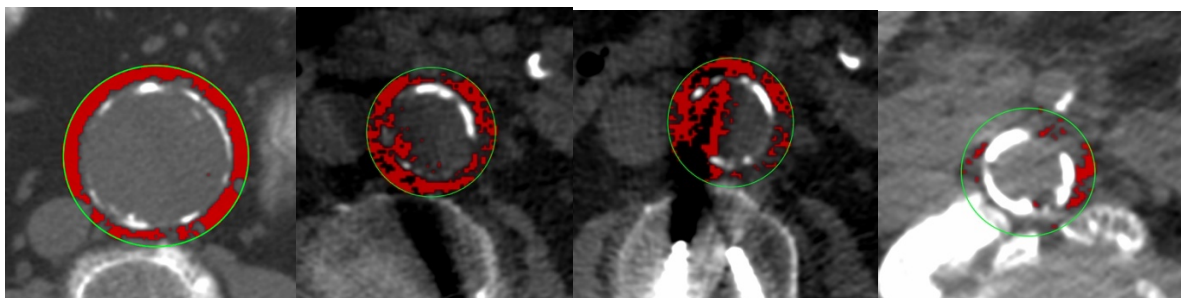


Figure 40. Presence of intraluminal pixels with values -45 to -195 HU in native CT scans. Usually, only solitary pixels in few axial CT images are seen (left image). Such pixels can be seen in the vicinity of metal/high density foreign objects, for instance near spinal osteosynthesis materials (middle two images). Alternatively, they can arise near very high-density calcium deposits in the aorta or vertebral column (right image).

In order to examine the potential impact of intraluminal voxels with fat tissue attenuation values in the native scans and the possible need to exclude the aortic disc from the PaFT measurement within the periaortic ROI, the number of such pixels was counted in all the native scans of the derivation cohort.

As seen in **Figure 41** the number of such pixels is so low that the exclusion of the aortic disc from the periaortic ROI is not necessary.

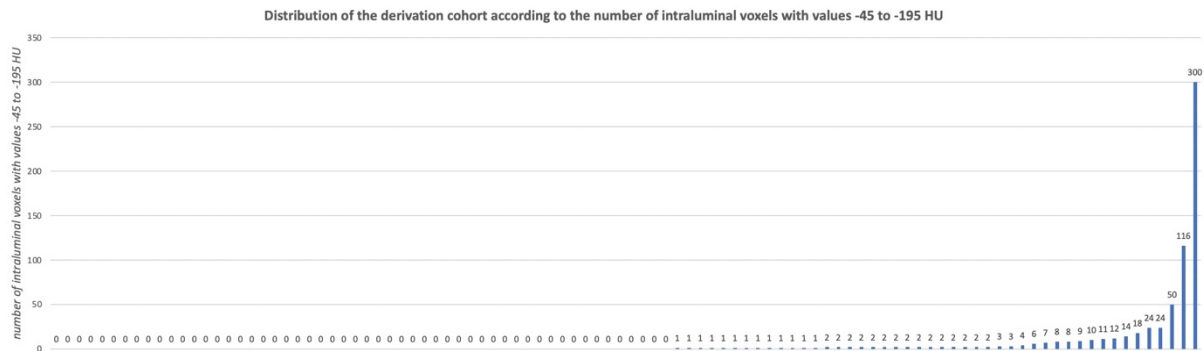


Figure 41. The distribution of unenhanced CT scans of the derivation cohort, sorted with increasing number of intraluminal voxels with values of -45 to -195 HU. More than half CT-scans (55/101) had zero voxels, two-thirds (67/101) had 1 or less voxels, 83/101 had 2 or less voxels and 91/101 had 10 or less voxels. Of the 10 examinations with > 10 voxels, the number of false positive voxels was still miniscule compared to the total number of fat-containing voxels (typically 1500 - 25000). Considering the difference of fat-containing voxels between the unenhanced and enhanced data sets, the false positive voxels of these ten last examinations would account only for 0.27 % to 2.67 % of the measured difference in voxels -45 HU to -195 HU between the unenhanced and enhanced phases. Thus, the number of intraluminal voxels with fat tissue values in the aortic lumen of unenhanced scans does not warrant the exclusion of the unenhanced aortic disc when counting voxels with values -45 to -195 HU.

Oval shaped periaortic ROIs. Non-circular aortic discs in axial images lead to non-circular periaortic ROIs. While this can be an issue for the standardization of the method, it was not relevant in this study, since it was ensured that identical periaortic ROIs and thus identical cylinders of periaortic tissue were compared in the two phases (**Figure 42**).

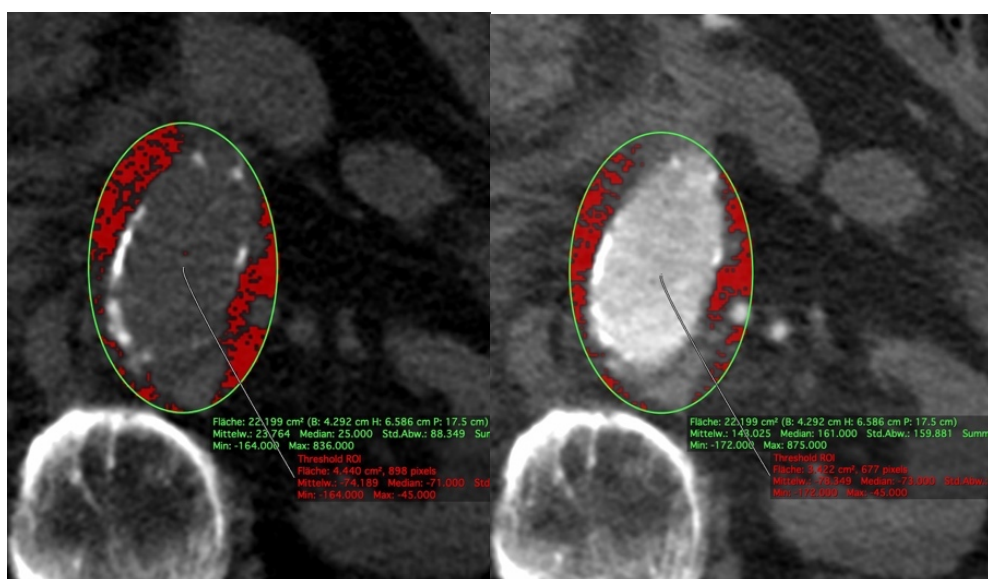


Figure 42. Non-circular periaortic ROIs. They posed no limitation for the present study, since identical segments of periaortic tissue were compared in the two CT phases.

There are a number of ways to deal with **non-circular aortic discs** in the axial images. One approach is to reject them. *Schlett* et al. made sure to apply their method strictly to images with nearly circular aortic discs. To achieve that, they included in their measurement aortic segments upwards from the aortic bifurcation beginning with the first axial image containing a nearly circular aortic disc (defined as a < 1 mm difference between the transversal and anterior-posterior diameters). Subsequently, they excluded data sets containing images with a > 5 mm difference between transverse and anterior-posterior diameters throughout the volume of interest. They justified that because „the oval shape of the aorta precluded a standardized measurement of the periaortic adipose tissue cylinder.“⁴⁰ Having ensured near-circular aortic discs, they then defined the periaortic ROI in every axial image as a circle with a diameter 10 mm larger than the anterior-posterior aortic diameter.⁴⁰ This periaortic ROI was concentric to the aortic disc. While this approach does ensure a more homogeneous sample, helpful when establishing a standard measuring protocol, it comes with certain disadvantages: while the concept is easier to apply in shorter aortic segments (*Schlett* examined only 40 mm long aortic segments), it becomes increasingly difficult when the entire infrarenal aortic segment is examined, whereby any angulation of the aorta would immediately exclude the patient. Secondly, nearly circular aortic discs are more ubiquitous in non-aneurysmatic aortas (*Schlett* examined non-aneurysmatic aortas) and less so in AAAs.

Dias-Neto et al. used concentric rings calibrated to the aortic diameter, whereby in each axial image a ROI was traced with a diameter of „10 mm circumferential to the outer contour of the aorta“, concentric with the aortic disc.⁴¹ According to the authors, this process allowed the designation of a hollow cylinder of aortic PaFT.⁴¹ The authors, however, did not elaborate further on how their method accounted for non-circular aortic segments and they simply stated that „measurements of PaFT were based on the method described by *Schlett* et al.“⁴¹

Another option explored in the present study was to apply the OsirixMD tools to perform a stretched MPR reconstruction of the aortic segment and then generate axial images of the aorta orthogonally to the longitudinal axis of the reconstructed aorta. While the aortic disc is mostly nearly circular in the new axial images, the software can no longer perform the necessary volume reconstructions because of the variable (uneven) slice thickness of the newly reconstructed axial images.

Since the objective of this study was to explore the feasibility of PaFT measurement in contrast enhanced CT images compared to unenhanced CT images and not to establish a standard protocol for PaFT measurement, the standardisation of the periaortic cylinder was not considered a priority. Therefore, non-circular aortic discs were included in the measurement by simply adjusting the aortic ROIs to match the contour of the aortic wall, ending up with a number of oval-shaped aortic ROIs. As long as the aortic ROIs (and periaortic ROIs) were identical in size and location in both the unenhanced and enhanced phase, it was ensured that the same periaortic volume containing the same PaFT was examined in both CT phases, allowing for a direct comparison of tissue densities.

Irregular aortic contour. Just like non-circular ROIs, irregular aortic shapes were not an issue, since identical ROIs were compared in the two phases (**Figure 43**).

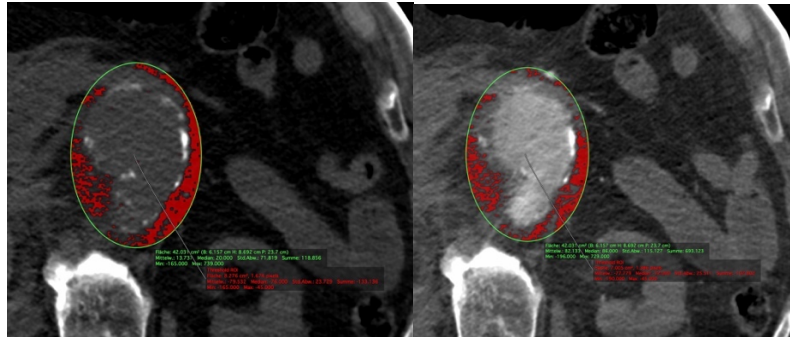


Figure 43. Irregular aortic disc shapes. Being identical on both phases, they posed no issue for the current study.

Periaortic blood in ruptured AAAs. As expected, the presence of blood and hematin-containing tissue in close proximity to the aortic wall will interfere with the detection of fat-containing voxels. This was not an issue in this study, however, because of the identical paired image sets (**Figure 44**).

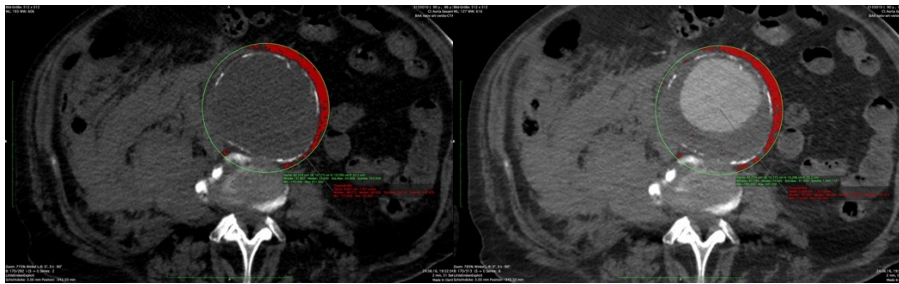


Figure 44. Presence of periaortic hematoma. While this will interfere with the identification of PaFT, this was not an issue with the identical paired image sets in the present study.

Organs in close vicinity to the aortic wall. A further issue with PaFT quantification arises when the presence of periaortic organs or foreign objects displaces normal periaortic tissue. This, again, was not an issue in this study because of the identical paired image sets (**Figure 45**).

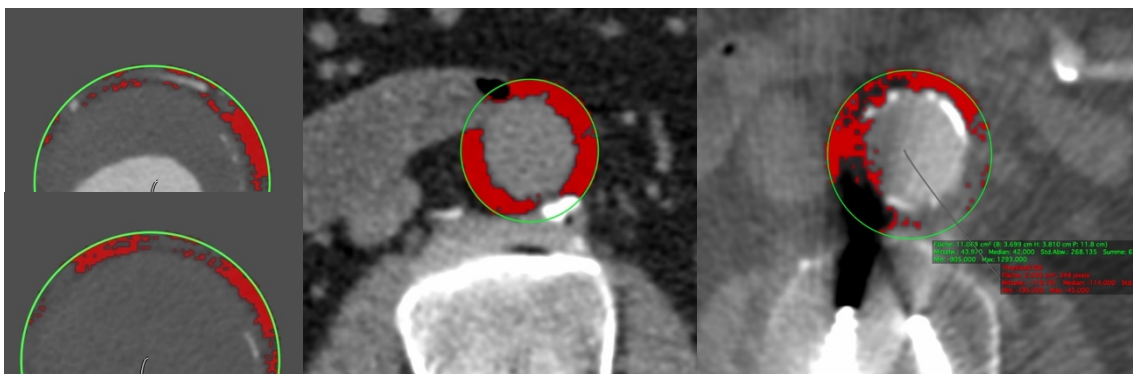


Figure 45. Presence of periaortic organs and foreign objects. The presence of blood vessels (left image) or intestinal segments (middle image) can interfere with the measurement of PaFT. Artifacts from foreign objects can cause the loss of PaFT tissue voxels (right image). While para-aortic foreign tissue will interfere with PaFT Volume quantification, the mean PaFT HU value is not affected, since it is measured only in periaortic areas within the -195 to -45 HU range and not in the entire periaortic ring.

5.4 Conclusion – Future prospectives

This study examined the feasibility of PaFT quantification within a 5 mm-wide periaortic ring volume using a newly introduced method based on the OsirixMD post-processing platform (which was applied for this purpose before) and the GlobalThresholding Plugin (newly introduced for this purpose). The latter simplifies the process of PaFT quantification significantly, since it automatically constructs a specific PaFT-ROI of fat tissue-containing voxels within the specified area. From this PaFT-ROI then, the total volume and the mean HU value of PaFT along an entire aortic segment can be very simply determined by simple volume reconstruction. Previous methods based on the Osirix platform required determining a PaFT “density” by painstakingly dividing the number of PaFT pixels by the aortic disc area in every single axial image,⁴¹ whereas with the present method, after defining the periaortic ROIs, the Plugin automatically creates a ROI only from PaFT containing pixels.

The study showed for the first time that intraluminal contrast medium affects (underestimates) the measurement of PaFT volume in a very consistent way, which necessitates a conversion factor of 1.1057 to be applied to PaFT Volume measurements in arterial scans for comparison reasons with unenhanced CT scans. On the other hand, the Mean HU value of PaFT-containing voxels remains practically unaltered by the intraluminal enhancement. Thus, PaFT Volumes and PaFT Mean HU values can be quantified in enhanced aortic CT scans with very high reliability, simply by correcting the former by 1.1057, whereas no correction is necessary for the latter.

The present study also focused on certain methodological issues and resolved a number of them. It demonstrated that PaFT Volume and mean HU value can be measured reliably and comparably in both unenhanced and enhanced scans, irrespective of intraluminal contrast densities, lateral or longitudinal contrast dispersion, extent of aortic wall calcification, aortic size or imaging parameters (slice thickness or CT-tube voltage). The aortic disc in the native phase does not need to be excluded from the measurement because of voxels with negative HU values. Volume measurements need to be standardized, e. g. per unit of aortic volume. The presence of non-adipose periaortic tissue can affect the total PaFT Volume but will not affect the mean PaFT HU value, since the latter is only determined by HU values within the area containing fat tissue and not the whole of the periaortic area.

The PaFT Mean HU value offers three methodological advantages: it is unaffected by contrast medium and the presence of non-fatty periaortic tissue (as demonstrated in the present study) and does not require aortic size adjustment. It is unknown, however, which PaFT value (mean HU or Volume) is more representative of PaFT properties. Overall, the results of this methodological study will help establish the methodology of PaFT quantification, enabling a further examination of the clinical importance and role of PaFT on vascular diseases (especially its potential prognostic value for AAAs) in additional studies.

Looking ahead, a number of issues need to be addressed before further implementation of this method. For PaFT quantification in axial images, the issue of non-circular ROIs has to be addressed and may necessitate different primary processing of raw data (unavailable for this study), excluding non-circular images or measuring PaFT only in certain locations (infrarenal neck or maximum diameter) of AAAs. Other non-methodological issues beyond the scope of this study, like the position of the retroperitoneal lining, the width of the examined periaortic area or the effect of BMI and total abdominal fat tissue on the PaFT, also need to be addressed further.

6. REFERENCE LIST

1. Doyle B, Hoskins P, McGloughlin TM (2011) Computational Rupture Prediction of AAAs: What needs to be done next? *J Endovasc Ther* 18:226-229
2. Georgakarakos E, Ioannou CV, Katsamouris AN, Kostas T, Papaharilaou Y (2011) Computational Evaluation of Aortic Aneurysm Rupture Risk: What Have We Learned So Far? *J Endovasc Ther* 18:214-25
3. Doderer SA, Gäbel G, Hamming JF, Holdt LM, Kokje VBC, Lindeman JHN, Northoff BH (2018) Adventitial adipogenic degeneration is an unidentified contributor to aortic wall weakening in the abdominal aortic aneurysm. *J Vasc Surg* 67:1891-1900
4. Buijs RVC, Greuter M, Leemans EL, Tielliu IFJ, Willems TP, Zeebregts CJ (2018) Quantification of abdominal aortic calcification: Inherent measurement errors in current computed tomography imaging. *PLoS ONE* 13: e0193419
5. Fox CS, Cupples LA, D'Agostino RB Sr, Hoffmann U, Liu CY, Massaro JM, Maurovich-Horvat P, Meigs JB, Murabito JM, O'Donnell CJ, Pou KM, Vasani RS (2007) Abdominal visceral and subcutaneous adipose tissue compartments: association with metabolic risk factors in the Framingham Heart Study. *Circulation* 116:39-48
6. Barandier C, Montani JP, Yang Z (2005) Mature adipocytes and perivascular adipose tissue stimulate vascular smooth muscle cell proliferation: effects of aging and obesity. *Am J Physiol Heart Circ Physiol* 289:1807-1813
7. Bailey-Downs LC, Csiszar A, Gautam T, Sonntag WE, Sosnowska D, Toth P, Tucsek Z, Ungvari Z (2013) Aging Exacerbates Obesity-Induced Oxidative Stress and Inflammation in Perivascular Adipose Tissue in Mice: A Paracrine Mechanism Contributing to Vascular Redox Dysregulation and Inflammation. *J Gerontol A Biol Sci Med Sci* 68:780-792
8. Chatterjee TK, Blomkalns AL, Denning GM, Dickson EW, Harrelson A, Idelman G, Neltner B, Romig-Martin SA, Rothenberg FG, Rudich S, Stoll LL, Weintraub NL (2009) Proinflammatory phenotype of perivascular adipocytes: influence of high-fat feeding. *Circ Res* 104:541-549
9. Henrichot E, Chizzolini C, Dayer JM, Juge-Aubry CE, Meda P, Meier CA, Pache JC, Pernin A, Velebit V (2005) Production of Chemokines by Perivascular Adipose Tissue A Role in the Pathogenesis of Atherosclerosis? *Arterioscler Thromb Vasc Biol* 25:2594-2599
10. Spiroglou SG, Kostopoulos CG, Papadaki HH, Varakis JN (2010) Adipokines in periaortic and epicardial adipose tissue: differential expression and relation to atherosclerosis. *J Atheroscler Thromb* 17:115-130
11. Brinkley TE, Chughtai HL, Ding J, Hundley WG, Kitzman DW, Kritchevsky SB, Leng X, Nicklas BJ (2014) Periaortic Fat and Cardiovascular Risk: A Comparison of High-Risk Older Adults and Age-Matched Healthy Controls. *Int J Obes (Lond)* 38:1397-1402

12. Kawahito H, Akakabe Y, Ikeda K, Irie D, Kato T, Kishida S, Matoba S, Matsubara H, Mori Y, Ogata T, Takata H, Ueyama T, Wakana N, Yamada H (2013) Periaortic adipose tissue-specific activation of the renin-angiotensin system contributes to atherosclerosis development in uninephrectomized apoE/Mice. *Am J Physiol Heart Circ Physiol* 305:H667-75
13. Rajsheker S, Blomkalns AL, Chatterjee TK, Manka D, Stoll LL, Weintraub NL (2010) Crosstalk Between Perivascular Adipose Tissue and Blood Vessels. *Curr Opin Pharmacol* 10:191-196
14. Quesada I, Cannizzo B, Castro C, Cejas J, García R, Redondo A (2018) Vascular dysfunction elicited by a cross talk between periaortic adipose tissue and the vascular wall is reversed by pioglitazone. *Cardiovasc Ther* 36:e12322
15. Antonopoulos AS, Antoniades C, Bakogiannis C, Casadei B, Channon KM, Coutinho P, De Silva R, Digby J, Herdman L, Kessler B, Krasopoulos G, Lee R, Margaritis M, Petrou M, Psarros C, Reilly S, Sanna F, Sayeed R, Shirodaria C, Tousoulis D (2015) Adiponectin as a Link Between Type 2 Diabetes and Vascular NADPH Oxidase Activity in the Human Arterial Wall: The Regulatory Role of Perivascular Adipose Tissue. *Diabetes* 64:2207-2219
16. Padilla J, Bayless DS, Fleming NJ, Jenkins NT, Lansford KA, Laughlin MH, Rector RS, Sheldon RD, Thorne PK (2014) Differential regulation of adipose tissue and vascular inflammatory gene expression by chronic systemic inhibition of NOS in lean and obese rats. *Physiol Rep* 2:e00225
17. Watts SW, Burnett R, Dorrance AM, Shaw S (2011) Indoleamine 2,3-dioxygenase in periaortic fat: mechanisms of inhibition of contraction. *Am J Physiol Heart Circ Physiol* 301:H1236–H1247
18. Fox CS, Hoffmann U, Lehman SJ, Massaro JM, Meigs JB, Murabito JM, O'Donnell CJ, Schlett CL (2010) Peri-Aortic Fat Deposition Is Associated with Peripheral Arterial Disease: The Framingham Heart Study. *Circ Cardiovasc Imaging* 3:515-519
19. Britton KA, Corsini EM, Fox CS, Hoffmann U, Massaro JM, Murabito JM, Pedley A (2012) Prevalence, Distribution, and Risk Factor Correlates of High Thoracic Periaortic Fat in the Framingham Heart Study. *J Am Heart Assoc* 1:e004200
20. Akyürek Ö, Efe D, Kaya Z (2014) Thoracic periaortic adipose tissue in relation to cardiovascular risk in type 2 diabetes mellitus. *Wien Klin Wochenschr* 126:767–773
21. Britton KA, Fox CS, Hoffmann U, Kreger BE, Massaro JM, Murabito JM (2013) Body Fat Distribution, Incident Cardiovascular Disease, Cancer, and All-cause Mortality. *J Am Coll Cardiol* 62:921-925
22. Britton KA, Benjamin EJ, Corsini E, Fox CS, Hamburg NM, Hoffmann U, Larson MG, Mitchell GF, Palmisano J, Schlett CL, Vasan RS, Vita JA, Wang N (2013) Thoracic Periaortic and Visceral Adipose Tissue and Their Cross-sectional Associations with Measures of Vascular Function. *Obesity (Silver Spring)* 21:1496-1503
23. Du B, Eng JS, Fleenor BS, Ouyang (2015) A Aortic perivascular adipose-derived interleukin-6 contributes to arterial stiffness in low-density lipoprotein receptor deficient mice. *Am J Physiol Heart Circ Physiol* 308:H1382-390

-
24. Efe D, Aygün F, Keser A, Ulucan Ş (2015) Relationship of Coronary Artery Disease with Pericardial and Periaortic Adipose Tissue and Their Volume Detected by MSCT. *Hellenic J Cardiol* 56:44-54
25. Kaess BM, Corsini E, Fox CS, Hoffmann U, Larson MG, Massaro JM, Pedley A, Sawyer DB, Smith HM, Vasan RS (2012) Relation of Vascular Growth Factors with CT-Derived Measures of Body Fat Distribution: The Framingham Heart Study. *J Clin Endocrinol Metab* 97:987-994
26. Lee JJ, Hoffmann U, Levy D, Long MT, Massaro JM, Pedley A (2018) Visceral and intrahepatic fat are associated with cardiometabolic risk factors above other ectopic fat depots: The Framingham Heart Study. *Am J Med* 131: 684-692
27. Maurovich-Horvat P, Engel LC, Hoffmann U, Kallianos K, Koenig W, Schlett CL, Szymonifka J, Truong QA (2015) Relationship of Thoracic Adipose Tissue Depots with Coronary Atherosclerosis and Circulating Inflammatory Biomarkers. *Obesity (Silver Spring)* 23:1178-1184
28. Kranendonk ME, van Herwaarden JA, de Jager W, Kalkhoven E, Moll FL, Stupkova T, Vink A, Visseren FL (2015) Inflammatory characteristics of distinct abdominal adipose tissue depots relate differently to metabolic risk factors for cardiovascular disease: distinct fat depots and vascular risk factors. *Atherosclerosis* 239:419-427
29. Lehman SJ, Fox CS, Hoffmann U, Massaro JM, O'Donnell CJ, Schlett CL (2010) Peri-aortic Fat, Cardiovascular Disease Risk Factors, and Aortic Calcification: The Framingham Heart Study. *Atherosclerosis* 210:656-661
30. Rosito GA, Fox CS, Hoffmann U, Mahabadi AA, Massaro JM, O'Donnell CJ, Ruberg FL, Vasan RS (2008) Pericardial fat, visceral abdominal fat, cardiovascular disease risk factors, and vascular calcification in a community-based sample: the Framingham Heart Study. *Circulation* 117:605-613
31. Kurobe H, Hirata Y, Kitagawa T, Matsuoka Y, Maxfield MW, Sata M, Sugasawa N (2013) Azelnidipine suppresses the progression of aortic aneurysm in wild mice model through anti-inflammatory effects. *J Thorac Cardiovasc Surg* 146:1501-1508
32. Michel JB, Allaire E, Cockerill G, Egidio J, Lindholt J, Martin-Ventura JL, Sakalihan N, Swedenborg J, Thorsteinsdottir U, Treska V (2011) Novel aspects of the pathogenesis of aneurysms of the abdominal aorta in humans. *Cardiovasc Res* 90:18-27
33. Folkesson M, Eriksson P, Silveira A, Swedenborg J (2011) Protease activity in the multi-layered intra-luminal thrombus of abdominal aortic aneurysms. *Atherosclerosis* 218:294-299
34. Sano M, Baba S, Hirakawa S, Inuzuka K, Konno H, Ogawa M, Sakabe J, Sasaki T, Sato K, Setou M, Tanaka H, Unno N, Yamamoto N, Zaima N (2014) Lymphangiogenesis and Angiogenesis in Abdominal Aortic Aneurysm. *PLoS ONE* 9:e89830
35. Satta J, Juvonen T, Mosorin M, Soini Y (1998) Angiogenesis is associated with mononuclear inflammatory cells in abdominal aortic aneurysms. *Ann Chir Gynaecol* 87:40-42
36. Villacorta L, Chang L (2015) The role of perivascular adipose tissue in vasoconstriction, arterial stiffness, and aneurysm. *Horm Mol Biol Clin Investig* 21:137-147

-
37. Thanassoulis G, Corsini E, Fox CS, Hoffmann U, Massaro JM, Meigs JB, O'Donnell CJ, Rogers I, Schlett CL (2012) Periaortic Adipose Tissue and Aortic Dimensions in the Framingham Heart Study. *J Am Heart Assoc* 1:e000885
38. Folkesson M, Gulbins E, Japtok L, Kleuser B, Länne T, Vorkapic E, Wågsäter D, Welander M (2017) Inflammatory cells, ceramides, and expression of proteases in perivascular adipose tissue adjacent to human abdominal aortic aneurysms. *J Vasc Surg* 65:1171-1179
39. Police SB, Cassis LA, Charnigo R, Daugherty A, Thatcher SE (2009) Obesity Promotes Inflammation in Periaortic Adipose Tissue and Angiotensin II-Induced Abdominal Aortic Aneurysm Formation. *Arterioscler Thromb Vasc Biol* 29:1458-1464
40. Schlett CL, Bamberg F, Fox CS, Hoffmann U, Lehman SJ, Massaro JM, O'Donnell CJ (2009) Novel measurements of periaortic adipose tissue in comparison to anthropometric measures of obesity, and abdominal adipose tissue. *Int J Obes (Lond)* 33:226-232
41. Dias-Neto M, Meekel JP, van Schaik TG, Hoozemans J, Sousa-Nunes F, Henriques-Coelho T, Lely RJ, Wisselink W, Blankensteijn JD, Yeung KK (2018) High Density of Periaortic Adipose Tissue in Abdominal Aortic Aneurysm. *Eur J Vasc Endovasc Surg* 56:663-671
42. Okamoto E, Couse T, De Leon H, Goodman RB, Scott NA, Vinten-Johansen J, Wilcox JN (2001) Perivascular inflammation after balloon angioplasty of porcine coronary arteries. *Circulation* 104:2228-2235
43. Abbara S, Butler J, Cury RC, Desai JC, Nieman K, Reddy V (2006) Mapping epicardial fat with multi-detector computed tomography to facilitate percutaneous transepical arrhythmia ablation. *Eur J Radiol.* 57:417-422
44. Kvist H, Cederblad A, Chowdhury B, Sjöström L, Tylén U (1988) Adipose tissue volume determination in males by computed tomography and 40K. *J Obes* 12:249-266
45. Nelson JC, Carr JJ, Detrano R, Goldin JG, Kronmal RA, Loria CM, McNitt-Gray MF, Williams OD, Wong ND (2005) Measuring coronary calcium on CT images adjusted for attenuation differences. *Radiology* 235:403-414
46. Otton JM, Bester L, Boshell D, Feneley M, Hayen A, Lønborg JT, McCrohon J, Sammel N, Sesel K (2012) A method for coronary artery calcium scoring using contrast-enhanced computed tomography. *J Cardiovasc Comput Tomogr* 6:37-44
47. Bischoff B, Hadamitzky M, Hausleiter J, Hein F, Martinoff S, Meyer T, Schömig A (2009) MD Impact of a Reduced Tube Voltage on CT Angiography and Radiation Dose: Results of the PROTECTION I Study. *JACC Cardiovasc Imaging* 2:940-946
48. Huda W, Levin G, Scalzetti EM (2000) Technique factors and image quality as functions of patient weight at abdominal CT. *Radiology* 217:430-435
49. Bischoff B, Hadamitzky M, Hausleiter J, Kantert C, Martinoff S, Meyer T, Schömig A (2012) Cardiovascular risk assessment based on the quantification of coronary calcium in contrast-enhanced coronary computed tomography angiography. *Eur Heart J Cardiovasc Imaging* 13:468-475

50. Marwan M, Achenbach S, Daniel WG, Mettin C, Muschiol G, Pflederer T, Ropers D, Schuhbäck A, Seltmann M (2013) Very low-dose coronary artery calcium scanning with high-pitch spiral acquisition mode: comparison between 120-kV and 100-kV tube voltage protocols. *J Cardiovasc Comput Tomogr* 7:32-38
51. Schlosser T, Barkhausen J, Hunold P, Schmermund A, Voigtländer T (2007) Coronary artery calcium scoring: influence of reconstruction interval and reconstruction increment using 64-MDCT. *AJR Am J Roentgenol* 188:1063-1068
52. Groen JM, Greuter MJ, Oudkerk M, Schmidt B, Suess C, Vliegenthart R (2007) The influence of heart rate, slice thickness, and calcification density on calcium scores using 64-slice multidetector computed tomography: a systematic phantom study. *Invest Radiol* 42:848-855
53. Mühlenbruch G, Das M, Günther RW, Hohl C, Katoh M, Koos R, Mahnken AH, Thomas C, Wildberger JE (2005) Effect of varying slice thickness on coronary calcium scoring with multislice computed tomography in vitro and in vivo. *Invest Radiol* 40:695-699
54. Mühlenbruch G, Das M, Günther RW, Hohl C, Honnef D, Klotz E, Koos R, Mahnken AH, Niethammer M, Thomas C, Wildberger JE (2007) The accuracy of 1- and 3-mm slices in coronary calcium scoring using multi-slice CT in vitro and in vivo. *Eur Radiol* 17:321-329
55. Glodny B, Helmelt B, Petersen J, Schenk C, Strasak A, Taferner B, Trieb T, Unterholzner V (2009) A method for calcium quantification by means of CT coronary angiography using 64-multidetector CT: very high correlation with agatston and volume scores. *Eur Radiol* 19:1661-1668
56. Pavitt CW, Gordon D, Harron K, Lindsay AC, Nicol ED, Padley SP, Ray R, Rubens MB, Zielke S (2016) Technical feasibility and validation of a coronary artery calcium scoring system using CT coronary angiography images. *Eur Radiol* 26:1493-1502
57. Bowden DJ, Aitken SR, Wilkinson IB, Dixon AK (2009) Interobserver variability in the measurement of abdominal aortic calcification using unenhanced CT. *Br J Radiol* 82: 69-72
58. Gitsioudis G, Atsiatorne E, Buss SJ, Giannitsis E, Hofmann NP, Hosch W, Iwan J, Katus HA, Kauczor HU, Korosoglou G, Siebert S, Voss A (2014) When Do We Really Need Coronary Calcium Scoring Prior to Contrast-Enhanced Coronary Computed Tomography Angiography? Analysis by Age, Gender and Coronary Risk Factors. *PLoS ONE* 9:e92396
59. Shimizu K, Libby P, Mitchell RN (2006) Inflammation and cellular immune responses in abdominal aortic aneurysms. *Arterioscler Thromb Vasc Biol* 26:987-994
60. Rizas KD, Ippagunta N, Tilson MD 3rd (2009) Immune cells and molecular mediators in the pathogenesis of the abdominal aortic aneurysm. *Cardiol Rev* 17:201-210
61. Kwon HM, Edwards WD, Holmes DR, Lerman A, McKenna C, Ritman EL, Sangiorgi G, Schwartz RS, Virmani R (1998) Adventitial vasa vasorum in balloon-injured coronary arteries: visualization and quantitation by a microscopic three-dimensional computed tomography technique. *J Am Coll Cardiol* 32:2072-2079

62. Gössl M, Galili O, Herrmann J, Lerman A, Lerman LO, Mannheim D, Rajkumar SV, Tang H, Versari D (2009) Prevention of Vasa Vasorum Neovascularization Attenuates Early Neointima Formation in Experimental Hypercholesterolemia. *Basic Res Cardiol* 104:695-706
63. Antonopoulos AS, Achenbach S, Akoumianakis I, Alexopoulos N, Anthony S, Antoniadis, Brophy CM, Channon KM, Ciccone P, Digby J, Herdman L, Kampoli AM, Kelion A, Krasopoulos G, Margaritis M, Neubauer S, Oikonomou EK, Petrou M, Psarros C, Sabharwal N, Sanna F, Sayeed R, Shirodaria C, Tousoulis D, Thomas S, Uberoi R (2017) Detecting human coronary inflammation by imaging perivascular fat. *C.Sci Transl Med* 12;9:eaal2658
64. Buijs RVC, Boersma HH, Slart RHJA, Tielliu IFJ, Tio RA, Willems TP, Zeebregts CJ (2013) Calcification as a risk factor for rupture of abdominal aortic aneurysm. *Eur J Vasc Endovasc Surg* 46:542-8
65. Gupta A, Fürtjes G, Gilkeson R, Große Hokamp N, Jordan M, Laukamp KR, Lennartz S, Obmann MM, Obmann VC, Pennig L, Ramaiya N, Zopfs D (2021) CT artifacts after contrast media injection in chest imaging: evaluation of post-processing algorithms, virtual monoenergetic images and their combination for artifact reduction. *Quant Imaging Med Surg* 11:226-239
66. Ghekiere O, Buls N, Dendale P, Leiner T, Mancini I, Nchimi A, Salgado R, Vanhoenacker P (2017) Image quality in coronary CT angiography: challenges and technical solutions. *Br J Radiol* 90:20160567
67. Laukamp KR, Gilkeson R, Graner FP, Große Hokamp N, Gupta A, Ho V, Obmann VC, Ramaiya N, Ros P (2020) Role of spectral-detector CT in reduction of artifacts from contrast media in axillary and subclavian veins: single institution study in 50 patients. *Acta Radiol* 61:450-460
68. Haage P, Günther RW, Hübner D, Piroth W, Schmitz-Rode T (2000) Reduction of contrast material dose and artifacts by a saline flush using a double power injector in helical CT of the thorax. *JR Am J Roentgenol* 174:1049-53
69. Takeyama N, Gokan T, Hashimoto T, Hayashi T, Kato K, Kinebuchi Y, Nakashima J, Ohgiya Y, Takahashi T, Takasu D (2011) Comparison of different volumes of saline flush in the assessment of perivenous artefacts in the subclavian vein during cervical CT angiography. *Br J Radiol* 84:427-434
70. Lee EJ, Cho NJ, Han DC, Jeon JS, Kim H, Kim SH, Kwon SH, Nam B, Noh H (2022) Abdominal periaortic and renal sinus fat attenuation indices measured on computed tomography are associated with metabolic syndrome. *Eur Radiol* 32:395-404
71. Mylonas I, Alam M, Amily N, Chen L, Chow BJ, Hibbert B, Small G, Yam Y (2014) Quantifying coronary artery calcification from a contrast-enhanced cardiac computed tomography angiography study. *Eur Heart J Cardiovasc Imaging* 15:210-215

7. PUBLICATIONS/ACKNOWLEDGEMENTS

1. The complete work was published on 26.02.2022 as an original research article in the International Journal of Cardiovascular Imaging as:

Apostolos T. Mamopoulos, Patrick Freyhardt, Aristotelis Touloumtzidis, Alexander Zapenko, Marcus Katoh, Gabor Gaebel (2022) *Quantification of periaortic adipose tissue in contrast-enhanced CT angiography: technical feasibility and methodological considerations*. Int J Cardiovasc Imaging. 2022 Feb 26. <https://doi.org/10.1007/s10554-022-02561-8> .Online ahead of print. PMID: 35218465

2. The results of the work were published as an e-Poster at the 35th Annual Meeting of the European Society of Vascular Surgery (ESVS) on 28-29.09.2021 as:

A. Mamopoulos, M. Katoh, G. Gaebel. P-008 - *Technical feasibility of aortic wall calcium and periaortic fat tissue quantification using CT angiography images*.

3. The summary of the e-poster presentation at the 35th Annual Meeting of the European Society of Vascular Surgery (ESVS) was published as an abstract in the European Journal of Vascular and Endovascular Surgery-Vascular Forum as:

A. Mamopoulos, M. Katoh, G. Gaebel (2022) *Technical feasibility of aortic wall calcium and periaortic fat tissue quantification using CT angiography images*. EJVES Vasc Forum. Volume 54, 2022, Pages e18-e19. <https://doi.org/10.1016/j.ejvsf.2021.12.025>

The author would like to thank the thesis advisor, Professor Dr. med. M. Katoh, for his guidance and support during the process of the dissertation and Professor Dr. med. W. Reith for his interest in the subject and the acceptance to review the work.

The author would also like to thank PD Dr. med. G. Gäbel for his support and advice during the planning, execution and publication of the present study and PD Dr. med. P. Freyhardt for his support and especially his advice concerning technical issues.

The author would like to thank HELIOS Klinikum Krefeld for the availability of the data used in the study.

Lastly, the author would like to thank Rene Laqua for the free availability of the OsirixMD GlobalThresholding Plugin. According to his wish, a complete direct reference to the Plugin was made as an in-text citation.

The work is dedicated to my family and especially my mother.

8. CURRICULUM VITAE

The curriculum vitae is not included in the online version.

Eidesstattliche Erklärung

Erklärung gemäß § 7 Abs. 1 Nr. 2

Ich erkläre hiermit an Eides statt, dass ich die vorliegende Arbeit ohne unzulässige Hilfe Dritter und ohne Benutzung anderer als der angegebenen Hilfsmittel angefertigt habe. Die aus anderen Quellen direkt oder indirekt übernommenen Daten und Konzepte sind unter Angabe der Quelle gekennzeichnet.

Bei der Auswahl und Auswertung folgenden Materials haben mir die nachstehend aufgeführten Personen in der jeweils beschriebenen Weise unentgeltlich geholfen:

1. PD Dr. med. Gabor Gäbel, Manuskript Korrektur
2. PD Dr. med. Patrick Freyhardt, Datensammlung

Weitere Personen waren an der inhaltlich-materiellen Erstellung der vorliegenden Arbeit nicht beteiligt. Insbesondere habe ich nicht die entgeltliche Hilfe von Vermittlungs- bzw. Beratungsdiensten (Promotionsberaterinnen/Promotionsberater oder anderer Personen) in Anspruch genommen. Außer den Angegebenen hat niemand von mir unmittelbar oder mittelbar geldwerte Leistungen für Arbeiten erhalten, die im Zusammenhang mit dem Inhalt der vorgelegten Dissertation stehen.

Die Arbeit wurde bisher weder im Inland noch im Ausland in gleicher oder in ähnlicher Form in einem anderen Verfahren zur Erlangung des Doktorgrades einer anderen Prüfungsbehörde vorgelegt.

Ich versichere an Eides statt, dass ich nach bestem Wissen die Wahrheit gesagt und nichts verschwiegen habe.

Die Bedeutung der eidesstattlichen Erklärung und die strafrechtlichen Folgen einer unrichtigen oder unvollständigen eidesstattlichen Erklärung sind mir bekannt.

Ort, Datum

Unterschrift der/des Promovierenden

Eidesstattliche Versicherung

Belehrung

Die Medizinische Fakultät der Universität des Saarlandes verlangt eine Eidesstattliche Versicherung über die Eigenständigkeit der erbrachten wissenschaftlichen Leistungen. Weil der Gesetzgeber der Eidesstattlichen Versicherung eine besondere Bedeutung beimisst und sie erhebliche Folgen haben kann, hat der Gesetzgeber die Abgabe einer falschen eidesstattlichen Versicherung unter Strafe gestellt. Bei vorsätzlicher (also wissentlicher) Abgabe einer falschen Erklärung droht eine Freiheitsstrafe bis zu drei Jahren oder eine Geldstrafe. Eine fahrlässige Abgabe (also Abgabe, obwohl Sie hätten erkennen müssen, dass die Erklärung nicht den Tatsachen entspricht) kann eine Freiheitsstrafe bis zu einem Jahr oder eine Geldstrafe nach sich ziehen. Die entsprechenden Strafvorschriften sind in § 156 StGB (falsche Versicherungen an Eides Statt) und in § 161 StGB (fahrlässiger Falscheid, fahrlässige falsche Versicherung an Eides Statt) wiedergegeben.

§ 156 StGB: Falsche Versicherung an Eides Statt

Wer vor einer zur Abnahme einer Versicherung an Eides Statt zuständigen Behörde eine solche Versicherung falsch abgibt oder unter Berufung auf eine solche Versicherung falsch aussagt, wird mit Freiheitsstrafe bis zu drei Jahren oder mit Geldstrafe bestraft.

§ 161 StGB: Fahrlässiger Falscheid, fahrlässige falsche Versicherung an Eides Statt:

(1) Wenn eine der in den § 154 bis 156 bezeichneten Handlungen aus Fahrlässigkeit begangen worden ist, so tritt Freiheitsstrafe bis zu einem Jahr oder Geldstrafe ein.

(2) Strafflosigkeit tritt ein, wenn der Täter die falsche Angabe rechtzeitig berichtigt. Die Vorschriften des § 158 Abs. 2 und 3 gelten entsprechend.